10-19-2016 12:00 AM

Identification of a Nuclear Localization Signal (NLS) within the Pleckstrin Homology (PH) domain of Rho Guanine Nucleotide Exchange Factor (RGNEF)

Michael V. Tavolieri, *The University of Western Ontario*

Supervisor: Michael J. Strong, *The University of Western Ontario*
A thesis submitted in partial fulfillment of the requirements for the Master of Science degree in Pathology
© Michael V. Tavolieri 2016

Abstract

Rho Guanine Nucleotide Exchange factor (RGNEF) is a 180 kDa protein which forms pathological neuronal cytoplasmic inclusions in degenerating spinal motor neurons in amyotrophic lateral sclerosis (ALS) and for which the gene (*ARHGEF28*) is mutated in a subset of cases. Despite having previously been shown to localize to the nucleus and to undergo a nuclear cytosolic shift in response to cellular injury, the mechanism of its nuclear import has yet to be elucidated. Here we use site-directed mutagenesis with a combination of subcellular fractionation and confocal microscopy to identify a functional nuclear localization signal (NLS) within the Pleckstrin Homology (PH) domain of RGNEF. We show that the function of the NLS is conserved both in full length RGNEF and when expressed as only the PH domain. This advances the growing body of literature implicating dysfunction in the nuclear import and export pathways as a feature of ALS pathology. Additionally, this is the first PH domain-embedded NLS identified, despite the prevalence of PH domains in the human proteome and the similarities in their consensus motifs.

Keywords

Amyotrophic Lateral Sclerosis; Rho Guanine Nucleotide Exchange Factor; Pleckstrin Homology Domain; Nuclear Localization Signal; Confocal Microscopy; Subcellular Fractionation; Molecular Modeling

Dedication

I would like to dedicate this body of work to the memory of the following individuals: Oreste Tavolieri, in whom I saw the strength to overcome any obstacle; Mona Crow, who taught me the fortitude to endure any loss; Anna Tavolieri, who showed me unconditional love; and Linda Costella, who was truly my best friend for a very long time. One day the world will be free of disease. Until then, we carry with us your memory and your virtue.

Acknowledgments

Foremost I would like to thank my parents. They have always supported me even when they didn't understand the path that I was taking. They have always had faith in the decisions I've made and pride in my accomplishments. More than anything else though, they taught me humility in my success and to treat every person with respect. What they've taught me, I will carry with me no matter what mountain I climb. Thank you both so much for everything.

I would also like to acknowledge all of my lab mates in the Strong Lab. Thank you all for the support you've shown me over the past two years. They have been a second family to me: they have pushed me to be better, supported me, and enabled me to accomplish amazing things. Thank you all for letting me be part of your team.

In particular I would like to acknowledge Sali Farhan who has been one of the most supportive lab mates I've ever had. Graduate school can be a lonely place and Sali has always gone out of her way to make sure I had a friend in her. More than that, her ideals and integrity make her an exceptional role model and someone whom I'm proud to have in my life.

I would like to acknowledge Dr. Danae Campos-Melo and Dr. Cristian Droppelmann both for their contribution to this body of work and for their mentorship during my time at Western. Dr. Droppelmann has made some of the greatest contributions to this work both in his hands-on support and also in being incredibly accessible for questions and guidance. Undoubtedly, he is one of the most rational, intelligent and wise people I have ever met. Even more so, his obvious dedication to science often hides what a compassionate, thoughtful, and caring human being he is. He embodies so much of what I hope to be as a scientist and has been an outstanding role model for me over the past two years.

I would like to acknowledge all of my good friends who visited me and helped me get acclimated in London. In particular, I would like to thank my two best friends Sarah Voegeli and

always open and accessible any time I needed help and offered as much assistance as they could. Thank you three so much.

I would like to thank all of the investigators in my past who gave me the opportunity to learn and grow and whose support brought me to this point: Dr. David Taylor of the ALS Society of Canada and my three former supervisors at the University of Windsor: Dr. Jerome Cohen, Dr. Barbara Zielinski, and Dr. Michael Crawford. In particular I want to thank Dr. Jerome Cohen for the three years I spent in his lab. Dr. Cohen, thank you so much for all of the opportunities you gave me in undergrad. I didn't realize at the time all the things you were doing to prepare us for graduate school. I appreciate everything you've done for me and I'm so grateful for the time we spent working together.

I would like to acknowledge Sharon Colman of the Windsor-Essex County ALS Society. I can say from personal experience that for a family member of a person with ALS, no one is more knowledgeable, compassionate, or caring than Sharon Colman. She is a guardian angel to people in need.

Finally, I would like to thank my supervisor Dr. Michael Strong. Thank you so much for giving me the opportunity to make a contribution to fighting this disease. What I have accomplished under your leadership is one of the greatest achievements of my life. Thank you for the time and patience you have invested in me. I am so grateful for how I have grown under your guidance.

Table of Content

List of Tables

List of Figures

List of Appendices

List of Abbreviations

ALS   Amyotrophic lateral sclerosis

ARM   Armadillo repeat

BMAA   Beta-methylamino L-alanine

BTK   Burton's tyrosine kinase

C9orf72   Chromosome 9 open reading frame 72

CFTR   Cystic fibrosis transmembrane conductance regulator

Dbl   Diffuse B-cell lymphoma

DH   Dbl homology

DPR   Dipepetide repeat proteins

EF3   Elongation factor 3

EWS   Ewing's sarcoma protein

fALS   Familial amyotrophic lateral sclerosis

FTD   Frontotemporal dementia

FUS   Fused in sarcoma / translocated in liposarcoma

GAP   GTPase activating protein

GEF   Guanine exchange factor

HIV   Human immunodeficiency virus

hnRNP A1   Heterogeneous nuclear ribonucleoprotein A1

IBB   Importin-β binding domain

ICC   Immunocytochemistry

NCI   Neuronal cytoplasmic inclusion

NEFL	Low molecular weight neurofilament *gene*
NF	Neurofilament
NFH	High molecular weight neurofilament protein
NFL	Low molecular weight neurofilament protein
NFM	Medium molecular weight neurofilament protein
NLS	Nuclear localization signal
NNI	Neuronal nuclear inclusion
NPC	Nuclear pore complex
NUP	Nucleoporin
PCR	Polymerase chain reaction
PH	Pleckstrin homology
PIKE	Phosphoinositol 3-kinase enhancer
PP2A	Protein phosphatase 2A
PTHrP	Parathyroid hormone-related protein
PrLD	Prion-like domain
PRMT1	Protein arginine N-methyltransferase 1
PtdIns	Phosphoinositides
Ran	Ras-related nuclear protein
RCC1	Regulator of chromosome condensation
sALS	Sporadic amyotrophic lateral sclerosis
sPH	Split pleckstrin homology
STAT 5	Signal transducer and activator of transcription 5

TAF15	TATA-binding protein associated factor 2N
TDP-43	TAR DNA-binding protein of 43 kDa
TH	Tec homology
U snRNPs	Uridine-rich small nuclear ribonucleoprotein particles

Chapter 1

1   Thesis Rationale / Hypothesis

Amyotrophic lateral sclerosis (ALS) is a neurodegenerative disease often resulting in death within 5 years of symptom onset (1,2). Epidemiological research suggests ALS poses an increasing risk to Canadian health services as the number of individuals reaching the average age of symptom onset will double by 2026 (3). Currently, the only compound that is approved for treatment of ALS that has been shown to alter disease course, Riluzole, extends patient survival by approximately 3 months and the mechanism by which it slows disease pathology is still unknown (4).

Approximately 10% of ALS cases are classified as familial ALS (fALS) and show typical Mendelian inheritance (5). Forty percent of these are due to mutations in the gene *chromosome 9 open reading frame 72* (*C9orf72*) (6). The mechanism by which *C9orf72* mutations result in disease pathology is still unknown though a growing body of research has implicated *C9orf72* mutations in dysfunction in the nuclear transport pathways (7–9). Further evidence of nuclear transport dysfunction in ALS comes from the fact that many ALS-related proteins show nuclear depletion in ALS patient neurons.

The transport of large proteins in and out of the nucleus is a tightly controlled process (10). The classical nuclear import pathway is the best described mechanism and accounts for approximately 45% of protein import into the nucleus (11). It is distinguished from alternate mechanisms of import based on its use of nuclear localization signals (NLS) that interact directly with the transport receptor importin-α (12,13). A heterodimer forms between importin-α and importin-β1 to facilitate import through the nuclear pore complex (NPC) (14,15). This process is driven by the cycling of Ras-related Nuclear protein (Ran), which recycles the importin subunits from the nucleus into the cytoplasm (16).

Pleckstrin Homology (PH) domains are an invariable component of guanine exchange factors (GEFs), along with the Dbl Homology (DH) domain. Named for the protein in which it was first discovered, Diffuse B-Cell Lymphoma (Dbl), the DH domain performs catalytic exchange of GDP for GTP. The PH domain is thought to contribute to GEF activity by localizing the protein to substrate rich membranes (17). Although no PH domain has been shown to play a role in nuclear import, the Split Pleckstrin Homology (sPH) domain (a domain with similar characteristics) within the protein phosphoinositol 3-kinase enhancer (PIKE) has been shown to contain a functional NLS (18).

Rho guanine nucleotide exchange factor (RGNEF) is a 180 kDa ALS-linked protein that has been shown to localize to the nucleus in low levels (19). As an ALS-linked protein, it shares many hallmark characteristics of proteins linked to ALS including ALS-specific mutations (20), localization to neuronal cytoplasmic inclusions (NCIs) (21) and being a stability element for low molecular weight neurofilament mRNA (*NEFL* mRNA) (19,22). To date, no NLS has been identified within the protein sequence. RGNEF does however contain a PH domain, which has classically been known to contribute to subcellular localization.

Given the canonical function of PH domains in GEF activity, I hypothesize that the PH domain of RGNEF plays a role in its subcellular localization. Specifically, I hypothesize that it may contain a NLS responsible for RGNEF nuclear import.

1.1 Background of ALS

Amyotrophic lateral sclerosis (ALS) is a neurodegenerative disease characterized by the progressive loss of upper and lower motor neurons, often resulting in death within 5 years of symptom onset (1,2). Early symptoms vary depending on the site of onset: individuals with limb onset present with wasting or weakening of the distal muscles (hands or legs); individuals with bulbar onset present first with slurred speech and dysphagia (1). With both forms of onset, death

typically occurs as a result of respiratory failure within 5 years of symptom onset, though individuals with bulbar onset have a lower median length survival (23,24).

There are three recognized variants of ALS: sporadic (sALS), familial (fALS) and the Western Pacific or Guamanian variant. The latter is considered an example of an environmental trigger. Amongst the Chamorro peoples of Guam and the Japanese inhabitants of the Kii Peninsula ALS was hyperendemic with peak incidence rates between 1950 – 1954 (25), with a steady decline thereafter (26). The etiology of the Guamanian variant is still unknown. One hypothesis suggests that the high incidence of the disease observed in 1945 was the product of biomagnification of the neurotoxin beta-methylamino L-alanine (BMAA) in traditional foodstuffs. (27). However, further research on this topic has failed to show high levels of BMAA in Chamorro individuals (28). A second hypothesis suggests that the decrease in cases of ALS is the product of westernization of Guamanian Society and the influence of the United States on Guamanian foods and lifestyle (26).

The remaining cases of ALS are defined as either sALS or fALS. Cases of fALS are distinguished from sALS by genetic inheritance of the disease; sALS has no apparent family linkage and individuals do not harbour an ALS-causative genetic mutation. This classical classification system is being challenged, however, as ALS is increasingly described as a complex disease with a spectrum of genetic susceptibility factors. It has been proposed that fALS and sALS classifications represent gene effect size. Single genes with large affect sizes produce cases that are classified as fALS: genetic linkage is easy to identify. Cases where one or more genes contributes, each of which has a smaller affect size, are likely to present as sALS (23,29). This is supported by evidence of apparent genetic correlation in approximately 8 – 10% of cases of sALS. For example, relatives of individuals with apparent sALS have been shown to be at an increased risk for ALS (30).

In Canada, a growing population of individuals reaching the age of symptom onset pose a high burden for healthcare providers and medical systems. An epidemiological examination suggests

that the number of Canadians over the age of 60 will double by 2026, significantly increasing the number of individuals at risk of developing ALS (3). The only compound currently available for the treatment of ALS that alters disease course, Riluzole, has only been shown to have limited impact on patient survival (4). Greater research into the cause of the disease is still needed to identify treatment targets and to improve patient outcome.

1.2   Neuropathology and the disease process of ALS

The neuropathology of ALS is characterized by significant loss of muscle with thinning of the ventral spinal roots and atrophy of the spinal cord (31). The ventral and lateral corticospinal tracts show prominent pallor and gliosis as a result of loss of descending supraspinal motor neurons (1). At the microscopic level, key features of ALS include neuronal cytoplasmic inclusions (NCIs), neuronal nuclear inclusions (NNIs) and glial inclusions.

The most common NCI, ubiquitinated inclusions, are circular or fibrillar skeins observed in the perikarya of the motor neuron (32). They have been shown to contain ALS-related proteins including TDP-43 (33), FUS (34), and RGNEF (21). Hyaline conglomerate inclusions, a second type of NCI, occur in the perikarya of motor neurons (31,35) and are immunoreactive for neurofilament proteins (NF) (31,36). NFs are obligate heteropolymers composed of three subunits differentiated based on their molecular weight: low molecular weight neurofilament (NFL), medium molecular weight (NFM) and high molecular weight (NFH) (37). A loss of the normal stoichimetric balance of NF subunits is thought to be key to their recruitment to NCIs, in particular NFL expression (38). Several RNA binding proteins implicated in ALS have been shown to regulate NFL subunit expression (19,39).

A second form of inclusions, NNIs are more prevalent in cases of ALS with frontotemporal dementia (FTD) than ALS alone. A 2004 case study of an individual with ALS showed eosinophilic nuclear inclusions in pyramidial neurons of the motor cortex and hippocampus (40). Work done using a larger population of individuals with a diagnosis of either ALS-alone, FTD-

alone or ALS-FTD showed ubiquitin immunoreactive intraneuronal inclusions in one case of ALS-FTD, though no cases with a diagnosis of ALS only. NNIs were shown in about half (7 of 15) FTD cases, supporting the hypothesis that ALS and FTD may represent a spectrum of disorders (41).

Glial inclusions are another neuropathological marker supporting the hypothesis of ALS and FTD as a spectrum of disorders. An examination of TDP-43 immunoreactive ubiquitin-positive inclusions in the neostriatum showed glial inclusions in all cases of ALS-FTD and most (12 of 14) cases of ALS-alone (42). Work done examining FUS immunoreative inclusions showed that glial inclusions are present in oligodendrocytes and are more common in late onset cases (43).

1.3   Nuclear transport dysfunction in ALS

1.3.1 Chromosome 9 open reading frame 72: a regulator of nuclear transport

Mutations in *Chromosome 9 open reading frame 72* (*C9orf72*) account for approximately 40% of all fALS cases (44). The mutation is observed as a massive intronic hexanucleotide (GGGCC) repeat expansion (6,45). While healthy individuals appear to have about 23 repeats, ALS patients range between 600 to 2000 repeats (45,46). The expanded RNA undergoes an unconventional form of translation, called repeat associated non-ATG-initiated translation. This gives rise to three distinct dipeptide repeat proteins (DPRs) depending on the reading frame translated from the RNA bearing the expanded repeats (47). Despite the prevalence of *C9orf72* repeats in ALS patients, the mechanism underlying its pathogenesis remains unknown.

Many ALS-associated proteins show nuclear-cytoplasmic mislocalization. One hypothesis for how mutations in *C9orf72* may contribute to ALS pathology is by causing dysfunction in the nuclear transport system of motor neurons. Supporting data has been shown in human, yeast, and drosophila. First, the expression of the DPRs of *C9orf72* in cultured human astrocytes results in altered splicing of Ran GTPase: DPR expression causes exon 2-skipping, resulting in the

removal of the first 88 residues of the protein (9). Ran GTPase provides the energy necessary for nuclear transport, including non-classical nuclear import (see section 1.4.2). As well, two unbiased screens performed in yeast have shown that both karyopherins and effectors of Ran-mediated nucleocytoplasmic transport are modifiers of *C9orf72* toxicity (8). Finally, in a Drosophila model of *C9orf72*, a targeted RNAi screen using a library of 121 RNAi lines – which encoded nuclear pore complex proteins, importins, regulators of the RanGTP cycle, and arginine methylases - identified 15 enhancers and 4 suppressors of eye phenotype. These included both RCC1 and RanGAP, 2 importin-α subunits, importin-β1, karyopherin-β2, and PRMT1 (7). This suggests that alterations in nuclear transport may be a key component of *C9orf72*-mediated toxicity.

1.3.2 TAR DNA-binding protein of 43 kDa

TAR DNA-binding protein of 43 kDa (TDP43) has become a major protein of interest in ALS since it was identified in 2006 as a core component of ubiquitinated aggregates in motor neurons and glial cells in the vast majority of ALS cases (48,49). Mutations in the gene encoding TDP-43, *TAR DNA Binding Protein* (*TARDBP*) are found in 4% of fALS cases (50). It had also been shown to have a role in RNA splicing of the cystic fibrosis transmembrane conductance regulator (CFTR) (51). In the context of ALS, TDP-43 has been implicated in multiple aspects of the disease pathogenesis. Key to this thesis, nuclear depletion of TDP-43 is a hallmark of disease pathology in ALS (52).

The N-terminal TDP-43 contains a NLS, which facilitates its nuclear localization via the classical nuclear import pathway (discussed in greater detail in section 1.4.2) (53). In healthy cells, TDP-43 is found predominantly in the nucleus (54,55). However, in motor neurons of individuals with ALS, TDP-43 is localized predominantly to the cytoplasm (56). In the cytoplasm, TDP-43 has been shown to be a major component of ubiquitinated aggregates in ALS motor neurons (48,49).

Although TDP-43 nuclear depletion appears to be linked to ALS pathology, none of the ALS-related TDP-43 mutations are located within the NLS (57). Past research from our lab has shown upregulation of TDP-43 expression with prominent cytosolic localization in axotomized mouse motor neurons (58). This suggests that TDP-43 nuclear depletion may occur after motor neurons have begun degeneration and are in a state of stress.

1.3.3 Heterogeneous nuclear ribonucleoprotein A1

Heterogeneous nuclear ribonucleoprotein A1 (hnRNP A1) is another RNA-binding protein with a link to ALS. It has been shown to shuttle mature mRNA through the nuclear pore complex and to interact with the Drosha complex in miRNA biogenesis (59). The prion-like domain (PrLD) of hnRNP A1 is thought to contribute to its role in RNA binding. A rare mutation found in ALS patients in the PrLD of hnRNP A1 increases hnRNP A1's localization to stress granules (60). Stress conditions have been shown to induce the translocation of wild-type hnRNP A1 from the nucleus to stress granules (61).

The mechanism by which hnRNP A1 achieves nuclear shuttling is unique for two reasons. The first is that the N-terminal M9 domain of hnRNP A1 acts both as a nuclear import (62,63) and nuclear export signal (64,65). The second is that the M9 domain is capable of binding two transport receptors: both karyopherin-β2 (66) and karyopherin-β2B (67). This dual-binding illustrates the important and necessary role that hnRNP A1 plays in mRNA nuclear export in normal, healthy cells.

1.3.4 The FET Family of proteins

The FET family contains three member proteins, from which it gets its name: Fused in sarcoma/translocated in liposarcoma, Ewing's sarcoma protein, and TATA-binding protein associated factor 2N. The FET family of proteins all localize predominantly to the nucleus and show nuclear depletion in ALS motor neurons.

Fused in sarcoma / translocated in liposarcoma

Fused in sarcoma/translocated in liposarcoma (FUS) has many similarities to TDP-43, including ubiquitous expression and the ability to bind both DNA and RNA. It has been found to form irreversible inclusions when cells are exposed to environmental stress (68). FUS-immunoreactive skeins and aggregates have been found in ALS motor neurons (21,34). Nuclear import of FUS is achieved by binding Karyopherin-β1 (68). Mutations in FUS occur in approximately 4% of fALS cases (44). Of interest, those mutations which affect nuclear localization have been shown to cause more severe disease phenotype (52).

Ewing's sarcoma protein

Another member of the FET family, Ewing's sarcoma protein (EWS) is normally localized to the nucleus and functions in RNA regulation (69). Mutational screening of ALS patients has shown three missense variants of the gene encoding EWS (*EWSR1)*. These variants affect EWS localization (70). Post-mortem analysis of individuals with sporadic ALS have shown redistribution of EWS to the cytoplasm (71). The C-terminal of EWS contains a PY-NLS (discussed in section 1.4.3; 73,74). Its localization may be regulated by post-translational modification: phosphorylation of a single tyrosine residue adjacent to the PY-NLS has been shown to be necessary for karyopherin-β2 binding (73).

TATA-binding protein associated factor 2N

The third member of the FET family, TATA-binding protein associated factor 2N (TAF15), has also been identified as having missense variants occurring in ALS patients (74). Like the other members of the FET family, it is predominantly localized to the nucleus in healthy cells. When mislocalized to the cytoplasm, it is found in stress granules (70,74). A NLS has been identified in the C-terminal region of TAF15 (75). Methylation of the C-terminal region by protein arginine N-methyltransferase 1 (PRMT1) of TAF15 is required for proper nuclear localization (76). The observation that PRMT1 expression is affected by mutations in *C9orf72* (7) raises the possibility that mutations in *C9orf72* may cause nuclear depletion of TAF15 by regulating PRMT1 expression.

1.4 Nuclear transport

The preceding sections suggest that disruptions in nuclear transport may be a critical component of ALS pathogenesis. The entry and exit of large macromolecules in and out of the nucleus is a tightly regulated process. Like the plasma membrane, the nuclear envelope is an impermeable barrier consisting of an inner and outer membrane. Movement through the nuclear envelope occurs only through specialized pores, which are gated by large complexes of proteins termed nuclear pore complexes (NPCs) (10). Figure 1 illustrates the NPC. A NPC is a large supramolecular assembly composed of approximately 30 different proteins, termed nucleoporins (NUPs). The total molecular weight of the complex is approximately 125 MDa, of which approximately 55 MDa consists of the luminal domain embedded in the nuclear envelope.

Approximately 32 MDa of the complex consists of the cytoplasmic ring moiety, from which eight long (approximately 50 nm), kinky cytoplasmic filaments emanate (77,78). Though at its narrowest point the central pore is 45 – 50 nm in diameter, large proteins require active transport in order to pass through the NPC (79,80). The mechanism by which larger molecules are excluded from the nucleus is still unknown but may involve the nucleoplasmic basket (15). Although the exact mechanism whereby nuclear transport receptors facilitate import of large cargo proteins has not been determined, the interaction of transport receptors with NUPs composing the cytoplasmic filaments – specifically those rich in FG repeats – is necessary for the NPC conformational change required for import (81–83). A more thorough discussion on the role of transport receptors will be offered below (Section 1.4.2).
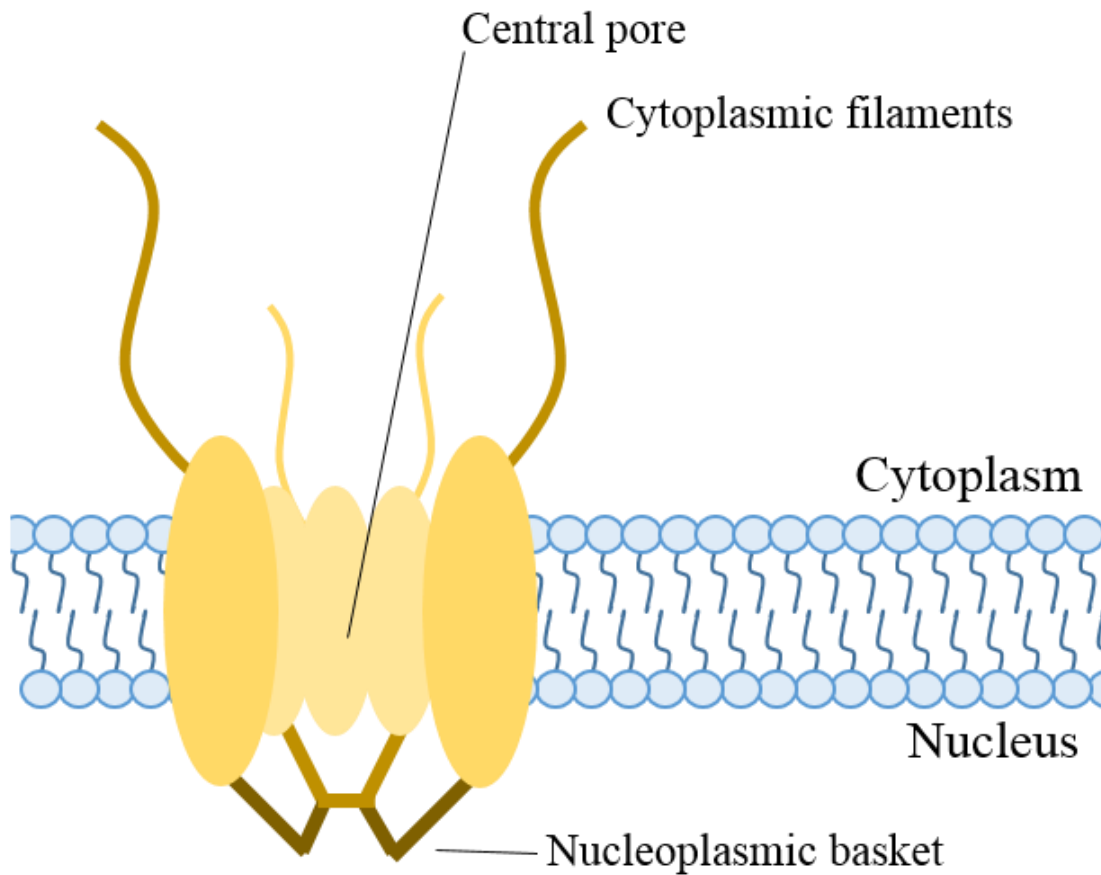
Figure 1: The nuclear pore complex. The nuclear pore complex (NPC) is a supramolecular structure of ~125MDa that spans the nuclear envelope. Small molecules are able to diffuse through the central pore. Larger molecules require transport receptors in order to pass through. The transport receptor importin-β1 is able to interact with Nucleoporins (NUPs) on the cytoplasmic filaments to initiate a conformational change in the NPC that allows for the import of it and its cargo. It is unclear what conformational changes are necessary as the central pore should be large enough (~50nm) to accommodate some large proteins. It is theorized that the nucleoplasmic basket may act to gate large molecules entering.

Though it is widely agreed that larger molecules require targeting signals to translocate, the literature still has not reached a consensus on the maximum molecular weight of a protein allowing for its passive diffusion into and out of the nucleus. Both 40 kDa (84,85) and 60 kDa (86–88) thresholds are often used in the literature. Others have suggested that this threshold may be as high as 110 kDa (89). Despite the dispute in threshold, we can say definitely that molecules greater than 110 kDa require active transport to enter the nucleus.

1.4.1 Nomenclature

For clarity, it is important to address nomenclature related to nuclear transport receptors. Karyopherin is a term that was first used in 1995 to describe all transport receptors relating to movement across the nuclear envelope, including the proteins responsible for nuclear export (90). The karyopherin-β family of protein contains ten subunits involved in nuclear transport (91). Importin-β1 is the first member of this family and is involved in classical nuclear import as described in section 1.4.2. The remaining members of the karyopherin-β family participate in alternate forms of nuclear transport. The names of some of these protein and the ALS-linked proteins they interact with are shown in Table 1.

1.4.2 Classical nuclear import

Classical nuclear import describes a mechanism whereby cargo proteins form a complex with both importin-α and importin-β1 subunits in order to translocate into the nucleus. It differs from other mechanisms of nuclear import in that it is the only one where the cargo protein binds importin-α. Its name harkens to the fact that it was the first identified mechanism of nuclear transport, having first been described in 1984 (12,13). Classical nuclear import is estimated to account for approximately 45% of import into the nucleus (11). Figure 2 illustrates the mechanism of classical nuclear import, which is discussed below.

Table 1: The members of the karyopherin-β family involved in nuclear import of ALS-related proteins

Name	Alternate Name	ALS-related proteins that use this receptor for nuclear localization
Importin-β1	Karyopherin-β1	TDP-43
Karyopherin-β2	Transportin-1	FUS, EWS, hnRNP A1
Karyopherin-β2B	Transportin-2	hnRNP A1
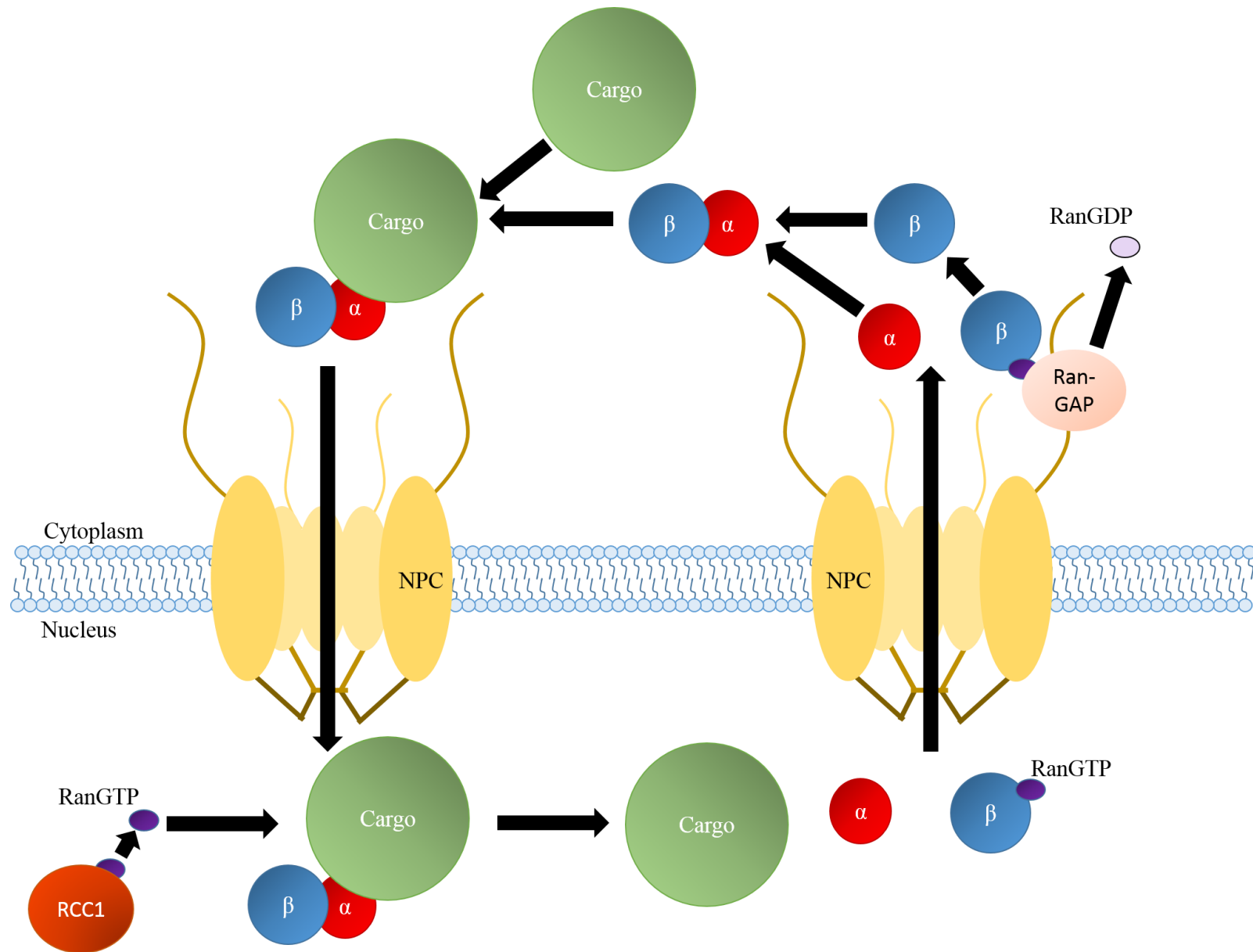
Figure 2: The classical nuclear import pathway. The classical nuclear import pathway is characterized by the interaction of a cargo protein with the importin-α – importin-β1 heterodimer. Importin-α (red) initially forms a heterodimer with importin-β1 (blue) through an importin-β binding domain (IBB). The cargo protein (green) can then bind importin-α directly via interaction of its NLS with the NLS-binding domain of importin-α Interaction between importin-β1 and NUPs of the NPC (yellow) allows for the import of the importin-cargo complex. The nucleus contains a high concentration of RanGTP, which binds importin-β1 and reduces its affinity for interacting with importin-α. This causes the importin-cargo complex to dissociate, releasing the cargo protein into the nucleus. Importin-α and importin-β1 are then able to exit the nucleus via the NPC. The concentration of RanGTP is highest in the nucleus where RCC1 (dark orange), the guanine exchange factor (GEF) responsible for its activation, is located. RanGDP concentration is highest in the cytoplasm. RanGAP (light orange), the GTPase activating protein (GAP) responsible for Ran's inactivation, has been shown to interact with NUPs of the cytoplasmic filaments, increasing the probability of it coming into contact with GTP-bound importin-β1 exiting via the NPC.

Interaction of importin-α with importin-β1

Importin-α and importin-β1 form a heterodimer before binding the cargo protein. It has been shown that importin-α is able to bind cargo protein in the absence of importin-β1 but that binding is greatly increased in the presence of importin-β1 (14). This is due to auto-inhibition of importin-α. Importin-α is composed of two functional domains: a short N-terminal importin-β binding (IBB) domain and a large NLS-binding domain. In the absence of importin-β1, the IBB acts as a pseudo-NLS, binds the NLS-binding domain and thus results in steric interference, greatly reducing cargo protein binding (92,93).

Interaction of importin-α with the cargo protein

Importin-α acts as a transport receptor for proteins directed to the nucleus. It does so by directly binding NLSs within cargo proteins. A NLS can be described as being either monopartite, having a single cluster of basic residues, or bipartite, containing two clusters of basic residues separated by a mutation tolerant linker sequence (94). Early work on bipartite signals described the linker sequence as being 9 to 12 amino acids long, though recent work has shown that the sequence can be as long as 29 amino acids (95). Basic residues of NLSs bind at two sites along the concave surface of importin-α. This surface is composed of ten armadillo repeats (ARM) with strictly conserved tryptophan and asparagine residues (96). The major NLS binding site, which is where monopartite sequences bind, is formed from ARMs 2-4. Bipartite sequences, however, bind both the major binding site and a second pocket formed by ARMs 7-9, termed the minor binding site (97). This direct binding facilitates nuclear import by linking the cargo protein to importin-β1.

Interaction between importin-β1 and its partners deposits cargo proteins into the nucleus

Once formed, the cargo-importin complex moves into the nucleus through the interaction of importin-β1 with the nuclear pore complex. Importin-β1 interacts with FG-rich NUPs located on the cytoplasmic filaments of the NPC and is shuttled through the central pore into the nucleosol (15). Within the nucleus, RanGTP binds importin-β1, inhibiting its interaction with importin-α. When the IBB site of importin-α is no longer bound by importin-β1, the IBB acts as a high

affinity pseudo-NLS, displacing the cargo protein and releasing it into the nucleus (98). The cargo protein will remain in the nucleus unless actively exported by the nuclear export pathway. This process also recycles importin-α and importin-β1 into the cytoplasm and is dependent on RanGTP (16).

The Ran Cycle

The energy for nuclear import is provided by the Ran cycle. Ran, a member of the small Ras GTPase family, cycles between a GTP- and a GDP-bound state. A Ran gradient is established in the cell by the asymmetrical distribution of Ran regulators. The guanine exchange factor (GEF) responsible for RanGTP, known as regulator of chromosome condensation (RCC1), contains an NLS and is localized predominantly in the nucleus (99). Binding of RCC1 to Histone H2A and H2B increases RCC1 GEF activity by two fold (100). The GTPase Activating Protein (GAP) responsible for RanGDP, known as RanGAP, localizes predominantly to the cytoplasm and can interact with RanBP1 and the nucleoporin NUP358 (also known as RanBP2) on the cytoplasmic filament (15). This compartmentalization of regulators creates a high concentration of RanGTP within the nucleus, which is quickly converted to RanGDP upon exiting via the nuclear pore. This distribution is critical to nuclear import as the phosphorylation state of Ran affects karyopherin-cargo interactions in classical nuclear import.

1.4.3   Alternative nuclear import mechanisms

As mentioned, classical nuclear import accounts for approximately 45% of import (11); the remaining 55% of import is determined by alternate mechanisms. In addition to the well described classical model of nuclear import, there exist less well understood mechanisms. In application, these are easy to distinguish from the classical pathway as they do not utilize the importin-α subunit: they use a different adaptor protein or possibly bind karyopherin-β subunit directly.

Alternative import pathways using importin-β1

Import of the uridine-rich small nuclear ribonucleoprotein particles (U snRNPs), which are spliceosomal subunits, uses a similar process to classical nuclear import, though it uses an alternate adaptor protein. Rather than importin-α, U snRNPs bind the adaptor protein snurportin-1. Snurportin-1 contains an IBB similar to importin-α and is able to bind importin-β1 to facilitate nuclear import (101). Rather than a NLS, snurportin-1 recognizes its cargo by an m_3G-cap on the spliceosomal RNA (102–104).

Additionally, importin-β1 is capable of binding some cargo proteins directly without the use of an adaptor protein. These proteins include ribosomal proteins (105), parathyroid hormone-related protein (PTHrP) (106), CREB (107), cyclin B1 (108), the HIV proteins Rev and Tat (109), the human T-cell leukemia virus type 1 (HTLV-1) protein Rex (110), and others. Not all of these proteins bind importin-β1 at the same site as importin-α. For example, the binding site for PTHrP only partially overlaps the IBB binding site. The superhelix of importin-β1 is composed of 19 HEAT repeat domains. HEAT repeat domains get their name from four proteins in which they have been found: Huntingtin, elongation factor 3 (EF3), protein phosphatase 2A (PP2A), and the yeast kinase TOR1. Importin-α binds to repeats 2-11 and PTHrP binds to repeats 7-19 (111).

Alternative import pathways using other karyopherin-β family members

Karyopherin-β2, another member of the β-karyopherin subfamily, is responsible for the nuclear import of over 20 proteins involved in mRNA processing, including FUS (68), EWS (73), and hnRNP A1 (66). These proteins sometimes use the PY-NLS, named for a conserved PY C-terminal sequence. The ALS-linked protein EWS, for example, uses this type of NLS (72,73). PY-NLS are characterized as being structurally disordered, having an overall basic character, and as having the C-terminal consensus sequence $R/H/KX_{2-5}PY$ (112).

In addition to importin-β1 and karyopherin-β2, at least 8 other β-karyopherins play a role in nuclear import. However, much is still unknown about the cargo of these proteins and the mechanism by which they interact (91).

1.5   Pleckstrin homology domains

Pleckstrin homology (PH) domains are widely believed to contribute to the subcellular localization of proteins. They are invariably located at the C-terminus of a Dbl Homology (DH) domain and together these two domains are often sufficient to perform guanine exchange (17). The DH domain catalyzes exchange of GDP for GTP, activating the GTPase. The mechanism by which the PH domain contributes to guanine exchange is not fully known, though it is believed to be necessary to localize the protein to substrate rich membranes by binding phosphoinositides (113).

PH domains lack consensus gene homology and instead are identified by their characteristic molecular structure: a seven-stranded β-sandwich structure with a C-terminal α-helix (114). PH domains get their name from the platelet protein Pleckstrin, which contains two PH domains. Figure 3 shows the N-terminal PH domain of Pleckstrin (115). It is believed that PH domains facilitate membrane binding through interactions between basic residues located along the β-sandwich structure and phosphoinositides (PtdIns) embedded within the membrane. Only a minority of PH domains show high affinity for PtdIns though and the true mechanism of localization has yet to be elucidated (113).

To date, no PH domain has been shown to contribute to nuclear import. An NLS was, however, found within the intervening sequence of a Split-Pleckstrin Homology (sPH) domain (18). Like PH domains, sPH domains share the characteristic 7 β-sandwich structure with a C-terminal α-helix. However, they contain an autonomously folded, intervening module. In the absence of this intervening module, the sPH domain is still capable of folding to its characteristic molecular
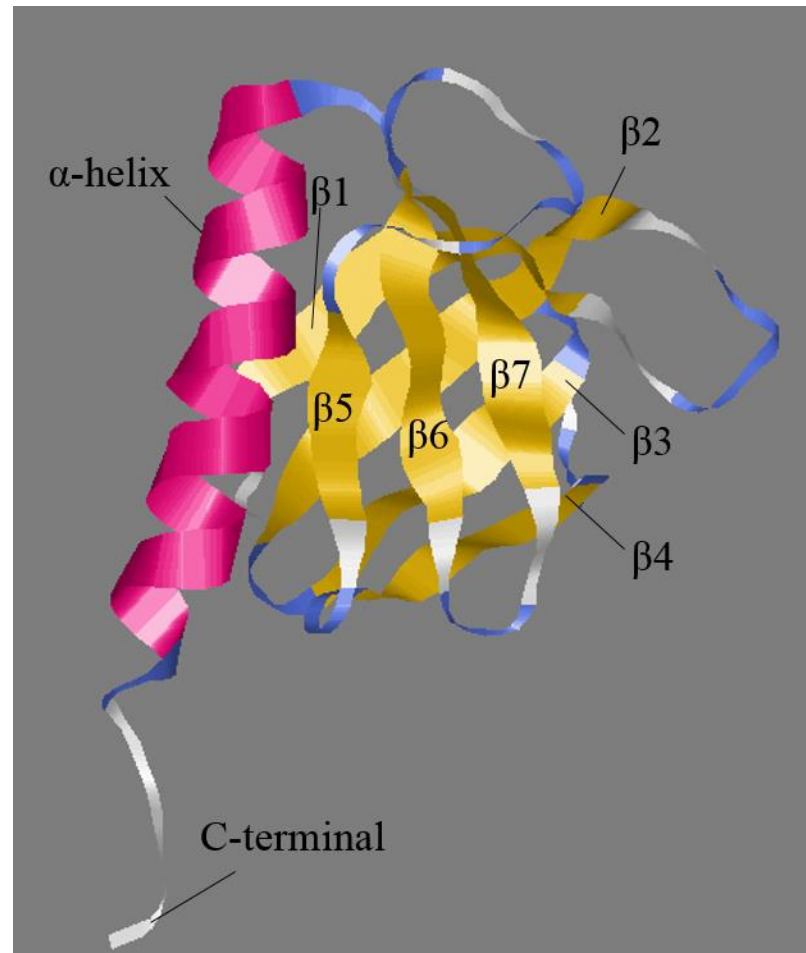
Figure 3: The N-terminal PH domain of Pleckstrin. The consensus characteristics of PH domains: 7 β-sandwich structure (yellow) with a C-terminal α-helix (pink). This figure was created using the protein sequence from PubMed. The model was created using I-Tasser (http://zhanglab.ccmb.med.umich.edu/I-TASSER/) (116–118) and manipulated using RasMol v2.7.5 (Bernstein + Sons, Shirley New York).

structure (119,120). The intervening sequence within the sPH domain of phosphoinositol 3-kinase enhancer (PIKE) has been shown to contain an NLS necessary for its localization to the nucleus. The mechanism by which this NLS affects nuclear import – classical vs non-classical pathway – has not been identified. The NLS, however, has been shown to increase the affinity of the PH domain for membrane binding (18). This may be because basic residues mediate both the binding of PH domains to PtdIns within membranes and interactions between NLSs and importin-α in classical nuclear import. Therefore, PH domains represent a likely location of NLS activity.

1.6   Rho guanine nucleotide exchange factor

Rho guanine nucleotide exchnage factor (RGNEF) is a 180 kDa protein unique in the human proteome for its ability to act both as a guanine exchange factor (GEF) and in its ability to bind RNA (19). Figure 4 shows the domains of RGNEF. Our lab identified RGNEF as a potential ALS-linked protein after confirming its ability to directly bind to and destabilize *NEFL* mRNA (19,22).

In addition to its role alongside TDP-43 as a regulator of *NEFL* mRNA stability, RGNEF shows further evidence of involvement in ALS. ALS-specific mutations have been identified by three independent labs (20,121,122). Figure 5 shows these mutations in *ARHGEF28*, the gene which encodes RGNEF. The deletion of a single nucleotide leading to either a frameshift or a splicing mutation has been observed for ALS cases. The resulting protein is predicted to be either 319 or 259 amino acids long and to lack functional domains including the RNA binding, DH and PH domains (20).

Ubiquitinated aggregates containing RGNEF have also been found in ALS spinal motor neurons. Our lab has shown that RGNEF NCIs can be observed in all variants of ALS except those with a mutation in the gene *superoxide dismutase 1* (*SOD1*). This includes cases of fALS with identified *C9orf72* expanded repeats, TDP-43 mutations, FUS mutations, and fALS cases for
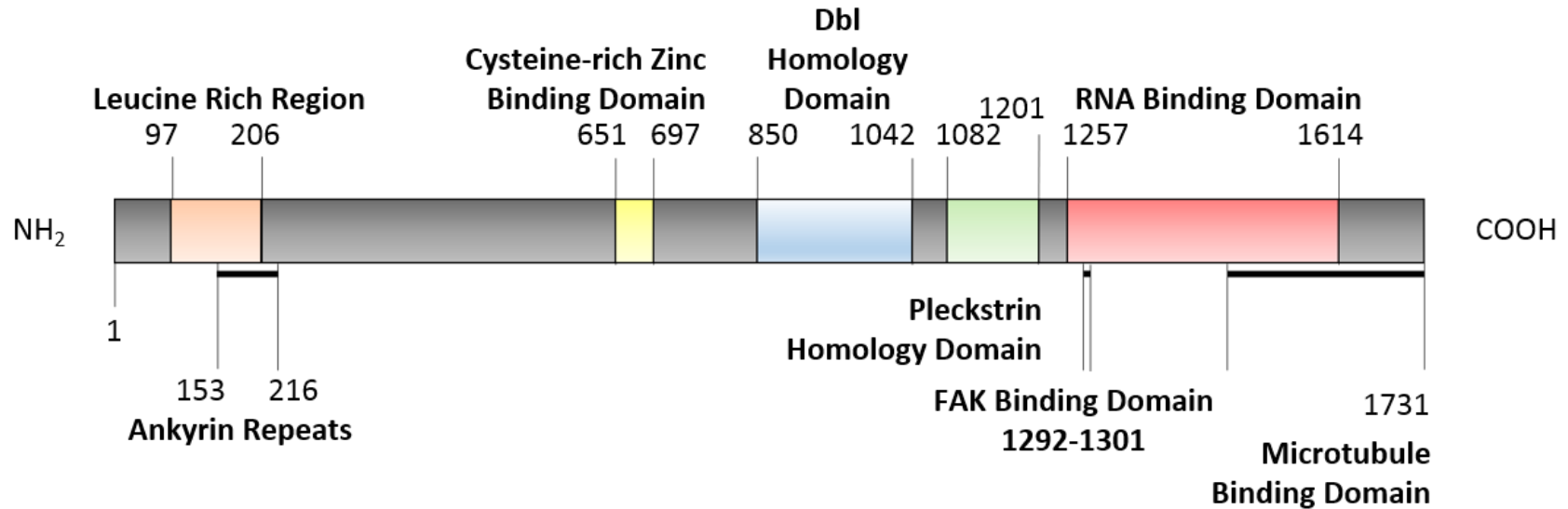
Figure 4: The domains of RGNEF. The leucine rich domain (orange) extends from amino acids 97 – 206. The Ankyrin Repeat domain (black line) partially overlap this region and extends from amino acids 153-216. The Cysteine-rich Zinc binding domain (yellow) extends from amino acids 651-697. The Dbl Homology (DH) domain (blue) extends from amino acids 850-697. The Pleckstrin Homology (PH) domain (green) extends from amino acids 1082-1201. The RNA binding domain (red) extends from amino acids 1257-1614. The RNA binding domain overlaps the FAK binding domain (black line) which extends from amino acids 1292 – 1301. The RNA binding domain partially overlaps the putative microtubule binding domain which extends from amino acids 1731
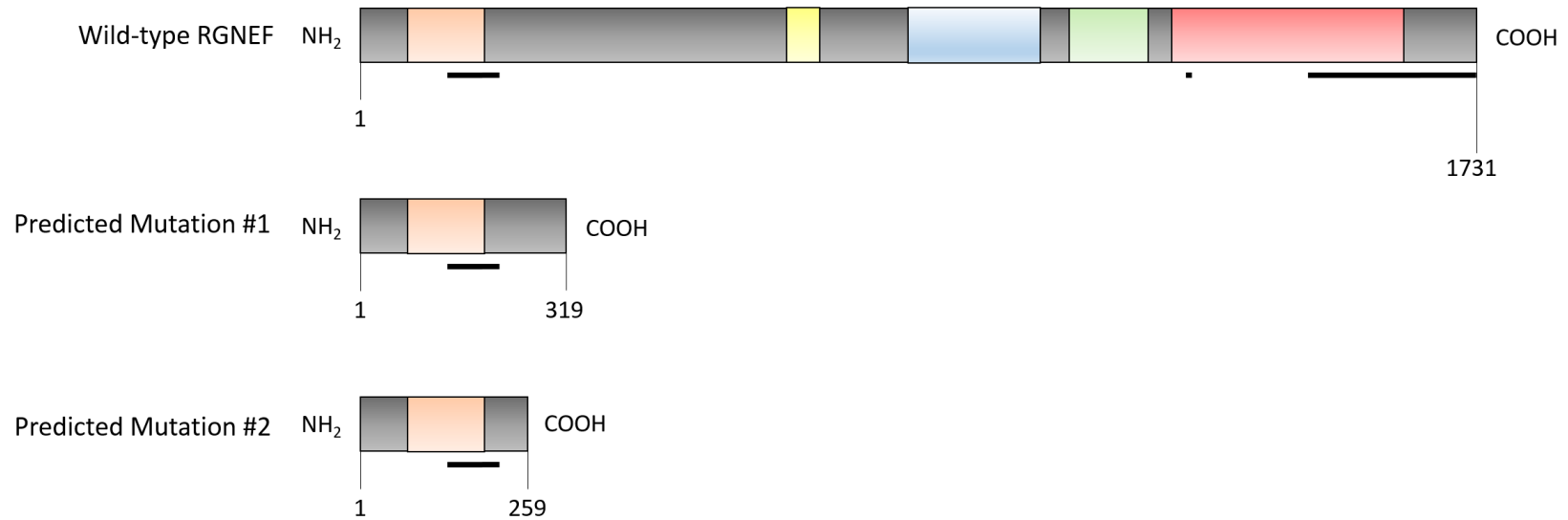
Figure 5: The frameshift mutation identified in ARHGEF28. The mutation observed in ARHGEF28, the gene which encodes for RGNEF, is predicted to cause a frameshift mutation resulting in a premature truncated protein. The resulting protein is predicted to be either 319 or 259 amino acid. Either protein would result in the complete loss of many of the functional domains of RGNEF, including the DH, PH, and RNA binding domains. The resulting proteins would express only the Leucine-Rich region and the Ankryn Repeats.

which the underlying genetic mutation is unknown. RGNEF immunoreactive inclusions are also seen in sALS, some of which harbour pathogenic *C9orf72* expansions in the absence of any family history of ALS. RGNEF also strongly co-localizes with TDP-43 and FUS immunoreactive NCIs in sALS motor neurons (21), further strengthening the relationship between RGNEF and those proteins that undergo nuclear depletion in ALS. Despite the overlap between RGNEF and other ALS-linked proteins, the mechanism by which RGNEF contributes to ALS pathology has not been elucidated. One potential way RGNEF may play a role in disease pathology is by providing cytoprotection to stress. Our lab has previously shown that HEK293T cells transfected with RGNEF showed increased survival under oxidative and osmotic stress conditions (123). Interestingly the data did not support the hypothesis that RhoA activation via the GEF activity may be responsible for this protection.

Despite previous literature having identified RGNEF within the nucleus (19), to date no mechanism for RGNEF nuclear import has been identified. As described in section 1.4, the maximum size for diffusion into the nucleus described in the literature is 110 kDa (89); RGNEF, with a molecular weight of 180 kDa, should not be able to penetrate the nuclear envelope without active transport. Therefore, it is likely that RGNEF contains a NLS. Of the domains in RGNEF, only the pleckstrin homology domain is linked to subcellular localization. Therefore, the PH domain of RGNEF is a likely site for the location of a NLS responsible for its nuclear import.

1.7 Hypothesis

Given the canonical function of PH domains in GEF activity, I hypothesize that the PH domain of RGNEF will play a role in its subcellular localization. Specifically, I hypothesize that it may contain a NLS responsible for RGNEF nuclear import.

Chapter 2

2 Specific Aims & Overview

2.1 Specific Aims

2.1.1 Aim 1: Determine the effects of the PH domain on subcellular localization of RGNEF

My first aim was to determine whether the PH domain of RGNEF contributes to its subcellular localization. To accomplish this I performed a series of polymerase chain reactions (PCRs) using flanking primers, which resulted in the creation of an RGNEF construct lacking the PH domain (RGNEF-ΔPH). The effects of this deletion were analyzed by immunocytochemistry (ICC) with confocal microscopy as well as by cellular fractionation followed by Western blot. All experiments were performed in HEK293T cells.

2.1.2 Aim 2: Determine the mechanism for the apparent PH domain dependent nuclear import of RGNEF using *in silico* techniques

My second aim was to use *in silico* techniques to determine the mechanism by which the PH domain of RGNEF contributes to its nuclear import. An online service, cNLS mapper (http://nls-mapper.iab.keio.ac.jp/cgi-bin/NLS_Mapper_form.cgi) (97,124,125), was used to identify a putative NLS responsible for nuclear import via the classical import pathway. The online modeling software I-Tasser (http://zhanglab.ccmb.med.umich.edu/I-TASSER/) (116–118) was then used to determine the molecular structure of the PH domain and RasMol (Bernstein + Sons, Shirley New York) was used to manipulate the image.

2.1.3 Aim 3: Confirm the functionality of the putative NLS in the PH domain of RGNEF

My third aim was to confirm the existence of the putative NLS within the PH domain of RGNEF. The basic residues of the putative NLS were point-mutated to neutral alanines creating a full length construct lacking the NLS (RGNEF-mNLS). We next created two sets of constructs expressing only the regions of interest. The first used the peGFP-C1 vector. Three constructs were created using this vector expressing the endogenous PH domain (PH-40 kDa), the endogenous NLS (NLS-26 kDa) or the PH domain with point-mutations (mNLS-40 kDa) with N-terminal GFP-tag. A second set of constructs used the pHM830 vector which causes the protein to express with both N-terminal GFP-tag and the addition of LacZ to the C-terminal. The endogenous PH domain (PH-160 kDa) and the PH domain with point-mutations (mNLS-160 kDa) were created.

The subcellular localization of all of these constructs was measured using confocal microscopy. Results obtained using the full length constructs – RGNEF, RGNEF-ΔPH, and RGNEF-mNLS – were confirmed by subcellular fractionation in HEK293T cells and by transfection of SH-SY5Y cells with ICC and confocal microscopy.

2.2   Cell lines and transfections

Two cells lines were used in these experiments: HEK293T and SH-SY5Y cells. The HEK293T cell line was chosen because it expresses the low molecular weight neurofilament mRNA (*NEFL* mRNA) (126) and because it is more amenable to transfection than neuronal cell lines. The SH-SY5Y cell line was chosen because it is a neuroblastoma cell line that can be differentiated to yield a dopaminergic neuron-like phenotype which expresses neuron specific proteins including neurofilaments (127).

Both cell lines were maintained in Dulbecco's modified eagle's medium (DMEM, Gibco, Life Technologies Inc., Burlington, Ontario) supplemented with 10% fetal bovine serum (Gibco, Life

Technologies Inc., Burlington, Ontario) and kept in a water-jacketed 37°C 5% CO$_2$ incubator (Forma Scientific, Thermo Fisher Scientific, Ottawa, Ontario).

Prior to transfection, SH-SY5Y cells were differentiated using retinoic acid to yield a neuron-like phenotype. To do this, non-differentiated cells at approximately 40% confluency were treated with 10 μM retinoic acid (Sigma-Aldrich, Oakville, Ontario) in DMEM media and incubated for 3 days. Because retinoic acid is light sensitive, plates were kept in the dark during this period.

2.3   RGNEF Constructs

In order to elucidate the role of the PH domain, 7 constructs were created. The primers for these processes are listed in Table 2. All mutagenesis PCRs were done using *Pfu* DNA polymerase (Thermo Fisher Scientific, Ottawa, Ontario). Figure 6 shows the 7 constructs created in this project. The full length RGNEF was created previously in our lab. RGNEF-ΔPH was created to study subcellular localization of RGNEF lacking the PH domain; it is a deletion of base pairs 3249-3603 (amino acids 1083-1201) with Kpn1 and Xho1 restriction sites on the 5'- and 3'-terminal, respectively. We then created a full length RGNEF that contained point-mutations at four sites designed to mutate the basic residues (arginine and lysine) of the putative NLS to alanines; this was called RGNEF-mNLS.

Having compared subcellular localization of these full length constructs - RGNEF, RGNEF-ΔPH, and RGNEF-mNLS - we next isolated the effects of only the regions of interest. For this purpose two sets of constructs expressing only specific regions were created. The first set used the peGFP-C1 vector which resulted in N-terminal GFP-tagged proteins. PH-40 kDa and NLS-26 kDA expressed only the PH domain (amino acids 1083-1202) or NLS (amino acids 1100-1128) of endogenous RGNEF, respectively. Their names originate from their predicted molecular mass: 40 kDa and 26 kDa. These used our full length RGNEF as a template. A third construct, mNLS-40 kDa, was created using RGNEF-mNLS as a template and expressed the PH domain of RGNEF-mNLS with point-mutations (amino acids 1083-1202; R1101A, K1103A, K1120A, K1123A).

Table 2: The primers used in PCR to generate the different RGNEF constructs.

Name	Forward or reverse primer	DNA sequence (5' to 3')
RGNEF ΔPH	Forward (1)	ATT<u>GGTACC</u>ATGGAGTTGAGCTGCAGCGAA
	Reverse (1)	GAAGACAAGAGGAAAGCTGAAGCCAGAGTG
	Forward (2)	CCTCTTGTCTTCTTCACTCATCAGTGCCTGCTT
	Reverse (2)	AGA<u>CTCGAG</u>CACCTTGAGGTCTACTTGATGTT
RGNEF mNLS	Forward (1) - R1101A	GTTTACTGGAAAACTGCTACAGGTGCTTTCAAAGATATCCTAGCTCTACT
	Reverse (1) - R1101A	AGTAGAGCTAGGATATCTTTGAAAGCACCTGTAGCAGTTTTCCAGTAAAC
	Forward (2) - K1103A	GAAAACTGCTACAGGTGCTTTCGCAGATATCCTAGCTCTACTTCTA
	Reverse (2) - K1103A	TAGAAGTAGAGCTAGGATATCTGCGAAAGCACCTGTAGCAGTTTTC
	Forward (3) - K1120A	GATGTGCTGCTCTTTTTACAAGAAGCAGACCAGAAATACATCTTTGCAGC
	Reverse (3) - K1120A	GCTGCAAAGATGTATTTCTGGTCTGCTTCTTGTAAAAAGAGCAGCACATC
	Forward (4) - K1123A	CTCTTTTTACAAGAAGCAGACCAGGCATACATCTTTGCAGCCGTTGATCA
	Reverse (4) - K1123A	TGATCAACGGCTGCAAAGATGTATGCCTGGTCTGCTTCTTGTAAAAAGAG
PH-40 kDa / mNLS-40 kDa	Forward	TA<u>CTCGAG</u>ATGAAAGGACTCTGTTATATGATGGC
	Reverse	ACT<u>GGTACC</u>TCAATCAGATTCACTTGTCCTTCC
NLS-26 kDa	Forward	TG<u>CTCGAG</u>ATGGTCGTTTCAAAGATATCCTAG
	Reverse	CACT<u>GGTACC</u>TCATGCAAAGATGTATTTCTGGTCTTTTTCTTG
PH-160 kDa / mNLS-160 kDa	Forward	AG<u>GCTAGC</u>GAAAGGACTCTGTTATATGATG
	Reverse	TAT<u>CTAGA</u>ATCAGATTCACTTGTCCTTCCC

*Restriction enzyme sequences are underlined. XhoI = CTCGAG; KpnI = GGTACC; NheI = GCTAGC; XbaI= TCTAGA

Full length RGNEF

NH₂ | KpnI ... XhoI | COOH

RGNEF-ΔPH

NH₂ | KpnI ... XhoI | COOH

RGNEF-mNLS

NH₂ | KpnI ... XhoI | COOH
R1101A K1120A
K1103A K1123A

PH-40 kDa

NH₂ | ... XhoI ... KpnI ... | COOH
GFP (238 amino acids)

NLS-26 kDa

NH₂ | ... XhoI KpnI ... | COOH
GFP (238 amino acids)

mNLS-40 kDa

NH₂ | ... XhoI ... KpnI ... | COOH
GFP (238 amino acids)
R1101A K1120A
K1103A K1123A

PH-160 kDa

NH₂ | ... NheI ... XbaI ... | COOH
GFP (238 amino acids)
LacZ (1016 amino acids)

mNLS-160 kDa

NH₂ | ... NheI ... XbaI ... | COOH
GFP (238 amino acids)
R1101A K1120A
K1103A K1123A
LacZ (1016 amino acids)

Figure 6: Comparison of the different constructs of RGNEF. Full length RGNEF was previously created in our lab. RGNEF-ΔPH and RGNEF-mNLS were ligated into the pcDNA3.1A(+)myc/his A plasmid resulting in the expressed protein containing a myc tag on their C-terminal. PH-40 kDa, NLS-26 kDa, and mNLS-40 kDa were all ligated into the eGFP-C1 vector resulting in the expressed protein containing GFP on their N-terminal. PH-160 kDa and mPH-160 kDa were ligated into the pHM830 vector resulting in the expressed protein containing GFP on their N-terminal and LacZ protein on their C-terminal.

RGNEF-ΔPH (deletion of amino acids 1082-1201; this construct lacks the PH domain)

RGNEF-mNLS (mutation of residue 1101 from an arginine to an alanine and of residues 1103, 1120 and 1123 from lysines to alanines; mutations in this construct are predicted to eliminate the putative NLS, thereby reducing import into the nucleus)

PH-40 kDa (expression of only the PH domain – residues 1082-1201 – with N-terminal GFP; this construct is predicted to localize to the nucleus)

NLS-26 kDa (expression of only the putative NLS – residues 1100-1128 – with N-terminal GFP; this construct is predicted to localize to the nucleus)

mPH-40 kDa (expression of only the mutated PH domain; residues 1082-1201 of the RGNEF-mNLS construct; contains the four mutations R1101A, K1103A, K1120A, and K1123A; contains N-terminal GFP and C-terminal LacZ; predicted to show reduced levels of nuclear localization compared with PH-40 kDa)

PH-160 kDa (expression of only the PH domain – residues 1082-1201 – with N-terminal GFP and C-terminal LacZ; this construct is predicted to localize to the nucleus)

mPH-160 kDa (expression of only the mutated PH domain; residues 1082-1201 of the RGNEF-mNLS construct; contains the four mutations R1101A, K1103A, K1120A, and K1123A; contains N-terminal GFP and C-terminal LacZ; predicted to show reduced levels of nuclear localization compared with PH-40 kDa)

The second set of constructs designed to isolate the effects of certain regions utilized the pHM830 vector (Addgene, Cambridge, Massachusetts) which encodes for an N-terminal GFP-tag and C-terminal addition of the LacZ protein. I designed these constructs but due to time constraints their synthesis was carried out by Dr. Cristian Droppelmann, a post-doctoral research associate in our lab. Similar to before, constructs expressing the PH domains of endogenous RGNEF and RGNEF-mNLS were created: PH-160 kDa and mNLS-160 kDa. With the addition of both the N-terminal GFP-tag and the C-terminal addition of LacZ protein the total molecular weight of the proteins was predicted to be 160 kDa.

2.3.1 PH domain deletion (RGNEF-ΔPH)

In order to determine the role of the PH domain on RGNEF localization, a construct lacking the domain was created. Given the size of the domain (357bp) and its location towards the centre of the gene, it was necessary to perform site-directed mutagenesis by primer extension. This process was first described by Ho et al. (128). In this process (see Figure 7) two independent PCR reactions using flanking internal primers produce fragments encoding the 5' and 3' outside of the PH domain (see top two panels of Figure 7). The flanking internal primers yield constructs with complementary overlap regions. A third PCR reaction is performed in which the two PCR products are mixed and their complementary regions hybridize, allowing one construct to act as the template for the other. The product of this PCR reaction is the desired construct: RGNEF lacking the PH domain. In the final PCR reaction, the two external primers are added to the product in order to amplify the yield. In my protocol, the reaction of PCR 3 underwent 10 cycles of extension, the external primers were added directly to the sample, and 40 more cycles occurred. Table 3 shows the program conditions for all PCR protocols and Table 2 shows the list of primer used. Note that following PCR reactions 1, 2 and 4 it was necessary to purify the product by gel extraction using a NucleoSpin Gel Extraction Kit (Macherey-Nagel Inc., Bethlehem Pennsylvania, USA) and DNA concentration were quantified using a Nanodrop Spectrophotometer (Thermo Fisher Scientific, Waltham, Massachusetts USA).

PCR 1: N-Terminal Fragment

PCR 2: C-Terminal Fragment

PCR 3: Final Construct

PCR 4: Amplification
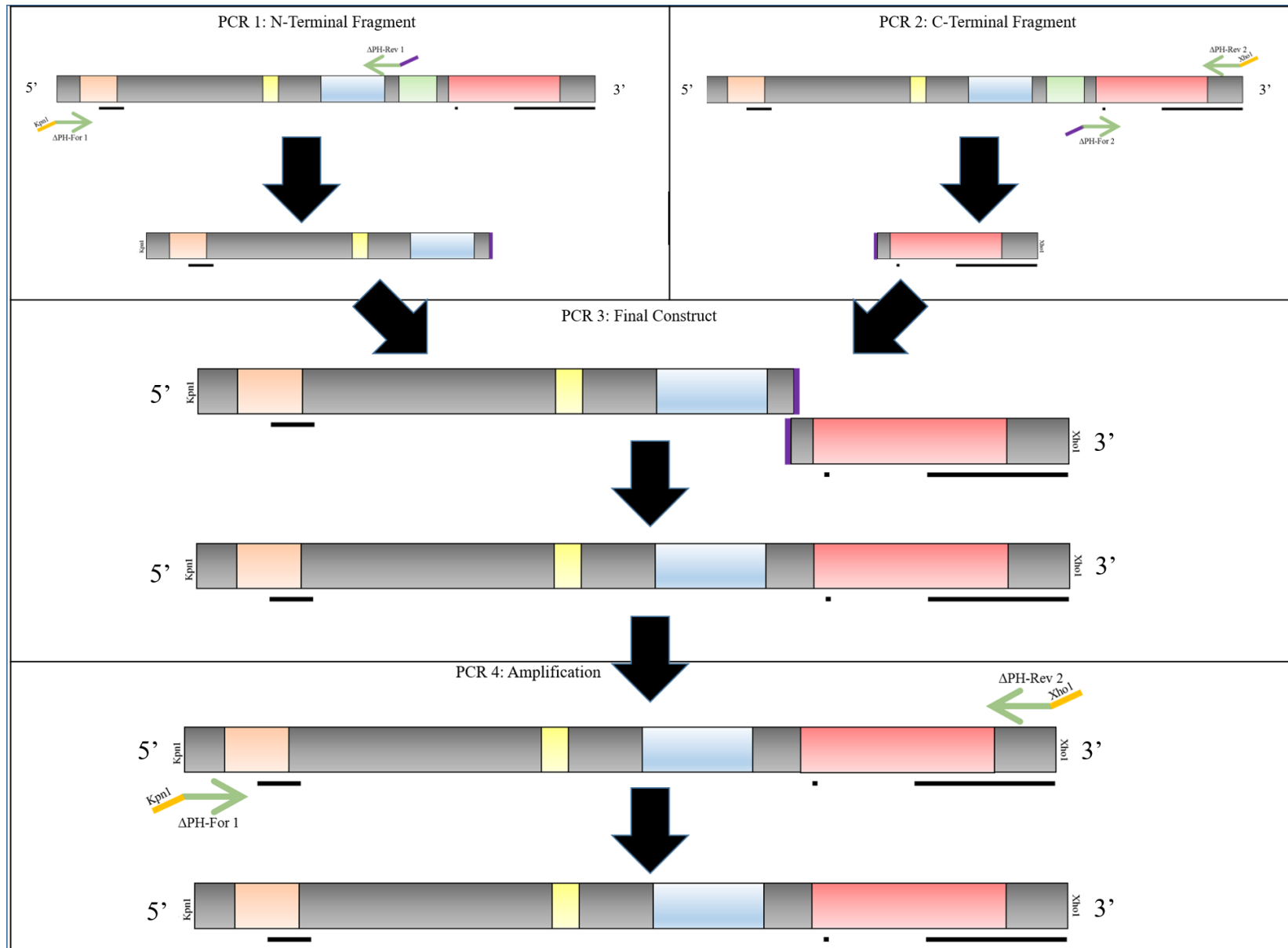
Figure 7: Flanking PCR. The mechanism for performing a flanking PCR. Green arrows represent primers. Yellow tails represent the added restriction sites (Kpn1 and Xho1). Purple tails represent the complementary shared sequence. The initial two PCR reactions use primers which result in complementary sequences. In the third PCR reaction, the final desired construct is created (in this case RGNEF-ΔPH) by adding the N- and C-terminal fragments in the first two PCRs together. Pfu DNA polymerase binds the complementary region and used the opposite fragment as a template for synthesis. In PCR 4, external primers are added, allowing for amplification of the desired product.

All reactions were carried out using *Pfu* DNA polymerase (Thermo Fisher Scientific, Waltham, Massachusetts USA). The manufacturer's protocol was followed, though dimethyl sulfoxide (DMSO; VWR International, Mississauga, Ontario) was added to a final concentration of 5%; this was done to reduce the non-specific amplification. The external primers encoded for the addition of the Kpn1 and Xho1 restriction sites to the 5' and 3' ends, respectively.

Following the final PCR reaction the product was purified by gel extraction and the insert was prepared for ligation into the pGEM-T Easy backbone using the pGEM –T Easy Vector System (Promega Corporation, Madison, Wisconsin, USA). The pGEM-T Easy is convenient for easy ligation and amplification of the insert. As described in the protocol provided by the manufacturer, the pGEM-T vector comes with 3'T-overhangs at the insertion site for simple AT Cloning. For this reason our PCR product was first a-tailed using Taq DNA polymerase. Ligation occurred as described in the protocol with the maximum volume of PCR product (3 µl) added to the reaction.

The product of the ligation was used to transform chemically competent DH5α Escherichia coli (*E. coli*, Invitrogen, Life Technologies Inc., Burlington, Ontario). Bacteria were plated onto an agar plate containing the selective antibiotic ampicillin and incubated at $37^{O}C$ overnight. Colonies were selected and grown in LB Broth with 0.1 μg/μl ampicillin at $37^{o}C$ for 15 hours. DNA was extracted by Miniprep kit (Invitrogen, Life Technologies Inc., Burlington, Ontario) for subsequent cloning. Colonies were screened to contain the insert and plasmid first by 1% agar gel and then by sequencing at the London Regional Genomics Centre (London, Ontario).

Given the utility of its affinity tag system, appropriate DNA was then ligated into the pcDNA 3.1(+)/myc-His A backbone, which when expressed adds a myc-tag to the C-terminal end of the protein. The insert was liberated from the pGEM vector using the Kpn1 and Xho1 restrictions sites added to the construct by our external primers. The pcDNA 3.1(+)/myc-His A was likewise

Table 3: The conditions for Flanking Primer PCR

	Stage 1	1 Cycle
PCR 1: N-Terminal Fragment & PCR 2: C-Terminal Fragment	95ºC	3:00 min
	Stage 2	**42 Cycles**
	95ºC	0:45 min
	62ºC	0:45 min
	72ºC	6:30 min
	Stage 3	**1 Cycle**
	72ºC	20:00 min
	Stage 4	**1 Cycle**
	4ºC	∞
PCR 3: Final Construct	**Stage 1**	**1 Cycle**
	95ºC	3:00 min
	Stage 2	**10 Cycles**
	95ºC	0:45 min
	58ºC	0:45 min
	72ºC	9:45 min
	Add external primers	
PCR 4: Amplification	**Stage 3**	**40 Cycles**
	95ºC	0:45 min
	60ºC	0:45 min
	72ºC	9:45 min
	Stage 4	**1 Cycle**
	72ºC	20:00 min
	Stage 5	**1 Cycle**
	4ºC	∞

cut within the multiple cloning site. Both Kpn1 and Xho1 were purchased from Invitrogen (Invitrogen, Life Technologies Inc., Burlington, Ontario). The pcDNA 3.1(+)/myc-His A was then dephosphorylated using shrimp alkaline phosphatase. The insert and backbone were incubated with T4 DNA Ligase (Promega Corporation, Madison, Wisconsin, USA) overnight at room temperature.

As previously described, the ligation product was used to transform chemically competent DH5α *E. coli* (Invitrogen, Life Technologies Inc., Burlington, Ontario). Bacteria were plated on ampicillin containing agar plates and grown overnight. Colonies were selected, grown in LB broth with 0.1 μg/μl ampicillin overnight, and a Miniprep kit (Invitrogen, Life Technologies Inc., Burlington, Ontario) was used to extract DNA. The DNA was screened both by 1% agar gel and then by DNA sequencing. The construct was then used to transfect of mammalian cell lines (See 2.3 Transfection).

2.2.2 NLS point-mutations (RGNEF-mNLS)

Having identified four residues likely to act as the putative NLS, we performed site-directed mutagenesis to point-mutate these basic residues to neutral alanine residues. The primers for this are listed in Table 2. Four sets of primers and four successive PCR reactions were necessary to accomplish this task. The reactions were performed in sequence: the product of the first PCR became the template for the second reaction and so on. The first reaction mutated arginine residue at 1101 to an alanine. The remaining mutations changed lysine residues to alanine residues and occurred at sites 1103, 1120, and 1123.

All four reactions utilized the QuickChange Lightning Multi Site-Directed Mutagenesis Kit (Agilent Technologies, Santa Clara, California). All four PCR were performed as described in the protocol provided in the QuickChange Kit. Following each PCR reaction, XL10-Gold Ultracompetent *E. coli* (Agilent Technologies, Santa Clara, California) were transformed using the PCR product as per the protocol provided in the QuickChange Kit. *E. coli* cells were plated

on agar plates containing the selective antibiotic ampicillin. Plates were incubated at 37°C overnight. Colonies were selected from these plates, grown in LB broth containing 0.1 μg/μl ampicillin overnight, purified by Miniprep kit (Invitrogen, Life Technologies Inc., Burlington, Ontario) and the DNA was screened by 1% agarose gel and DNA sequencing at the London Regional Genomics Centre (London, Ontario). Note that because site-directed mutagenesis occurs while the coding sequence of the gene is still within the circular plasmid - pcDNA 3.1(+)/myc-His A in this case – it was not necessary to ligate the PCR product into the plasmid prior to transformation as it was in the PH deletion protocol.

2.3.3 PH-, NLS- and mNLS-only constructs in peGFP-C1 (PH-40 kDa, NLS-26 kDa, & mNLS-40 kDa)

In order to isolate the localization effects of the PH domain without the influence of the remainder of the protein, three constructs were created: one composed of only the PH domain (amino acids 1082 – 1201), one composed of only the NLS sequence (amino acids 1100 -1128), and one composed of only the PH domain of the RGNEF-mNLS construct created in section 2.2.2 (amino acids 1082 – 1201; R1101A, K1103A, K1120A, K1123A). The primers for these are listed in Table 2. Notice in Figure 6 that, similar to those for the ΔPH construct, the primers for these constructs include the addition of an Xho1 and Kpn1 restriction site, though at opposite ends.

Following the PCRs, the products were purified by gel extraction using NucleoSpin Gel Extraction Kit (Macherey-Nagel Inc., Bethlehem Pennsylvania, USA) and concentration was determined using a Nanodrop Spectrophotometer (Thermo Fisher Scientific, Waltham, Massachusetts USA). Xho1 and Kpn1 (Invitrogen, Life Technologies Inc., Burlington, Ontario) restriction enzymes were used to digest the product of these PCR reactions. The peGFP-C1 backbone was also cut with Kpn1 and Xho1 restriction enzymes and dephosphorylated using shrimp alkaline phosphatase. Each construct was independently ligated into the peGFP-C1 vector using T4 Ligase (Promega Corporation, Madison, Wisconsin, USA). Following ligation, DH5α *E. coli* (Invitrogen, Life Technologies Inc., Burlington, Ontario) were transformed with the

respective products. Transformed cells were plated on agar plates with the selective antibiotic kanamycin. Plates were incubated at 37°C overnight. Colonies were selected and were grown overnight in LB broth containing 0.1 μg/μl kanamycin on an orbital shaker at 300 rpm at 37°C. A Miniprep kit (Invitrogen, Life Technologies Inc., Burlington, Ontario) was used to extract DNA from E. *Coli*. The DNA was then confirmed first by 1% agarose gel and by DNA sequencing London Regional Genomics Centre (London, Ontario).

2.3.4 PH- and mNLS-only constructs in pHM830 (PH-160 kDa & mNLS-160 kDa)

Because nuclear localization is dependent on molecular weight, we next created constructs with molecular weight of 160 kDa using the pHM830 vector (Addgene, Cambridge, Massachusetts). Due to time constraints, I designed these constructs though Dr. Cristian Droppelmann, a post-doctoral research associate in our lab, carried out the experiments. The primers for these constructs are listed in Table 2. These primers encode for the addition of NheI and XbaI sites to the 5' and 3' ends respectively.

Similar to in 2.3.3 after PCR, the products were purified by gel extraction using NucleoSpin Gel Extraction Kit (Macherey-Nagel Inc., Bethlehem Pennsylvania, USA) and concentration was determined using a Nanodrop Spectrophotometer (Thermo Fisher Scientific, Waltham, Massachusetts USA). NheI and XbaI (Invitrogen, Life Technologies Inc., Burlington, Ontario) restriction enzymes were used to digest the product of these PCR reactions. The pHM830 backbone was also cut with NheI and XbaI restriction enzymes and dephosphorylated using shrimp alkaline phosphatase. Each construct was independently ligated into the pMH830 vector using T4 Ligase (Promega Corporation, Madison, Wisconsin, USA). Following ligation, DH5α *E. coli* (Invitrogen, Life Technologies Inc., Burlington, Ontario) were transformed with the respective products. Transformed cells were plated on agar plates with the selective antibiotic ampicillin. Plates were incubated at 37°C overnight. Colonies were selected and were grown overnight in LB broth containing 0.1 μg/μl ampicillin on an orbital shaker at 300 rpm at 37°C. A Miniprep kit (Invitrogen, Life Technologies Inc., Burlington, Ontario) was used to extract DNA

from E. *Coli*. The DNA was then confirmed first by 1% agarose gel and by DNA sequencing London Regional Genomics Centre (London, Ontario).

2.4   Seeding and transfection of mammalian cell lines

Both HEK293T cells and SY5Y cells were used for these experiments. All cells used in this experiment were maintained in a water-jacketed 37^OC 5% CO_2 incubator (Forma Scientific, Thermo Fisher Scientific, Ottawa, Ontario).

For immunocytochemistry (ICC), a coverslip was placed at the bottom of a 6-well plate. The coverslip was coated with 1X attachment factor (Gibco, Life Technologies Inc., Burlington, Ontario) to increase cell adhesion. HEK293T cells were seeded at 230 000 cells per well. Cells were allowed to incubate one day until they reached approximately 70% confluency. They were then transfected using Lipofectamine 2000 (Thermo Fisher Scientific, Ottawa, Ontario) using 2 µg of DNA and 5 µl of Lipofectamine 2000 per well. As per the protocol provided, cells were incubated with Lipofectamine and DNA for 3 hours. Cells were incubated overnight in DMEM media described above.

The HEK293T cell line was also used for the purpose of fractionation. The bottom of a 150mm plate was coated with 1X attachment factor (Gibco, Life Technologies Inc., Burlington, Ontario). Cells were seeded at 2 200 000 per 150 mm plate and 26 µg of DNA and 65 µl of Lipofectamine 2000 were used per plate. All other conditions were the same.

The SH-SY5Y cell line was used for ICC and confocal microscopy. Again, coverslips were coated with 1X attachment factor (Gibco, Life Technologies Inc., Burlington, Ontario) and placed in the bottom of a 6-well plate. As described in section 2.2, SH-SY5Y cells were seeded at approximately 40% confluency and treated with 10 µM retinoic acid for 3 days prior to transfection. On the day of transfection, SH-SY5Y cells were at approximately 80% confluency.

2.5 µg of DNA and 7.5 µl of Lipofectamine 2000 were added per well. Cells were incubated with Lipofectamine and DNA for 3 hours. Afterwards cells were incubated for 48 hours in DMEM media with 10 µM retinoic acid.

2.5   Immunocytochemistry (ICC) and confocal microscopy

Following transfection, immunocytochemistry (ICC) was performed to visualize protein localization. Coverslips were fixed in 4% paraformaldehyde in 1X PBS. Coverslips were then washed with 1X PBS three times and permeabilized using 0.2% Triton X-100 in 1X PBS for 10 minutes. Coverslips were washed once and then incubated in 50 mM Ammonium Chloride in 1X PBS for 30 minutes in order to quench aldehyde groups and reduce background staining. Non-specific antibody interactions were reduced by incubating cover slips for 60 minutes at room temperature in blocking solution: 8% bovine serum albumin (BSA; Fisher Scientific Company, Ottawa, Ontario) in 1X PBS. Primary antibodies were diluted in blocking solution as described in Table 4. Coverslips were incubated in primary antibody for 90 minutes at room temperature in a humidifying chamber. Following incubation, coverslips were washed twice in blocking solution. Fluorescent AlexaFluor® antibodies (Life Technologies), shown in Table 4, were diluted in blocking solution and coverslips were incubated for 60 minutes at room temperature in a humidifying chamber. In order to visualize nuclei, coverslips with HEK293T cells were then incubated in 1 µg/mL Hoechst stain in PBS for 10 minutes. Coverslips with SH-SY5Y cells were found to stain better with DAPI stain and so were incubated in 1 µg/mL DAPI stain in PBS for 7 minutes. Coverslips were washed, first with PBS and then with deionized water, and left to dry overnight. Once dry, cover slips were mounted to frosted glass microscope slides using a fluorescent mounting media (Dako Canada Inc., Burlington, Ontario).

All cover slips in Aim 1 were examined using a multi-photon confocal microscope (LSM 510 META; Carl Zeiss Canada Ltd., Toronto, ON) and ZEN software (Carl Zeiss Canada Ltd., Toronto, ON). All coverslips in Aim 3 were examined using a Confocal Laser Scanning Platform Microscope (SP8; Leica Microsystems Inc, Richmond Hill, ON) and LAS X software (Leica

Table 4: The antibodies used in immunocytochemistry for confocal microscopy

Name	Species	Dilution	Manufacturer	Secondary Antibody
c-Myc (monoclonal)	Mouse	1:250	Cedarlane (Burlington, Ontario)	Goat α- Mouse, 488 nm absorbance, Life Technologies (titre: 1:800)
β III Tubulin	Rabbit	1:60	Sigma-Aldrich (Oakville, Ontario).	Goat α-Rabbit, 546 nm absorbance, Life Technologies (titre: 1:800)

Microsystems Inc, Richmond Hill, ON). The optical settings used for confocal microscopy in aim 3 are listed in Appendix A. Both ZEN and Las X software were used to generate intensity profiles which aided in cell counting for nuclear localization.

2.6   Fractionation protocol

Figure 8 shows the fractionation protocol used to isolate nuclear from cytoplasmic cellular fractions (129). Cells were seeded on a 150 mm plate at 2 200 000, allowed to incubate overnight, and were transfected as described in section 2.4. Twenty-four hours after transfection plates were fractionated. Cells were washed once with 1X PBS and then semi-permeabilized using 42 µg/ml digitonin (Sigma-Aldrich, Oakville, Ontario) dissolved in 1X NEH buffer. Cells were incubated for 10 minutes at 4°C on bench top rocker (VWR International, Mississauga, Ontario). The digitonin solution was collected and stored as the "cytoplasmic fraction". Cells were again washed with 1X PBS.

To each plate 500 µl of a low salt buffer was added, the surface of the plate was scraped using a cell scraper, and the contents of the plate were collected and transferred to a Dounce homogenizer (Corning Inc., Corning, New York, USA) where they were incubated on ice for 5 minutes. The low salt buffer contained 20 mM Hepes and 0.2 mM EDTA dissolved in 1X NEH buffer. In order to prevent protein degradation, two protease inhibitor cocktails were added. The first was the commercially available "cOmplete protease inhibitor" (Hoffman-La Roche Ltd., Mississauga, Ontario) dissolved in 1X NEH and diluted to 1X concentration. The second contained 50 mM PMSF and 0.1 mg/ml TLCK dissolved in isopropanol.

Following incubation on ice, cells were homogenized by passing 50 strokes through tight-fitted Dounce homogenizer. To the homogenate 500 µl of a high salt buffer was added and then passed an additional 50 strokes. The high salt buffer contained 1 mM DTT, 300 mM NaCl, 200 mM

Digitonin Solution
42 μg/ml digitonin, 2 mM DTT, 2 mM MgCl$_2$ in 1 X NEH buffer

Membrane semi-permeablization

Media
Cytosolic Proteins

Low Salt Homogenization Buffer
20 mM Hepes-NaOH (pH 7.4), 0.2 mM EDTA

Apply Low Salt Buffer and scrape cells

5 Minute incubation on ice

50 Strokes with homogenizer

High Salt Homogenization Buffer
300 mM NaCl, 200 mM Hepes-NaOH (pH 7.4), 0.2 mM EDTA, 1 mM DTT

Add equal volume High Salt Buffer
50 Strokes with homogenizer

Supernatant
Nucleosolic Proteins

Low speed centrifuge
1,000g for 10 minutes

Pellet
Membrane Bound Proteins

Figure 8: Fractionation protocol. Transfected HEK293T cells are first washed with 1X PBS. Membranes of HEK293T cells are then semi-permeabilized using a solution containing 42µg/ml digitonin (Sigma-Aldrich, Oakville, Ontario) dissolved in 1X NEH buffer. Cells are incubated for 10 minutes at 4°C in this solution. The digitonin solution is then collected and saved as the Cytoplasmic Fraction. Cells are washed once with 1X PBS. A Low Salt Homogenization Buffer is then added to the plate, the plate is scraped, the contents are gathered, and the sample is incubated on ice in a Dounce homogenizer (Corning Inc., Corning, New York, USA). The sample is then passed with 50 strokes using the tight fitting pestle. An equal volume of High Salt Homogenization Buffer is added and an additional 50 strokes are performed. Finally, the sample is transferred to a centrifuge tube and centrifuged at 1000g for 10 minutes. The pellet is saved as the Membrane Bound Proteins. The supernatant is saved as the Nucleosolic Proteins.

Hepes, and 0.2 mM EDTA dissolved in 1X NEH as well as the two protease inhibitor cocktails described above.

Following homogenization, the sample was collected and centrifuged at 1,000 g for 10 minutes at 4^OC. The resulting supernatant was collected and saved as the "nucleosolic fraction".

Prior to analysis by Western blot, cytosolic fractions were concentrated using Microsep microconcentrators (Pall Corporation, Port Washington, New York, USA) by centrifugation at 3000 g for 5 hours at 4^OC. The protein concentration of all samples was determined using Bio-Rad Dc protein assay according to the manufacturer's protocol and colorimetric analysis was performed using a microplate reader (Microplate Reader Benchmark; Bio-Rad Laboratories Canada Ltd., Mississauga, Ontario) reading at 655 nm.

2.7   Western blot

Western blots were performed to study the expression of target proteins in samples. Polyacrylamide gels were made at 10% and all samples were loaded at 50 μg per well based on protein concentrations determined by Dc assay. A loading buffer containing 62.5 mM Tris base (pH to 6.8), 2% SDS, 10% glycerol, 0.006% Bromophenol blue and 50% β-mercaptoethanol diluted in water was prepared. Gels were run at a constant 100V for 2.5 hours. The running buffer contained 50 mM Tris base, 200 mM glycine, and 2 mM SDS diluted in deionized water. Gels were transferred to nitrocellulose membrane at a constant 300 mA for 90 minutes. Transfer buffer was composed of 20% methanol dissolved in the above described running buffer. All equipment used for running and transferring gels was manufactured by Bio-Rad (Bio-Rad Laboratories Canada Ltd., Mississauga, Ontario). Nitrocellulose was kept at 4^OC overnight in washing solution. Washing solution was composed of 50 mM Tris base, 100 mM NaCl and 1% Tween20 with pH 7.4.

In order to reduce non-specific binding, nitrocellulose membranes were incubated in 5% skim milk blocking solution in washing buffer at room temperature for 1 hour. Primary antibodies were diluted in blocking solution and nitrocellulose membranes were incubated at room temperature for 90 minutes on an orbital shaker. The nitrocellulose membrane was then washed 3 times using 5% milk blocking solution. Secondary antibody was diluted in 5% milk blocking solution. The membrane was incubated in secondary antibody at room temperature for 60 minutes. Table 5 lists the primary and secondary antibodies used for Western blots.

After secondary antibody incubation, the nitrocellulose membrane was washed 3 times with washing buffer. Each wash occurred at room temperature on orbital shaker for 10 minutes. Western Lighting ECL reagents (PerkingElmer Woodbridge, Ontario) were used to generate chemiluminescence signal. Nitrocellulose blots were incubated at room temperature in ECL reagents for 2 minutes. Chemiluminescence was visualized using a Gel Doc system using Image Lab 5.2 software (Bio-Rad Laboratories Canada Ltd., Mississauga, Ontario). Relative band intensity was determined by densitometry using ImageJ (version 1.48v; National Institutes of Health, USA).

2.8 *In silico* analysis

2.8.1 Molecular modeling

All molecular modeling was done using I-Tasser online (http://zhanglab.ccmb.med.umich.edu/I-TASSER/). I-Tasser predicts protein structure using modeling by iterative threading assembly simulation (116–118). The 3D model provided by I-Tasser was then manipulated using RasMol v2.7.5 (Bernstein + Sons, Shirley New York).

Table 5: The antibodies used for Western blots

Name	Species	Dilution	Manufacturer	Secondary Antibody
c-Myc (monoclonal)	Mouse	1:4000	Cedarlane (Burlington, Ontario)	Goat α-Mouse, linked to horseradish peroxidase (titre: 1:5000) (Bio-Rad)
GAPDH	Rabbit	1:2000	Abcam (Toronto, Ontario)	Swine α-Rabbit linked to horseradish peroxidase (titre: 1:2500) (DAKO)
Lamin A/C	Goat	1:500	Santa Cruz (Dallas, Texas)	Mouse α-Goat, linked to horseradish peroxidase (titre: 1:500) (Santa Cruz)
Flotillin-1	Rabbit	1:500	Abcam (Toronto, Ontario)	Swine α-Rabbit linked to horseradish peroxidase (titre: 1:2500) (DAKO)

2.8.2 Identification of putative classical NLS

cNLS Mapper (http://nls-mapper.iab.keio.ac.jp/cgi-bin/NLS_Mapper_form.cgi), an online
service for the detection of importin-α dependent nuclear localization signals was used to analyze
the PH domain of RGNEF for possible NLSs. cNLS mapper is based on the results of an activity
based profile for different importin-α dependent NLSs created by systematic amino acid
replacement analysis in budding yeast (97,124,125).

2.8.3 Statistical analysis

All statistical analyses, including bar graphs, were performed or generated using

GraphPad Prism 6 (GraphPad Software, Inc., La Jolla, California, USA).

Chapter 3

3 Experimental results

3.1 Aim 1: Determine the effects of the PH domain on subcellular localization of RGNEF

3.1.1 The PH domain of RGNEF has the molecular shape consistent with PH domains

It was first necessary to confirm that the PH domain of RGNEF contained the 7 β-sandwich structure with C-terminal α-helix characteristic of PH domains. Figure 9 shows a side by side comparison of the N-terminal PH domain of Pleckstrin – the protein in which the PH domain was first identified - next to the PH domain of RGNEF (amino acids 1082-1201). The PH domain of RGNEF does show 7 β-sheets with a C-terminal α-helix. The β-sheets and the α-helix are of approximately the same size and in the same orientation between the two models. This is consistent with past findings in our lab that showed RGNEF acts as a GEF for RhoA as PH domains are a necessary component of GEF activity (17,19)

3.1.2 The transfection efficiency is not significantly different between RGNEF and RGNEF-ΔPH constructs in HEK293T cells

Transfection efficiency was determined by cell counting. Transfected HEK293T cells were stained by ICC and the percentage of cells expressing the myc tagged construct was determined by confocal microscopy. There was no significant difference in number of cells expressing RGNEF-ΔPH from full length RGNEF (Fig. 10; 90% ± 3% vs 92% ± 2%, respectively; p = 0.438) as measured by a two-tailed independent sample T-test.

3.1.3 RGNEF-ΔPH shows differential localization to the nucleus

Both fractionation and ICC show RGNEF-ΔPH was localized to the nucleus to a lower proportion than full length RGNEF; though differential levels of localization to the plasma membrane could not be
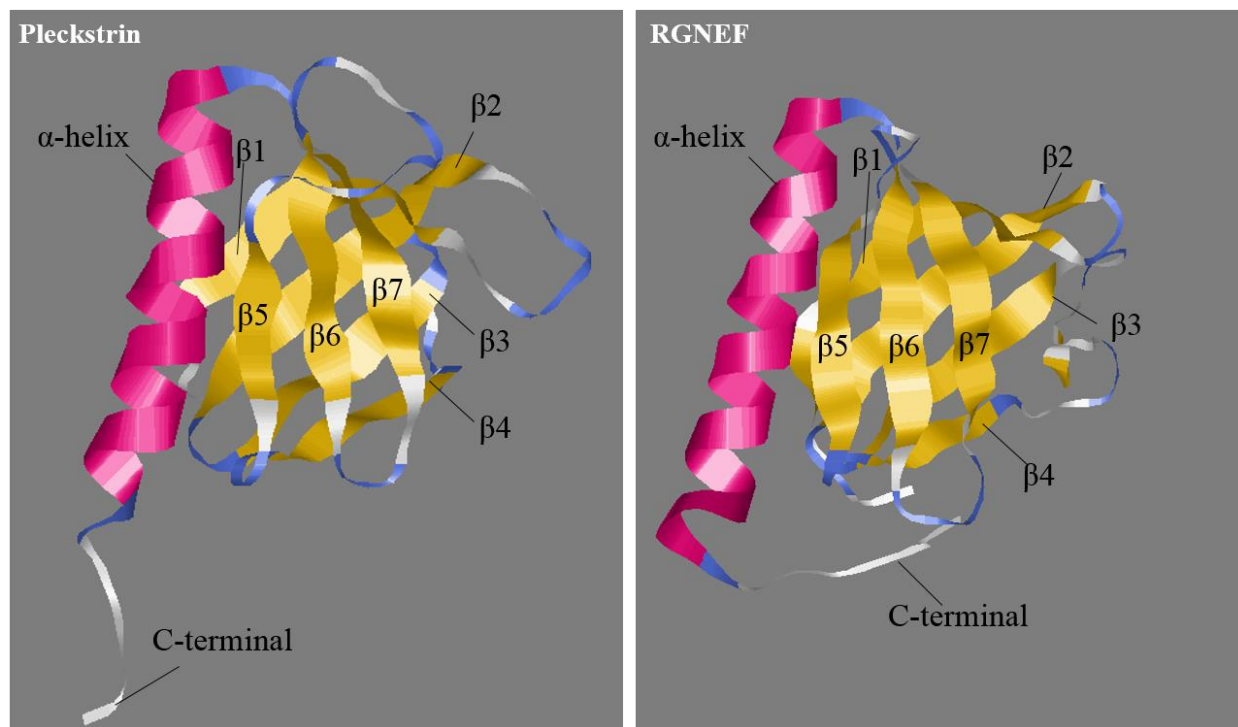
Figure 8: Comparison of the molecular structures of the N-terminal Pleckstrin and RGNEF PH domains. Molecular modeling of the PH domains of Pleckstrin and RGNEF. The PH domain of RGNEF shares the molecular shape used to define PH domains. This includes a 7 β-sandwich structure with a C-terminal α-helix. The model was created using I-Tasser (http://zhanglab.ccmb.med.umich.edu/I-TASSER/) (116–118) and manipulated using RasMol v2.7.5 (Bernstein + Sons, Shirley New York). The amino acid sequence of Pleckstrin was obtained from PubMed.
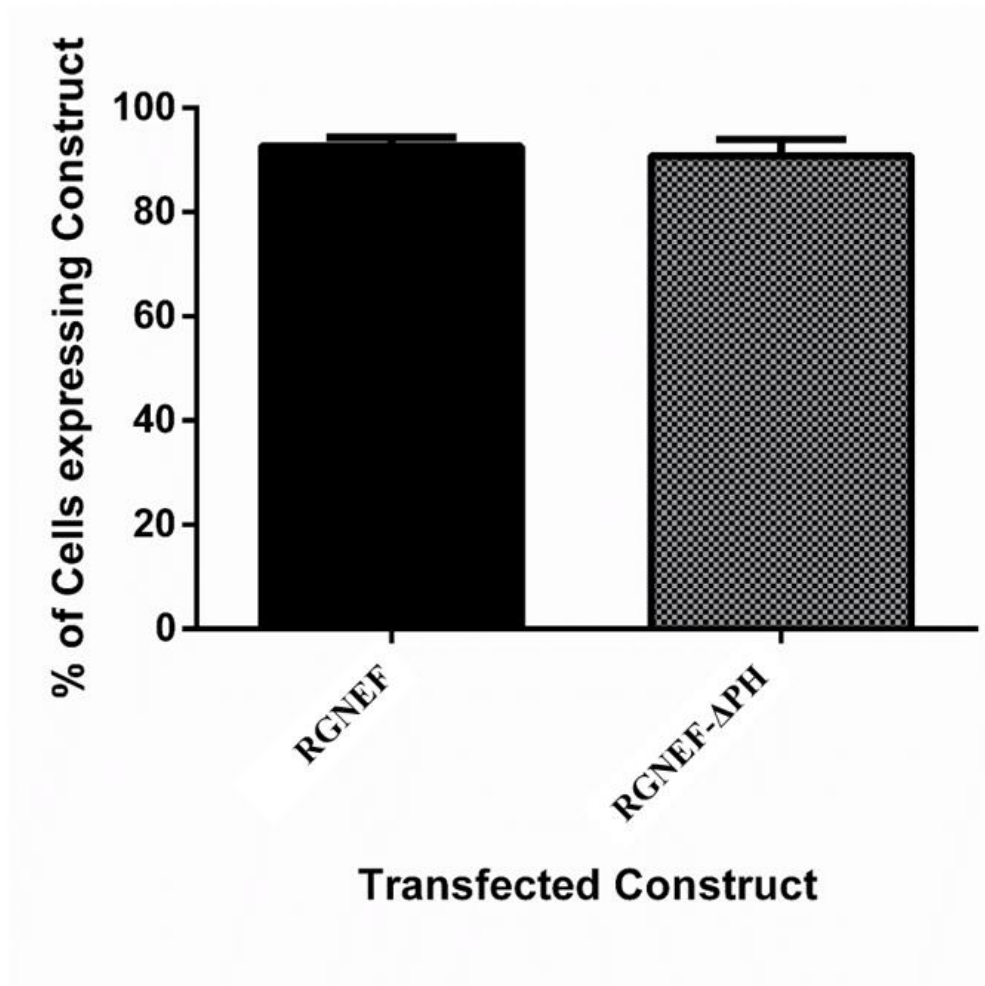
Figure 10: The transfection efficiency of RGNEF and RGNEF-ΔPH constructs measured by cell counting. The two construct show no significant difference (92% ± 2% vs 90% ± 3%, RGNEF and RGNEF-ΔPH respectively; p = 0.438) in the percentage of cells expressing each construct as measured by cell counting with confocal microscopy. Error bars show standard deviation.

confirmed. Transfected cells imaged by ICC confirm a reduced level of RGNEF-ΔPH recruitment to the nucleus with no apparent difference between constructs in membrane or cytosolic localization (Fig. 11). Confocal images of neither construct show high levels of recruitment to the plasma membrane. Cytosolic expression of both constructs appears diffuse. Differential localization of either construct to the nucleus was quantified by manual counting aided by intensity profiles generated by ZEN software (Carl Zeiss Canada; Fig. 12). RGNEF-ΔPH showed a significant decrease compared to RGNEF in the percentage of cells showing nuclear localization of the construct (Fig. 13; 12% ± 5% vs 39% ± 8%, respectively; p = 0.014).

Subcellular fractionation of HEK293T cells transfected with either construct showed a lower level of RGNEF-ΔPH in nucleosolic fraction compared to cells transfected with RGNEF (Fig. 14 A & B). Nucleosolic fractions from RGNEF-ΔPH transfected HEK293T cells showed no α-myc stained band at 180 kDa, suggesting RGNEF-ΔPH is completely absent from the nucleus. Densitometry confirmed a significant reduction in nuclear localization of respective constructs in RGNEF-ΔPH compared to RGNEF transfected cells (0.3 ± 0.1 vs 2.1 ± 0.6, respectively; p = 0.009). No significant difference was shown in the cytosolic fractions (Fig. 14 C & D; 2.4 ± 0.1 vs 2.3 ± 0.4, respectively; p = 0.379). Membrane fractions showed an apparent decrease in RGNEF-ΔPH recruitment to membranes compared to RGNEF that was not observed in confocal images (Fig 14E).
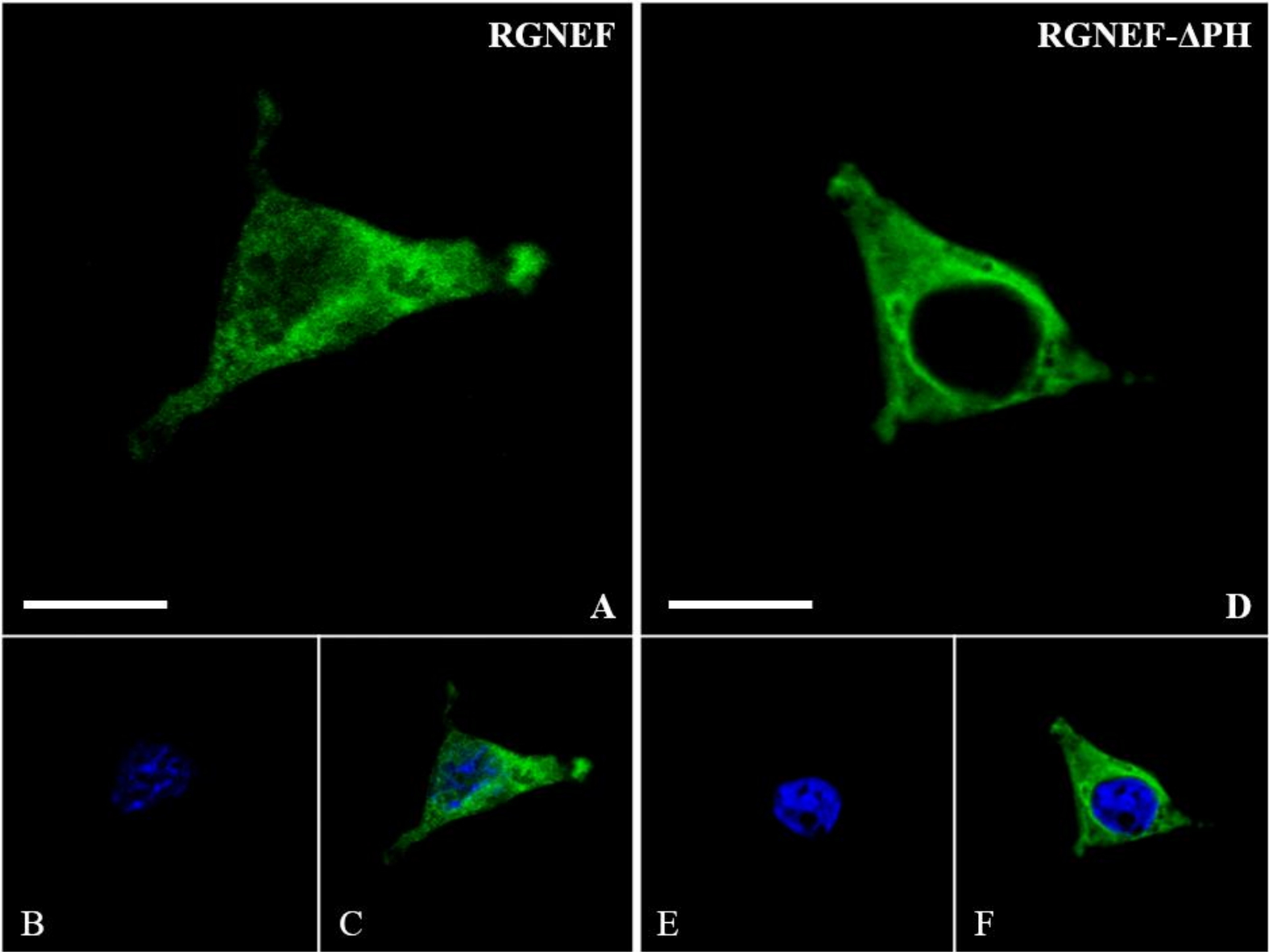
Figure 11: The subcellular localization of RGNEF and RGNEF-ΔPH as demonstrated by confocal microscopy. The subcellular localization in HEK293T cells as demonstrated by ICC with confocal microscopy. Panel A shows a high level of full length RGNEF localized throughout the cell, including within the nucleus (Panels B and C). Panel D-F shows that RGNEF-ΔPH is absent from the nucleus. Neither construct shows high levels of recruitment to the plasma membrane. Myc-tagged proteins were visualized using anti-myc antibody and Alexa 488 secondary antibody (green). The nucleic acid was visualized using Hoechst (blue). Scale bar represent 15 μm.
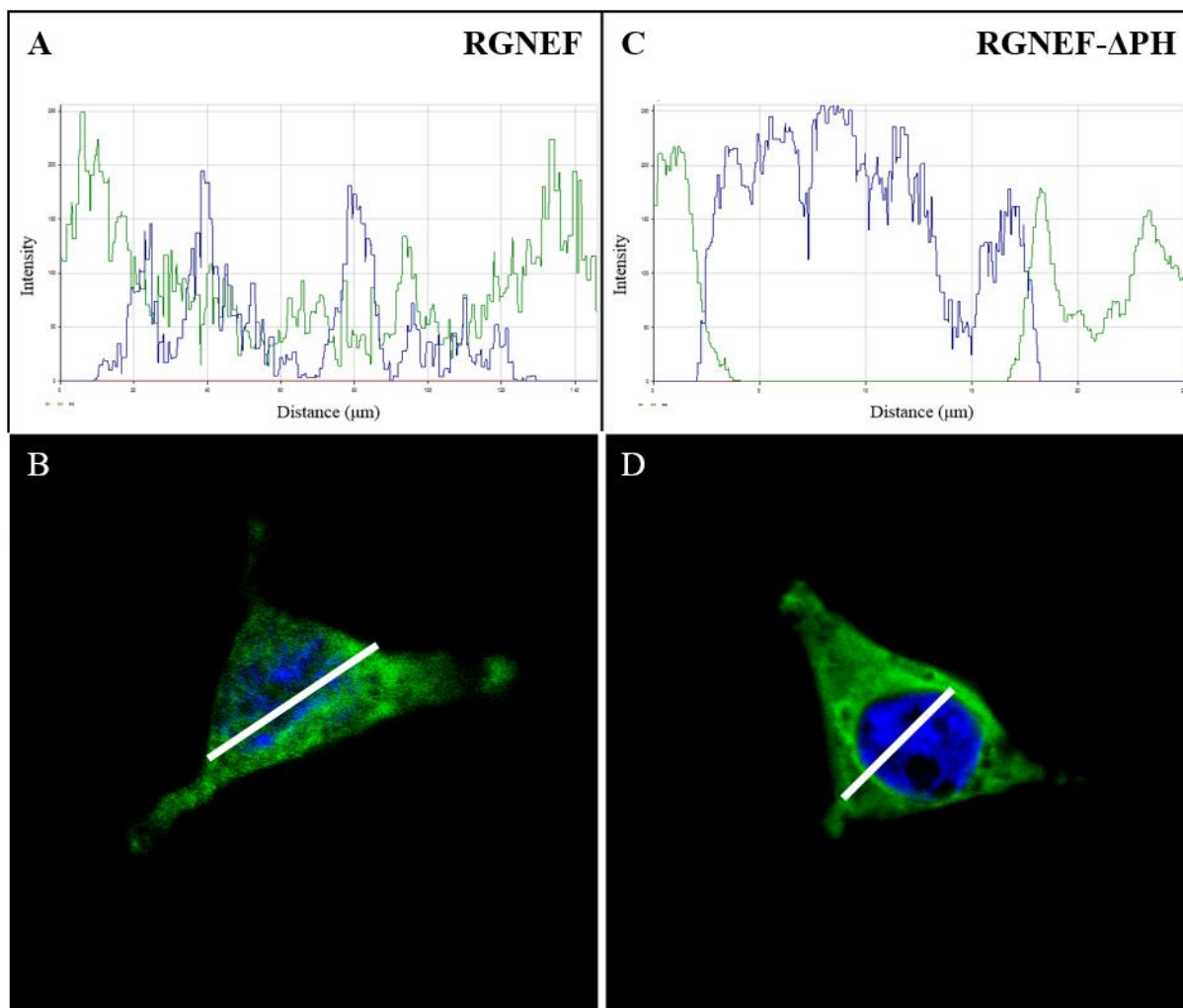
Figure 11: Intensity profiles generated using Zen Software of confocal images for RGNEF and RGNEF-ΔPH. Profiles (Panels A and C) show intensity profiles generated using ZEN software. Intensity (Y-Axis) is mapped against distance (X-Axis) across the cell, which is indicated by the white bar in panels B and D. The intensity profile (Panel A) for RGNEF shows consistently high levels of signal intensity of green channel (α-myc staining for our construct) as levels of blue (Hoechst) increase. The intensity profile for RGNEF-ΔPH (Panels C) shows the intensity of green drops off as blue increases. Myc-tagged proteins were visualized using anti-myc antibody and Alexa 488 secondary antibody (green). The nucleic acid was visualized using Hoechst (blue).
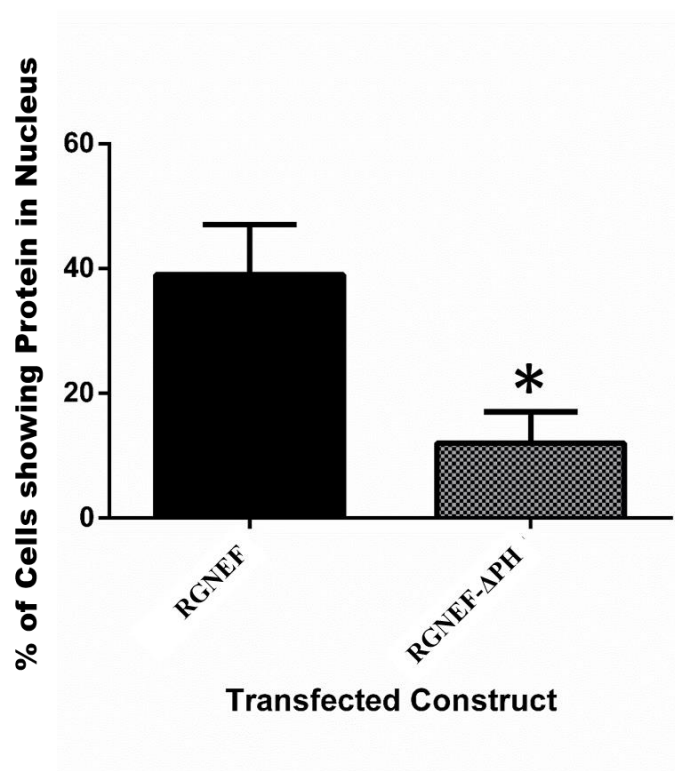
Figure 13: Subcellular localization measured as the percentage of cells showing nuclear localization of RGNEF and RGNEF-ΔPH as determined by cell counting. Manual cell counting, aided by intensity profiles, was performed to determine average number of cells with nuclear localization of the construct. HEK293T cells transfected with RGNEF-ΔPH showed significantly lower levels of cells with construct nuclear localization than those transfected with full length RGNEF (12% ± 5% vs 39% ± 8%, respectively; p = 0.014) as determined using a two-tailed independent sample T-Test. Error bars show standard deviation.

Nucleosolic Fraction

A

Cytosolic Fraction

C

Membrane Fraction

E

B

D
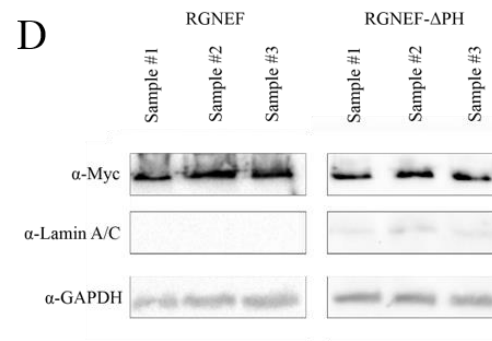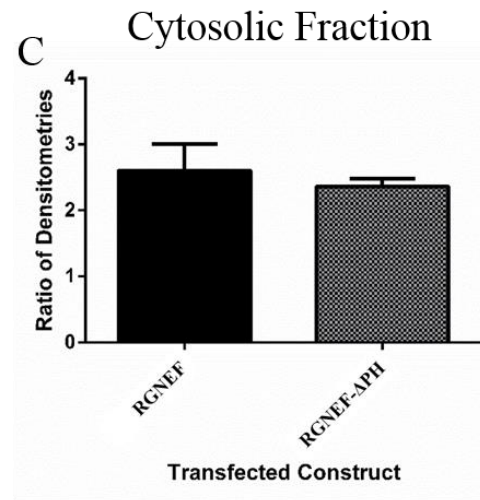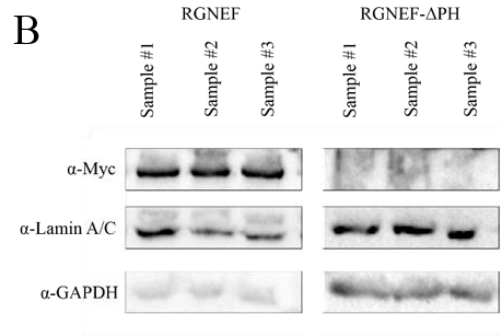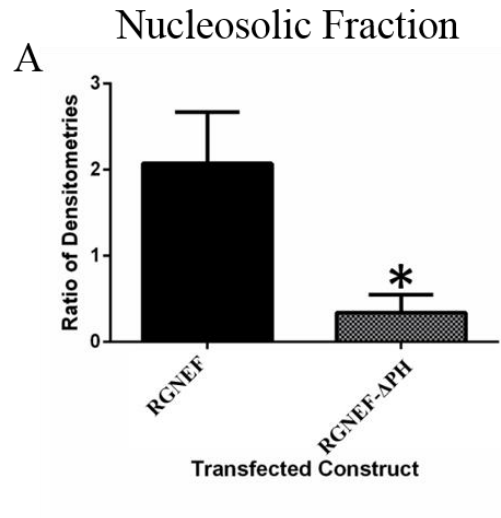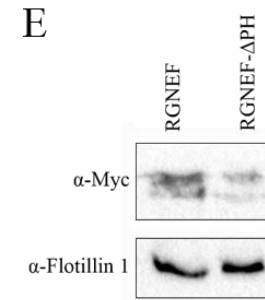
Figure 13: Subcellular localization measured by subcellular fraction with Western blot and densitometry. Fractionation of HEK293T cells transfected with either construct show a reduced level of RGNEF-ΔPH recruited to the nucleus compared to RGNEF (Panels A & B; 0.3 ± 0.1 vs 2.1 ± 0.6, respectively; p = 0.009). No significant difference was found between levels of RGNEF-ΔPH and RGNEF in the cytosolic fractions (Panels C & D; 2.4 ± 0.1 vs 2.3 ± 0.4, respectively; p = 0.379). A two-tailed independent sample T-test was used to determine significance. Low levels of the construct were shown in the membrane fraction of cells transfected with RGNEF. This was absent in cells transfected with RGNEF-ΔPH, suggesting a lower level of RGNEF-ΔPH recruitment to the membrane. Error bars show standard deviation.

3.2 Aim 2: Use of *in Silico* techniques to determine the apparent PH domain dependent mechanism of nuclear import of RGNEF

3.2.1 The analysis of the amino acid sequence of the PH domain using cNLS Mapper shows a putative NLS

The online software cNLS Mapper was used to predict the location of a putative NLS based on amino acid sequence. An NLS from residues 18 - 45 of the PH domain (residues 1100 – 1127 of full RGNEF) was predicted. Figure 15 shows the location of the NLS. The basic residues of the NLS are indicated by asterisks.

3.2.2 The molecular modeling of the NLS in the PH domain confirms that the basic residues are accessible for binding

Predictions by cNLS mapper are based on the amino acid sequence of a protein (98, 125, 126). Therefore, we used the molecular modeling software RasMol (Bernstein + Sons, Shirley New York) to map the position of the NLS to our existing model of the PH domain of RGNEF (Section 3.1.1). Figure 16 shows that the basic residues (yellow) of the NLS (red) are located on the exterior of the protein suggesting they are accessible for interaction with the concave surface of importin-α (96).

3.3 Aim 3: Confirm the functionality of the putative NLS in the PH domain of RGNEF

3.3.1 Mutagenesis to remove the basic residues of the NLS does not affect the molecular structure of RGNEF's PH domain

The four basic residues of the NLS were mutated to create RGNEF-mNLS, a construct that does not contain the basic residues necessary for binding to importin-α. In order to confirm that the mutations – either arginine to alanine or lysine to alanine – did not affect the molecular shape of

QALMSEERTLLYDGLVYWKTAT**GRFKDILALLLTDVLLFLQEKDQKYIFA**AVDQKPSVISL
QKLIAREVANEERGMFLISASSAGPEMYEIHTNSKEERNNWMRRIQQAVESCPEEKGGRTS
ESDEDKR
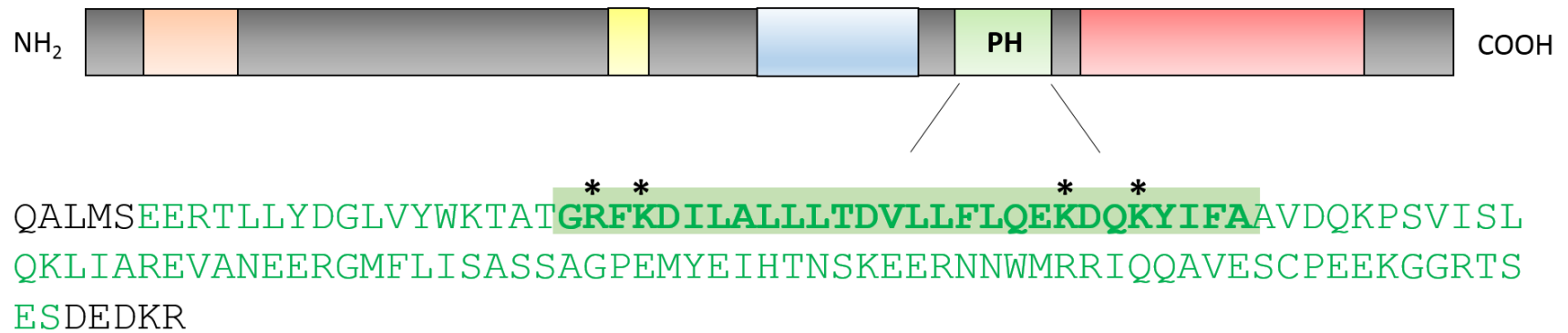
Figure 15: The location of the NLS predicted by cNLS mapper. The software cNLS predicted an NLS (highlighted green) from residues 18 – 45 of the PH domain (green font; residues 1100 – 1127 of full RGNEF). The basic residues (asterisks above) are located in two clusters separated by 16 residues.
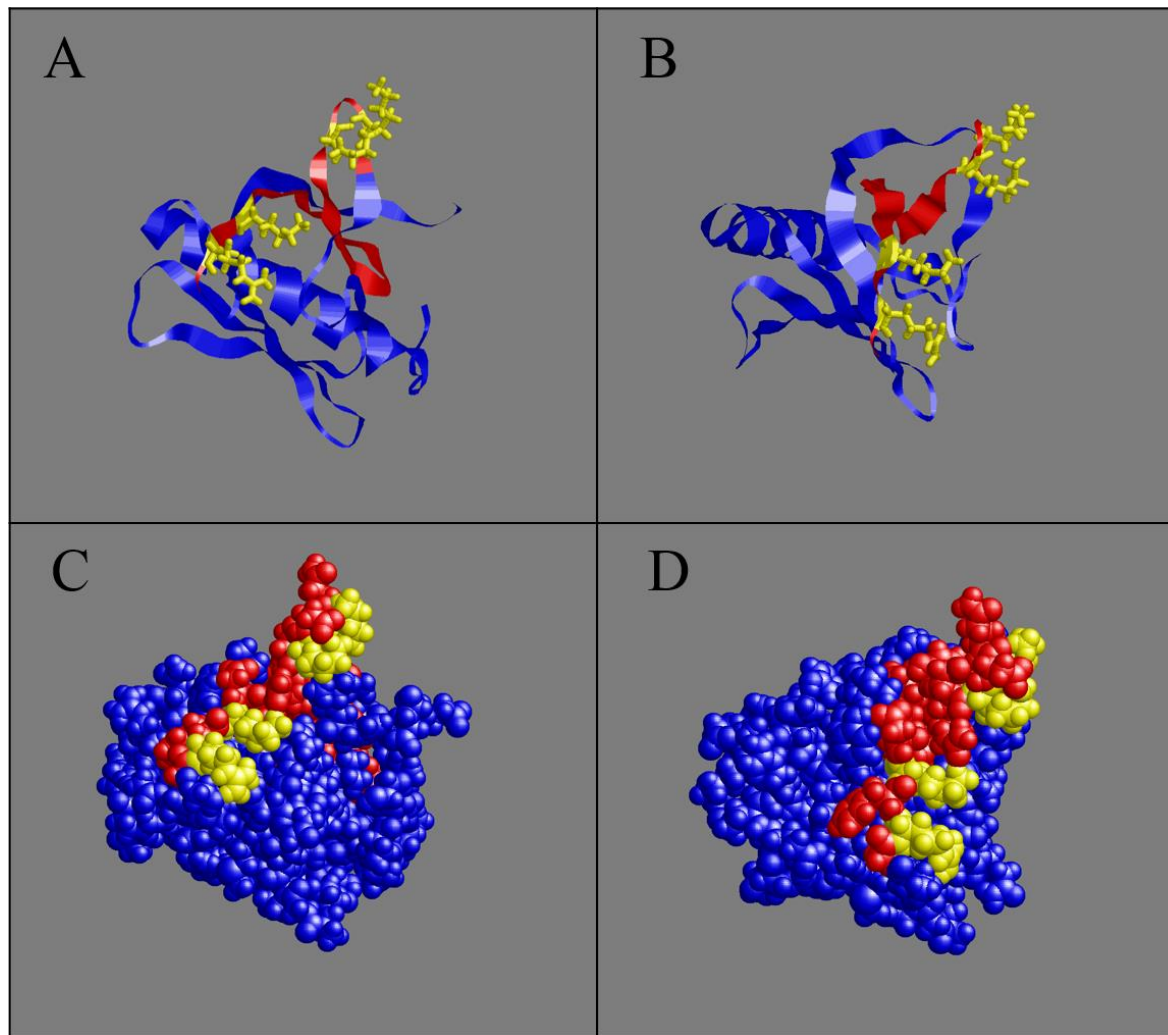
Figure 15: Molecular modeling of the NLS within the PH domain of RGNEF. Panels A & C and B & D show the same rotation with one being a ribbon model (A & B) and the other being a space fill model (C & D). The NLS (red) is shown to be located on the exterior of the PH domain with the basic residues (yellow).

the PH domain the amino acid sequence was submitted to the online software I-Tasser (117-119) and the model was oriented using RasMol. Figure 17A shows a side by side comparison of the PH domain of wild-type RGNEF against the mutated PH domain of RGNEF-mNLS. Figure 17B-E shows the model at the same various angles used in Figure 16. The PH domain of RGNEF-mNLS retains the same structure as the wild-type PH domain including the relative location of the NLS residues.

3.3.2 The expression efficiency of RGNEF-mNLS is not significantly different from that of full length RGNEF or RGNEF-ΔPH

The transfection efficiency for RGNEF-mNLS was determined using cell counting and Western blot. First, ICC and confocal microscopy was performed on transfected HEK293T cells because a new microscope was used for Aim 3 – a Leica SP8 replaced the Zeiss LSM 510 META used in Aim 1 - the percentage of cells expressing the construct was determined for RGNEF, RGNEF-ΔPH, and RGNEF-mNLS by cell counting. No significant difference in the percentage of cells expressing the construct was found between the three constructs when compared by a one-way ANOVA (Fig. 18A p = 0.091).

The overall expression was measured by lysing transfected HEK293T cells, running a Western blot, and performing densitometry (Fig 18B & C). Expression was normalized against GAPDH expression. No significant difference was found in protein levels between constructs when compared by a one-way ANOVA (p = 0.5403).

3.3.3 RGNEF-mNLS shows significantly lower levels of nuclear localization than full length RGNEF, consistent with RGNEF-ΔPH

Cells transfected with RGNEF-mNLS show significantly lower levels of localization to the nucleus as measured by confocal microscopy and Western blot. Transfected HEK293T cells were stained by ICC and confocal microscopy was performed. Figure 19 shows a comparison of

A
WT   mNLS

B
mNLS

C
mNLS

D
mNLS

E
mNLS
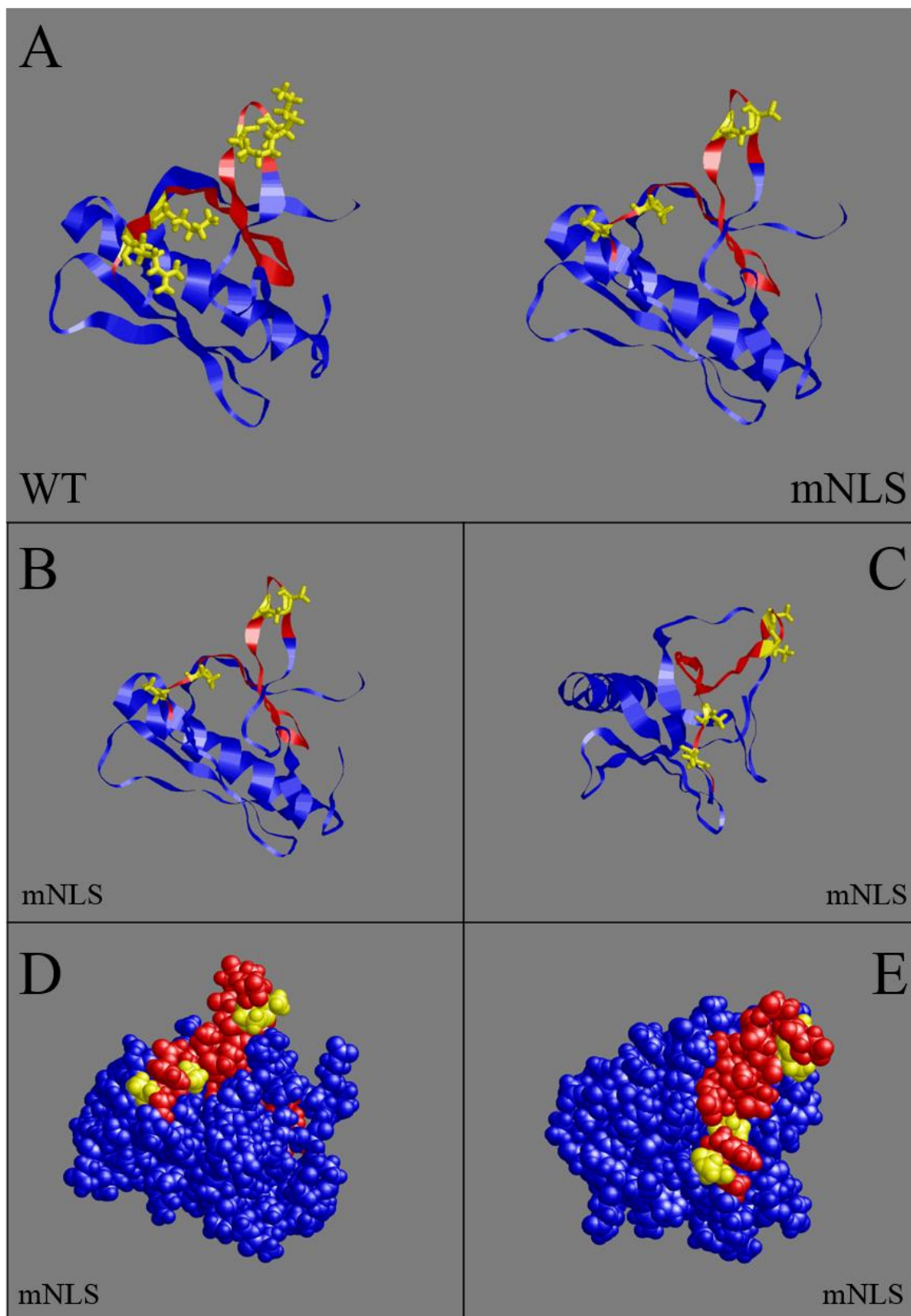
Figure 17: Comparison of the molecular structures of the wild-type RGNEF and RGNEF-mNLS PH domains. Panel A shows a side by side comparison of the PH domains of wild-type (WT) RGNEF against RGNEF-mNLS. Both PH domains show the same folding and relative location of the NLS. Panels B-E show rotations of the RGNEF-mNLS model.

A

B

C

α-myc

α-GAPDH

Figure 18: The transfection efficiency of RGNEF, RGNEF-ΔPH, and RGNEF-mNLS measured by cell counting and by Western blot. Panel A shows the results of cell counting using confocal microscopy. Cell counting for RGNEF and RGNEF-ΔPH was repeated from Aim 1 (Section 3.1.2). No significant difference was shown in percentage of cells between constructs when compared by a one-way ANOVA (p = 0.091). Panels B & C show levels of expression as measured by Western blot with densitometry. Relative protein amount was determined by comparing α-myc bands, which represent the expression of each construct, against GAPDH bands. We observed no significant difference in the relative protein amount between constructs as compared by a one-way ANOVA (p = 0.5403).
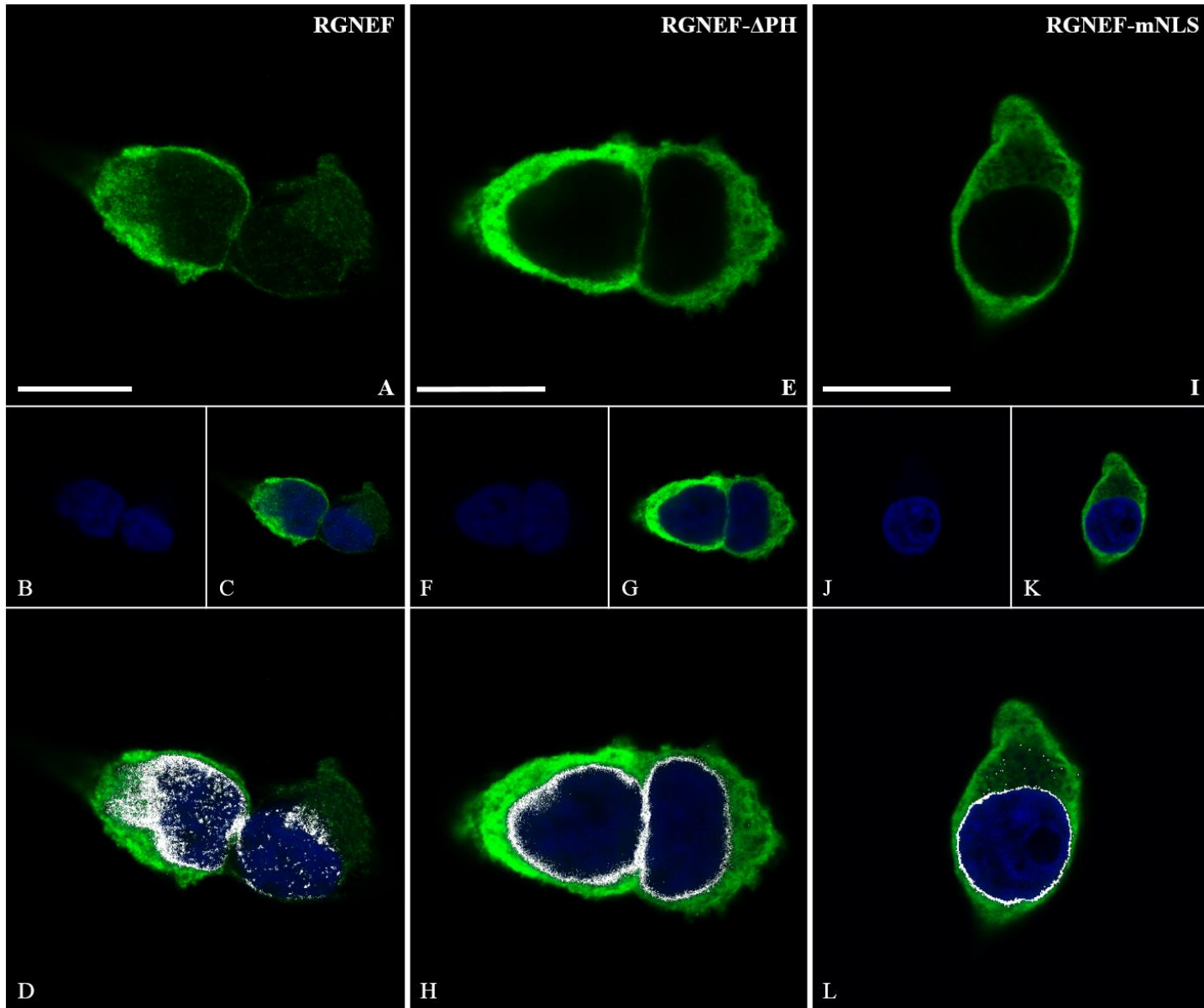
Figure 19: The subcellular localization of RGNEF, RGNEF-ΔPH, and RGNEF-mNLS shown by confocal microscopy.
HEK293T cells transfected with RGNEF (Panels A-D) shows localization of the construct to the nucleus. Co-localization analysis (Panel D) shows co-localization of RGNEF (green) with Hoechst stain (blue) within the nucleus. RGNEF-ΔPH (Panels K-H) and RGNEF-mNLS (Panels I-L) show no construct in the nucleus and co-localization analysis (Panels H & L) shows co-localization only around the periphery of the nucleus. Myc-tagged proteins were visualized using anti-myc antibody and Alexa 488 secondary antibody (green). The nucleic acid was visualized using Hoechst (blue). The scale bar represents 15 μm.

the three constructs. Panels D, H, and L show co-localization analysis; the regions where both green (myc tag) and blue (Hoechst stain) overlap are colored white. RGNEF shows some level of localization to the nucleus as shown by spots of co-localization seen throughout the nucleus. RGNEF-mNLS shows the same pattern of exclusion from the nucleus as RGNEF-ΔPH: co-localization is seen only along the periphery of the nucleus and not within. Co-localization at the periphery of the outer nuclear envelope likely represents our constructs collecting along the nuclear membrane possibly as an early step in nuclear import. Because they lack the basic residues for interaction with importin-α, they remain localized at the outer nuclear membrane.

The number of cells with our construct product protein in the nucleus were counted. Intensity profiles (Fig. 20) generated by LAS X software were used to examine the level of expression of the construct in the nucleus. We observed a significant difference in percentage of cells showing nuclear expression between constructs when compared by a one-way ANOVA ($p < 0.001$). A post-hoc Newman-Keuls test showed a significant difference in percentage of cells showing nuclear localization between HEK293T cells transfected with RGNEF (44%) and RGNEF-mNLS (11%; $p < 0.001$).

In order to complement the results observed in HEK293T cells, the neuronal cell type SH-SY5Y was transfected, ICC was performed and cells were imaged by confocal microscopy (Fig. 22). In addition to α-myc (green) and DAPI (blue), β-Tubulin III (red) was used as a marker of neuronal differentiation and to label the entirety of the cell. Subcellular localization of the constructs is similar in SH-SY5Y cells as to what is seen in HEK293T cells with reduced levels of RGNEF-ΔPH or RGNEF-mNLS localized to the nucleus compared to RGNEF. Co-localization analysis (Panels E, J, & O) demonstrated greater levels of nuclear localization of construct in those cells transfected with full length RGNEF than those transfected with either RGNEF-ΔPH (Panels F-J) or RGNEF-mNLS (Panels K-O), where co-localization was seen only around the periphery of the nucleus. This allows us greater ability to generalize our results to spinal motor neurons and to the ALS pathology. As well, because differentiated SH-SY5Y cells are neuron-like and have withdrawn from the cell cycle (127), it indicates that the nuclear localization observed in HEK293T cells is independent of cell cycle.
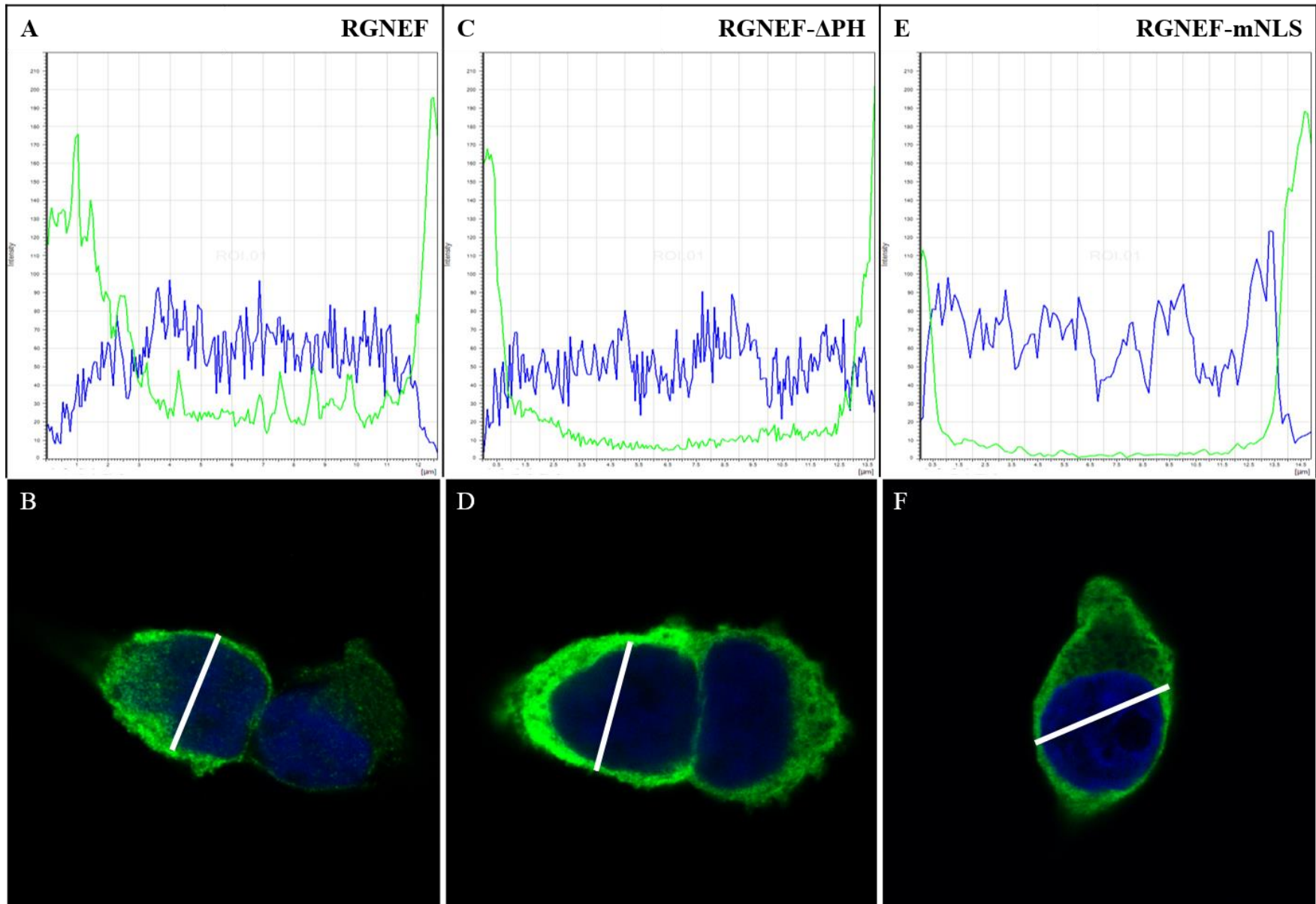
Figure 20: Intensity profiles generated using LAS X Software for confocal images of RGNEF, RGNEF-ΔPH, and RGNEF-mNLS. Profiles (Panels A, C, & E) show intensity profiles generated using LAS X software. Intensity (Y-Axis) is mapped against distance (X-Axis) across the HEK293T cell, which is indicated by the white bar in panels B, D, & F. The intensity profile (Panel A) for RGNEF shows consistently high levels of signal intensity of green channel (α-myc staining for our construct) as levels of blue (Hoechst) increase. For both RGNEF-ΔPH and RGNEF-mNLS (Panels C & E) the intensity of green drops off as blue increases. Myc-tagged proteins were visualized using anti-myc antibody and Alexa 488 secondary antibody (green). The nucleic acid was visualized using Hoechst (blue).
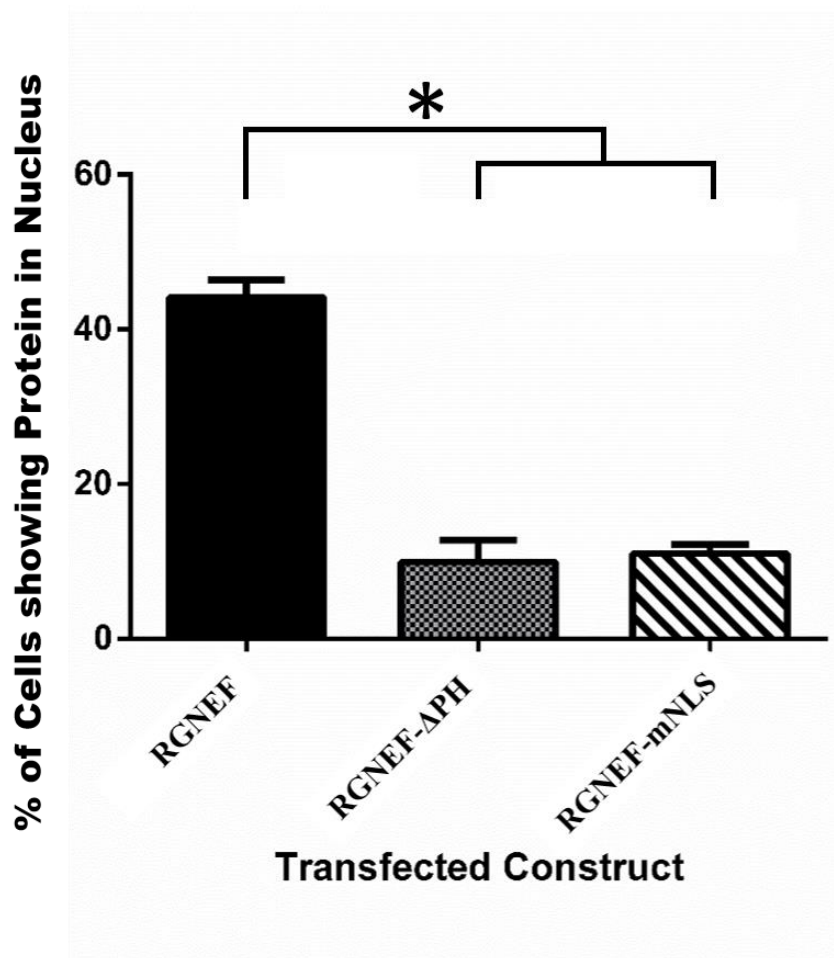
Figure 21: Subcellular localization measured as a percentage of cells showing nuclear localization of RGNEF, RGNEF-ΔPH, and RGNEF-mNLS. Manual cell counting aided by computer generated intensity profiles was used to determined average number of cells showing nuclear localization of respective constructs. A significant difference in percentage of cells showing construct in the nucleus was found between constructs ($p < 0.001$). A post-hoc Newman-Keuls test showed a significant difference in percentage of cells showing nuclear localization between HEK293T cells transfected with RGNEF (44%) and RGNEF-mNLS (11%; $p < 0.001$). A significant difference was also found between RGNEF and RGNEF-ΔPH (10%; $p < 0.001$). Error bars show standard deviation.
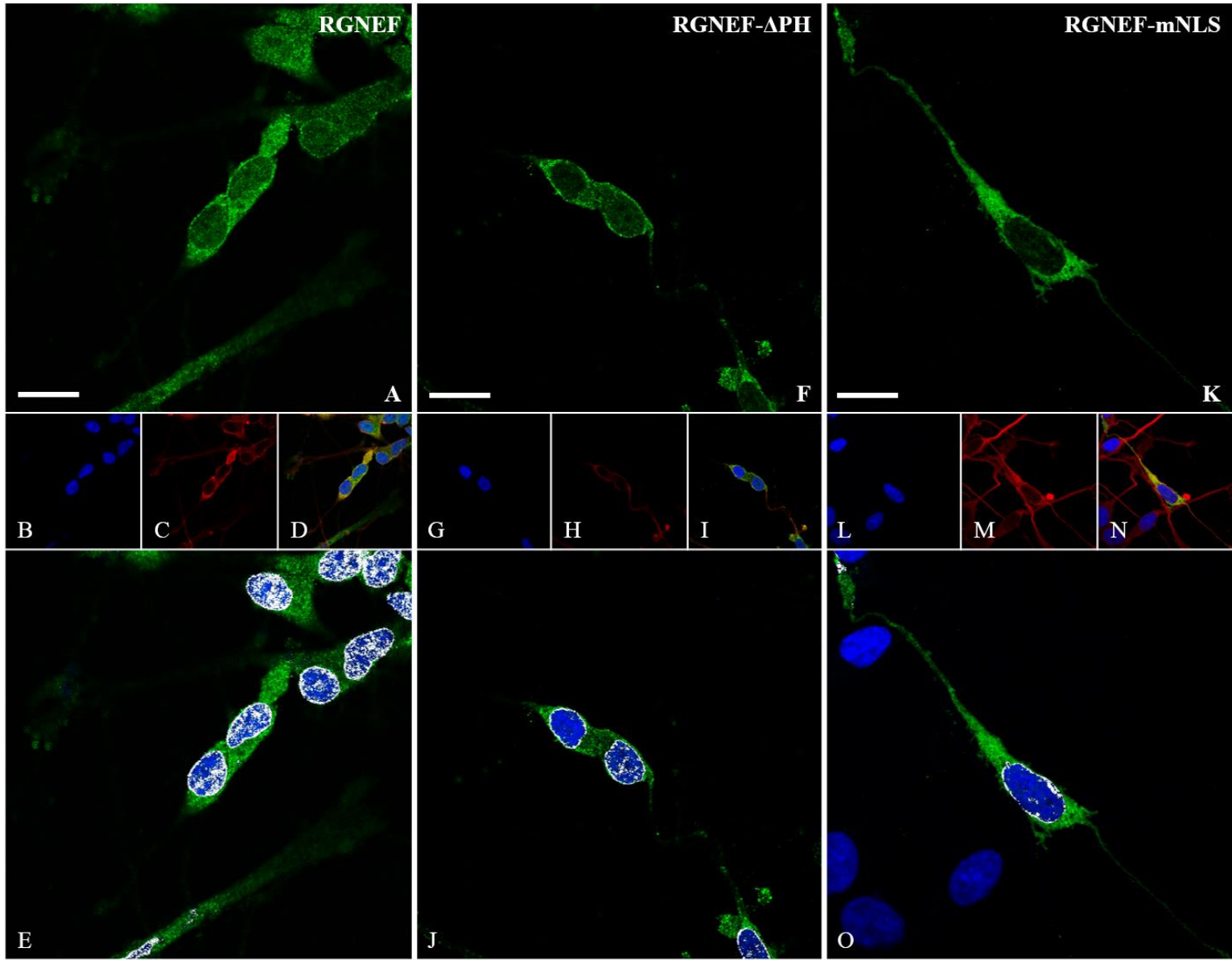
Figure 22: Confocal images showing subcellular localization of RGNEF, RGNEF-ΔPH, and RGNEF-mNLS in SH-SY5Y cells. High levels of nuclear localization of RGNEF were observed using confocal microscopy (Panels A-E) where as much lower levels of were observed for both RGNEF-ΔPH (Panels F-J) and RGNEF-mNLS (Panels K-O). Co-localization analysis (Panel E) demonstrated that RGNEF co-localized with DAPI stain within the nucleus. However, RGNEF-ΔPH (Panel J) and RGNEF-mNLS (Panel O) were co-localized largely around the periphery of the nucleus and at much lower levels within the nucleus itself. Myc-tagged proteins were visualized using anti-myc antibody and Alexa 488 secondary antibody (green). Beta Tubulin III was visualized using Beta Tubulin III antibody with Alexa 546 secondary antibody (red). Nucleic acid was visualized using DAPI (blue). The scale bar represent 15 μm.

The localization of RGNEF-mNLS in HEK293T cells was also measured by subcellular fractionation with Western blotting and densitometry (Fig. 23). For the nuclear fraction (Panels A & B), the level of construct was measured against Lamin A/C staining. A significant difference was found in relative protein levels in nuclear fractions between constructs (Panels A & B; p = 0.003). A Newman-Keuls test showed a significant difference between relative protein levels in cells transfected with RGNEF ($\bar{x}$ = 2.1) and either RGNEF-ΔPH ($\bar{x}$ = 0.3; p < 0.01) or RGNEF-mNLS ($\bar{x}$ = 0.4; p < 0.01). No significant difference was shown between RGNEF-ΔPH and RGNEF-mNLS p > 0.05). Expression in the cytosolic fraction was measured against GAPDH as an internal control. When comparing cytosolic fraction (Panel C & D), no significant difference in relative protein levels was shown between constructs (p = 0.434). Error bars represent standard deviations.

3.3.4 The expression of constructs of 40 kDa or less in HEK293T cells shows differential localization of PH-40 kDa and mNLS-40 kDa

In order to isolate the effects of the NLS on protein localization, three GFP-tagged constructs were created. The PH-40 kDa construct expressed only the wild-type PH domain (amino acids 1082 – 1201). The NLS-26 kDa construct expressed only the wild-type bipartite NLS sequence (amino acids 1100 -1128). The mNLS-40 kDa construct expressed only the PH domain from the NLS mutated (RGNEF-mNLS) template inclusive of point-mutations to eliminate importin-α binding (amino acids 1082 – 1201; R1101A, K1103A, K1120A, K1123A).

Figure 24 shows confocal microscope data for these three constructs with eGFP-C1 vector transfected HEK293T cells for reference (Fig. 24a). Cells transfected with the eGFP-C1 vector show diffuse expression including nuclear expression. Cells transfected with NLS-26 kDa (Fig. 24b) showed diffuse expression, comparable to that observed with eGFP-C1 transfected cells. Although we anticipated that this construct might preferentially localize to the nucleus, it is likely that because of its low molecular weight (26 kDa) that it was able to freely diffuse into and out of the nucleus, resulting in diffuse localization. It is also possible that by expressing only 27

A — Nucleosolic Fraction

C — Cytosolic Fraction
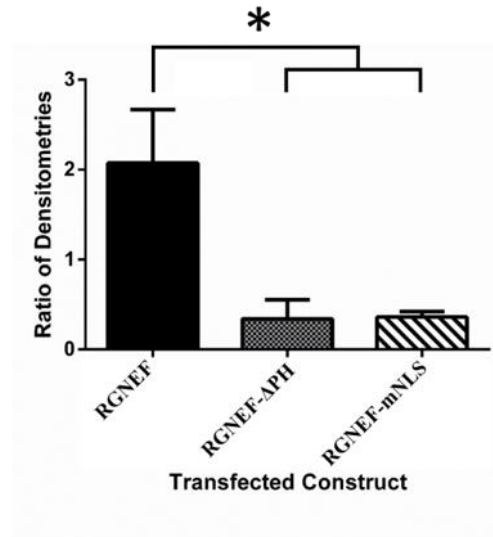
B — RGNEF-mNLS
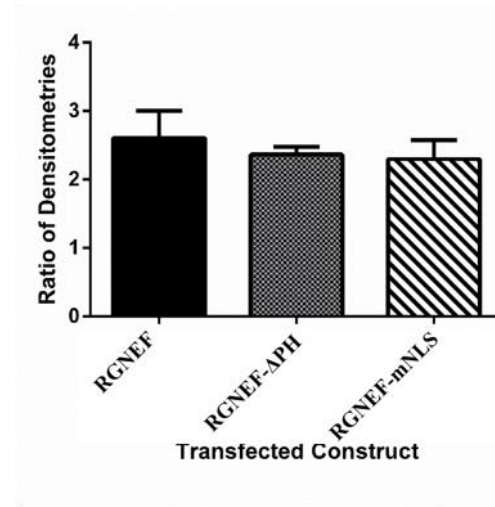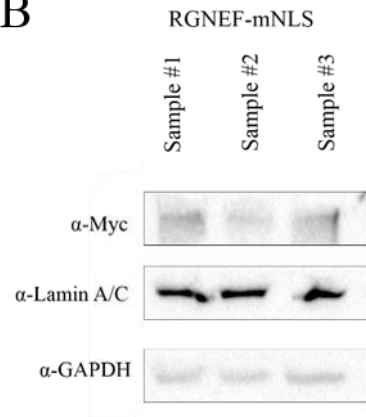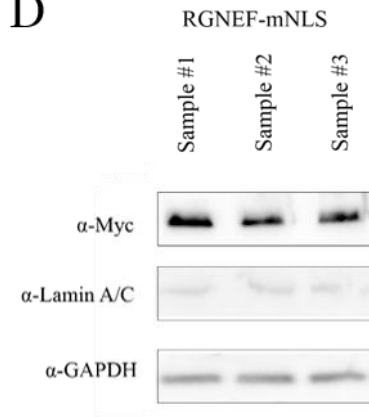
D — RGNEF-mNLS

Figure 23: Subcellular localization measured by cellular fractionation with Western blot and densitometry. Densitometry results (Panels A & C) for Western blots obtained from HEK293T transfected with RGNEF-mNLS were compared against data obtained for nuclear fractionation of RGNEF and RGNEF-ΔPH described previously (Section 3.1.3). A significant difference was found in relative protein levels in nuclear fractions between constructs (Panels A & B; p = 0.003). A Newman-Keuls test showed a significant difference between relative protein levels in cells transfected with RGNEF ($\overline{x}$ = 2.1) and either RGNEF-ΔPH ($\overline{x}$ = 0.3; p < 0.01) or RGNEF-mNLS ($\overline{x}$ = 0.4; p < 0.01). No significant difference was shown between RGNEF-ΔPH and RGNEF-mNLS p > 0.05). When comparing cytosolic fraction (Panel C & D), no significant difference in relative protein levels was shown between constructs (p = 0.434). Error bars represent standard deviations.

amino acids of the PH domain the resulting protein did not fold into the characteristic β-stranded structure seen in the endogenous PH domain (Fig. 9). As illustrated in Figure 16, the folding of the PH domain results in the basic residues of the NLS (yellow) collecting along the exterior of the domain. In the absence of the remainder of the PH domain it is possible that either the basic residues do not collect near one another or that they are subject to steric interference from the GFP-tag.

When transfected with the PH-40 kDa construct, HEK293T cells showed a variable pattern of protein localization. Figure 24c shows some level of construct recruitment to the nucleus in all cells at all levels of expression of the protein in the cell. Both cell 1 and cell 2 (as labelled in figure) show high expression of the construct. However cell 2 shows high levels of construct localized to the nucleus whereas cell 1 shows lower levels of expression in the nucleus. Cells 3 and 4 show moderate levels of construct expression although cell 3 shows nearly diffuse expression of the construct through the nucleus and cell 4 shows much lower level of nuclear expression. No cells showed higher levels of construct in the nucleus than in the cytoplasm. This suggests that NLS function may be regulated by some form of post-translational modification similar to the phosphorylation and methylation found in EWS and TAF15, respectively (73,76); cells showing high levels of construct nuclear localization may contain the NLS in an active state.

Figure 24d shows the expression of mNLS-40 kDa in HEK293T cells. As with PH-40 kDa, all transfected cells show some level of protein in the nucleus. The levels of construct in the nucleus appears lower than for PH-40 kDa, however no cell shows levels of nuclear expression as low as what was seen previously with RGNEF-ΔPH (see Figure 11).

Despite the support for our hypothesis that these low molecular weight constructs add, it is difficult to draw conclusive evidence from this data given that the literature offers three different thresholds for nuclear diffusion: 40 kDa (84,85), 60 kDa (86–88), and as high as 110 kDa (89). For example, cells transfected with PH-40 kDa or mNLS-40 kDa always showed some low level
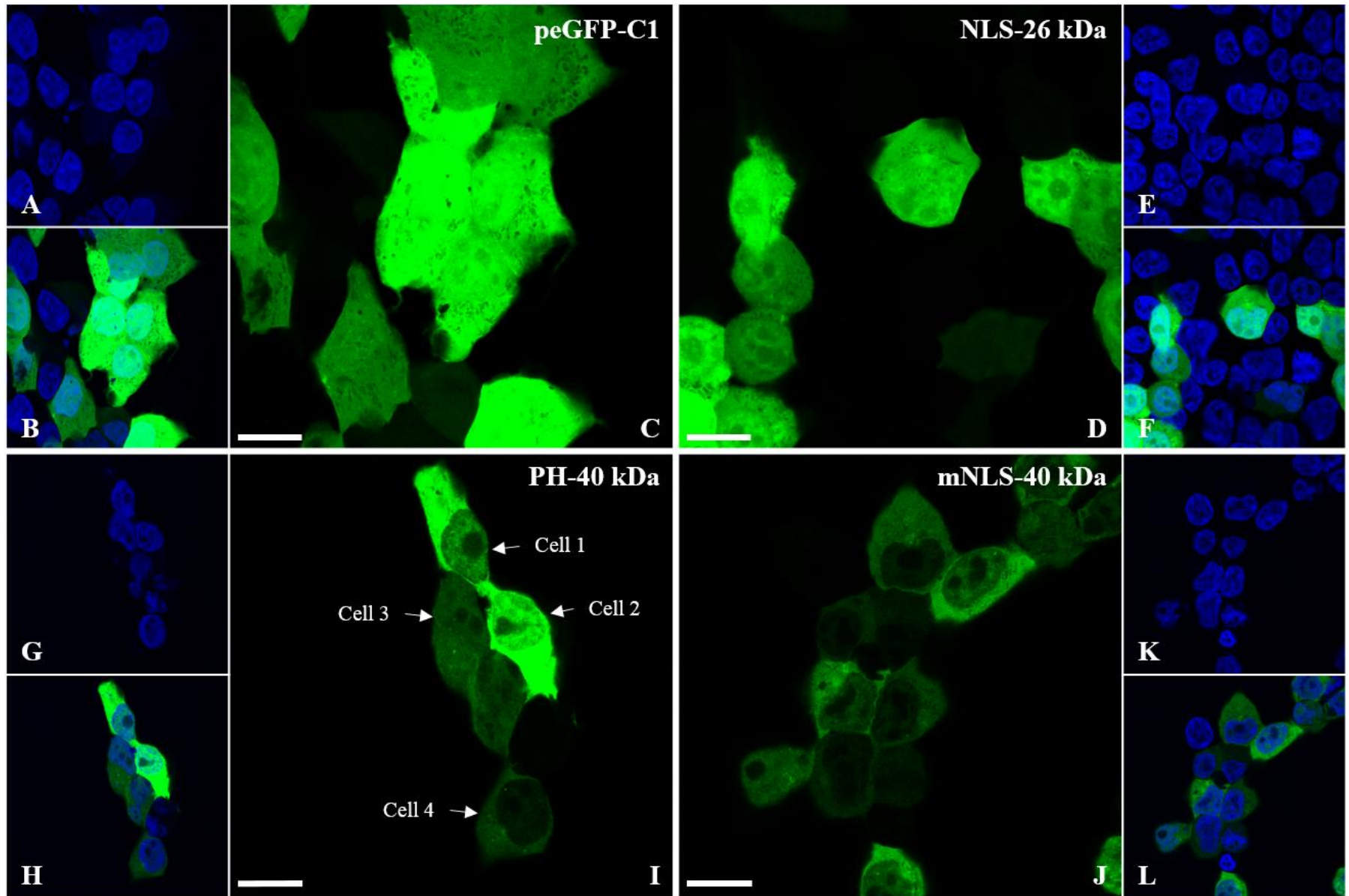
Figure 24: The subcellular localization of constructs of 40 kDa or less as shown by confocal microscopy. Examination of the subcellular localization by ICC and confocal microscopy shows diffuse expression of construct in eGFP-C1 (Panels A-C) and NLS-26 kDa (Panels D-F) transfected HEK293T cells. Cells transfected with PH-40 kDa (Panels G-I) show variable localization. Cell 1 & 2 (as indicated by label in figure) show high level of construct expression. Cell 1, however, shows much lower level of nuclear expression. Cells 3 & 4 show lower level of protein expression with cell 4 showing lower levels of nuclear expression. HEK293T cells transfected with mNLS-40 kDa (panels J-L) show lower levels of construct recruitment to the nucleus, though none as low as what was seen previously with RGNEF-ΔPH. In all panels, green represents fluorescence by N-terminal GFP-tag. The nucleic acid was visualized using Hoechst (blue). The scale bar represents 15 μm

of construct in the nucleus, suggesting that low levels of the constructs were diffusing into the nucleus. For this reason, we created constructs expressing proteins greater than the maximum threshold for nuclear diffusion.

3.3.5 The expression of 160 kDa constructs in HEK293T cells shows differential localization of PH-40 kDa and mNLS-40 kDa at levels equivalent to full length constructs

The expression of mNLS-40 kDa (see Section 3.3.4) exhibited lower nuclear expression than PH-40 kDa, though no cells showed levels as low as what had been previously seen in RGNEF-ΔPH or RGNEF-mNLS constructs. Therefore, we hypothesized that the nuclear localization of constructs seen was due to passive diffusion of the construct into the nucleus. Therefore, we created similar GFP-tagged constructs with the addition of the protein LacZ. This resulted in constructs of approximately 160 kDa. These constructs (PH-160 kDa and mNLS-160 kDa) far exceed the highest threshold estimate of 110 kDa for passive diffusion into the nucleus and therefore should not be able to diffuse.

Figure 25 shows confocal images of HEK293T cells transfected with these constructs. Panel A shows expression of only the pHM830 plasmid. This vector alone expresses the LacZ protein with N-terminal GFP-tag. The protein is absent from the nucleus, indicating that LacZ+GFP alone is sufficiently large enough to be excluded from the nucleus. Panel D shows high levels of nuclear localization of PH-160 kDa, comparable to levels of full length RGNEF (Figures 19, 22) and of PH-40 kDa (Figure 24). Panel G shows very low levels of nuclear localization of mNLS-160 kDa, comparable to levels of RGNEF-ΔPH and RGNEF-mNLS (Figures 19, 22).
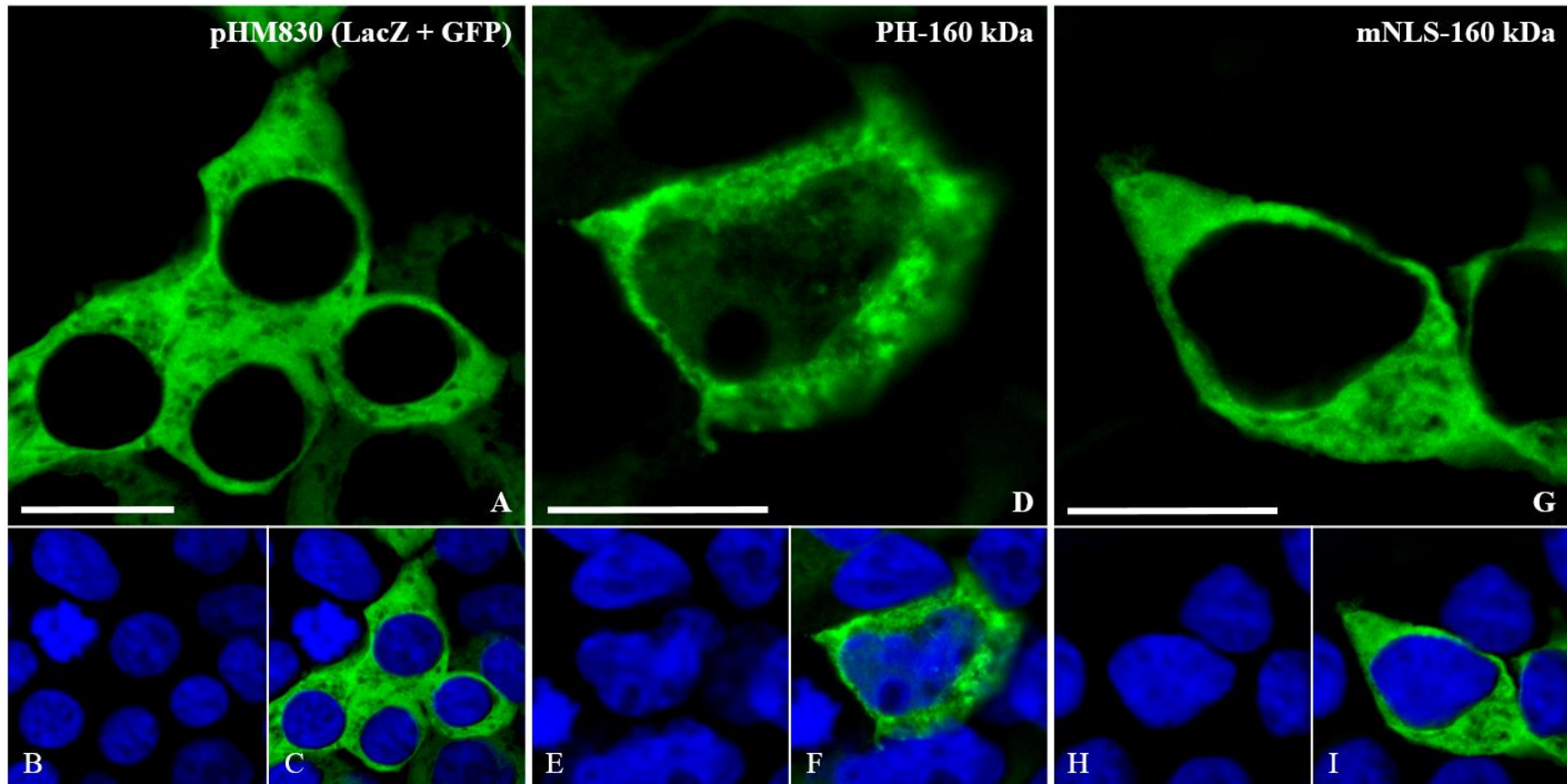
Figure 25: The subcellular localization of 160 kDa constructs as shown by confocal microscopy. Examination of subcellular localization by ICC and confocal microscopy shows cytoplasmic localization only of the pHM830 vector, which expresses GFP-tagged LacZ (Panel A-C). Panels D-F shows PH-160 kDa present in the nucleus. Panels G-I shows an absence of mNLS-160 kDa in the nucleus, comparable to what is seen in pHM830 transfected cells. In all panels Green channel represents florescence by GFP tag and blue represent florescence by Hoechst stain. The scale bar represents 15 μm.

Chapter 4

4 Discussion

Here we report multiple lines of evidence supporting the presence of a NLS within the PH domain of RGNEF. The interaction between cargo proteins and importin-α is facilitated by basic residues within NLSs (94). Point-mutations of the basic residues of our identified NLS reduced nuclear localization in both full-length constructs (RGNEF-mNLS) and in constructs expressing only the PH domain (mNLS-160 kDa). Molecular modeling confirms that these mutations did not change the overall molecular shape of the PH domain (Fig. 17). Our two lines of constructs, full length constructs and isolated PH domain constructs, complement one another well in that they confirm that NLS function also occurs in the full-length protein and that it functions independently of other regions of the protein. As well, our use of the neuron-like SH-SY5Y cell line to supplement data found in HEK293T cells allows us greater ability to generalize our findings towards our understanding of ALS pathology.

4.1 Implications for our understanding of RGNEF function

Our data presented here, particularly our identified NLS, offers significant insight into the function of RGNEF. It may also offer insight into the mechanism by which RGNEF destabilizes *NEFL* mRNA (19,22). The mechanism by which RGNEF destabilizes *NEFL* mRNA likely involves shuttling the mRNA species to a RNAse or complex in the cytoplasm to promote its degradation. Having shown the mechanism by which RGNEF is able to localize to the nucleus, it remains to be revealed whether RGNEF binds *NEFL* mRNA – or other target mRNA species – within the nucleus and may contribute to their nuclear export.

The protective effect of RGNEF on cellular stress is likely not due to its nuclear import. Our lab has previously shown that when transfected with full length RGNEF, HEK293T cells showed a significantly greater percentage of cell survival when exposed to oxidative stress than those cells which were transfected with empty vector. Cells transfected with constructs lacking the GEF region (both DH and PH domains) showed a significant increase in survival over cells

transfected with empty vector, suggesting that RGNEF's nuclear localization is not necessary for its function in stress protection (123).

It is of interest that regardless of the construct (full length RGNEF, RGNEF-ΔPH, or RGNEF-mNLS) or the cell type (HEK293T (Fig. 19) or SH-SY5Y (Fig. 22)) we observed a prominent localization of the construct at the nuclear membrane. We interpret this as our constructs collecting at the outer nuclear membrane as an initial step prior to nuclear import. This may implicate a second domain of RGNEF, the C-terminal microtubule binding domain (Fig. 4), as a contributor to nuclear import. The microtubule cytoskeleton has been shown to contribute to the nuclear import of parathyroid hormone-related protein (PTHrP), p53, retinoblastoma protein, and Signal transducer and activator of transcription 5 (STAT5) (130,131). It is thought that binding to microtubules facilitates transport through the cytoplasm to the nuclear envelope, where nuclear import is then carried out by conventional means (binding karyopherins). Whether the microtubule binding domain of RGNEF contributes to its transport to the nuclear envelope remains to be determined.

Our data also suggests that RGNEF nuclear localization undergoes some form of regulation. Figure 25 shows variable levels of nuclear localization between cells transfects with PH-160 kDa. Post-translational modifications of EWS and TAF15 have been shown to regulate their nuclear localization (73,76). Phosphorylation sites along RGNEF, including within the PH domain have previously been identified (132). Regulation of NLS activity likely occurs within the PH domain as the constructs in which we found differential localization between cells (PH-40 kDa, and PH-160 kDa) expressed only the PH domains of RGNEF. Regulation of RGNEF may contribute to its role in disease pathology.

4.2   Implications for our understanding of ALS pathology

The role of RGNEF in ALS pathology is currently unknown. It has been shown to destabilize *NEFL* mRNA (19), which encodes the NF subunit NFL. Stoichiometric balance of the NF

subunits and of NFL in particular is critical to the formation of the NCIs seen in ALS motor neurons (133). Like RGNEF, TDP-43 also acts as a stability factor for *NEFL* mRNA (39), forms ubiquitinated inclusions in ALS patients (48), and contains an NLS, allowing it to localize to the nucleus (53). Because TDP-43 acts to stabilize *NEFL* mRNA and RGNEF acts to destabilize *NEFL* mRNA, it is possible that together these two represent a feedback system that acts to maintain NFL expression levels. The ALS-specific mutations identified in *ARHGEF28* result in severely truncated proteins, which do not express either the RNA binding domain or the NLS-containing PH domain (20,121,122). It is possible that the loss of RGNEF as a regulator of *NEFL* mRNA increases susceptibility for ALS. As well, it is possible that the dysregulation of nuclear transport proteins – including importin-α, RCC1, and RanGAP – observed in cells expressing *C9orf72* expanded repeats (7) may result is the mislocalization of RGNEF and TDP-43, again resulting in the dysregulation of *NEFL* mRNA.

Measuring the localization of endogenously expressing RGNEF – rather than transient expression of artificial constructs – is critical to our understanding of its role in healthy cells. Our current study proved the capacity for RGNEF to undergo nuclear import in transiently transfected cells. Elucidating the endogenous localization of RGNEF in healthy and ALS motor neurons will help further our understanding of RGNEF's role in motor neuron degeneration.

4.3   Implications for our understanding of PH domains

Of note is our novel finding of a PH domain-embedded NLS. Though PH domains are the eleventh most common domain in the human genome (17), to date none have been reported to contain an NLS. Because importin-α binding by NLSs (94) and PtdIns (17) binding by PH domains is facilitated by basic residues, it is reasonable to believe that they occur in tandem more frequently than what has been found in the literature. One potential reason for under reporting NLSs within PH domains may be due to the highly conserved folding present in PH domains. Domain prediction software that does not take into consideration the molecular folding could easily yield false positive or false negatives in predicting NLSs. Notice in Figure 16 how the basic residues of the NLS are located on the edges of the β-sheets, which form the β-

sandwiches. This locates the residues on the exterior of the domain (Fig. 16) and reduces the probability of steric interference. Predictive software may falsely predict an NLS composed of basic residues within the β-sandwich, where they are inaccessible for interaction. As well, software using the classical definition of bipartite NLSs, which set the maximum length of the linker region between basic clusters at 12 residues, may fail to predict NLS. Work done in 2010 has since proven that the linker region may be as long as 29 residues (95). Software using this classical definition would fail to predict an NLS in a PH domain as the length of the β-sheets is fairly well conserved at around 16 residues (Fig. 9) meaning the software would not accurately predict residues located on the exterior of the molecule.

Table 6 shows the results derived from analysis using cNLS Mapper (http://nls-mapper.iab.keio.ac.jp/cgi-bin/NLS_Mapper_form.cgi) for 15 other PH domain-containing proteins. For reference, RGNEF is shown along the top and in italics. Proteins are sorted in descending ordered based on estimate molecular weight. Amino acids sequences for all proteins were obtained from PubMed. Accession numbers for all proteins are available in Appendix B. A score is assigned by cNLS mapper to predict the localization of the protein. Scores between three to five are predict that the protein will spend equal amounts of time in both the nucleus and cytoplasm. Scores above five indicate the protein is predicted to spend more time in the nucleus than the cytoplasm. Scores below three indicate the protein is predicted to spend more time in the cytoplasm than the nucleus (97,124,125). A putative bipartite NLS was identified in every PH domain analyzed using cNLS mapper and many identified obtained a score about three. Of note are proteins like Spectrin β 2 (134), Phospholipase C β (135), and Burton's tyrosine kinase (BTK) (136), which have previously been shown in the literature to localize to the nucleus despite their large molecular weight. For example, BTK is reported to localize predominantly to the cytoplasm but has also been observed within the nucleus (136). The mechanism by which BTK undergoes nucleus localization has not been identified (137). Work done in 2000 investigated a putative NLS within the PH domain of BTK and concluded that it was not responsible for nuclear import. However, it is worth noting that the techniques used in this work were not as sensitive as what we have outlined here. In particular, the only construct used to

Table 6: Results of analysis using cNLS Mapper on other PH domain-containing proteins

Protein Name	Score by cNLS Mapper	Length (AA)	Molecular Weight* (kDa)	
RGNEF	*4.4*	*1731*	*190.4*	G**R**F**K**DILALLLTDVLLFLQE**K**DQ**K**YIFA
Spectrin β 2	5.2	2390	262.9	EAFG**KK**AAN**R**SWQNVYCVL**RR**GSLGFY**K**DA**K**A
Phospholipase C γ	3.1	1290	141.9	EI**R**PG**K**TS**R**DFD**R**YQEDPAF**R**PDQSHCFVILY
Phospholipase C β	3.1	1181	129.9	**R**FG**K**FA**K**MP**K**SQ**K**L**R**DVFNMDFPDNSFLL**K**TLT
Dynamin-1	4.9	851	93.61	**K**GGS**K**EYWFVLTAENLSWY**K**DDEE**K**E**KK**YMLS
Phospholipase C δ	3.9	756	83.1	ES**RK**VM**R**TPESQLFSIEDIQEV**R**MGH**R**TEG
Burton's tyrosine kinase (BTK)	4.2	693	76.2	NF**KKR**LFLLTVH**K**LSYYEYDFE**R**G**RR**GS**K**
beta adrenergic receptor kinase	4.7	689	75.7	**RK**CLLL**K**I**R**GG**K**QFILQCDSDPELVQW**KK**EL**R**D
Tyrosine-protein kinase (TSK)	5.3	620	68.2	**RR**TSPSNF**K**V**R**FFVLT**K**ASLAYFED**R**HG**KK**RTL**K**
3-phosphoinositide-dependent protein kinase	5.6	556	61.1	**RK**GLFA**RRR**QLLLTEGPHLYYVDPVN**K**VL**K**GE
RAC-alpha serine/threonine-protein kinase	2.9	480	52.8	FIGY**K**E**R**PQDVDQ**R**EAPLNNFSVAQCQLM**K**TE
Pleckstrin homology domain-containing family A member 2 [N-Terminal PH domain]	5.7	425	46.7	**K**Q**K**P**K**TPFCFVINALSQ**R**YFLQANDQ**K**DM**K**DW

Pleckstrin homology domain-containing family A member 2 [C-Terminal PH domain]	4.2	425	46.7	**RK**SW**KRR**FFALDDFTICYF**K**CEQD**R**EPL**R**TI
Arno protein	4.2	399	43.8	**R**VK**TW**KRR**WFILTDNCLYYFEYTTD**K**EP**R**GIIP
Pleckstrin [N-Terminal PH domain]	4.4	350	38.5	ITTT**K**QQDHFFQAAFLEE**R**DAWV**R**DI**KK**AI
Pleckstrin [C-Terminal PH domain]	2.1	350	38.5	**RRK**NW**K**V**RK**FIL**R**EDPAYLHYYDPAGAEDPLGAIH
Pleckstrin homology domain-containing family A member 3	3.6	300	33	EI**K**VHSADNT**R**MELIIPGEQHFYM**K**AVNA
DAPP1 protein	2.8	280	30.8	EGYLT**K**QGGLV**K**TW**K**T**R**WFTLH**R**NEL**K**YF**K**D

* Molecular weight for each protein was estimated based on number of amino acids using the formula

number of amino acids X 110 dalton/amino acids = Molecular weight in dalton

Higher scores indicate stronger NLS activities. A score of 8, 9, or 10 is exclusively localized to the nucleus, a score

of 7 or 8 partially localized to the nucleus, a score of 3, 4, or 5 localized to both the nucleus and the cytoplasm , and a

score of 1 or 2 localized to the cytoplasm.

Values between three to five are highlighted in green. Values below three are highlighted in blue.

analyze the putative NLS involved the deletion of not only the entire PH domain but also the adjacent tec homology (TH) domain: a loss of about 200 amino acids or an estimated 22kDa (138). It is possible that this differential in molecular weight may have confounded their analysis of nuclear localization. As well, this large deletion may have affected molecular folding of the protein. We hypothesize that were we to use site directed mutagenesis to mutate only those basic residues likely to be involved in nuclear import we would be able to show differential nuclear localization. Figure 26 shows the location of the NLS which we have identified using cNLS mapper. Like for RGNEF, the model of the PH domain of BTK shows the basic residues collect along the exterior of the domain, suggesting they would be available for interaction with importin-α.

Given the evidence our analysis of 15 PH domain-containing proteins and our specific elucidation of the PH domain of RGNEF has yielded, it is likely that the number of PH domain-embedded NLS is underrepresented in the literature. The techniques outlined here should be used in future work to further validate this hypothesis.
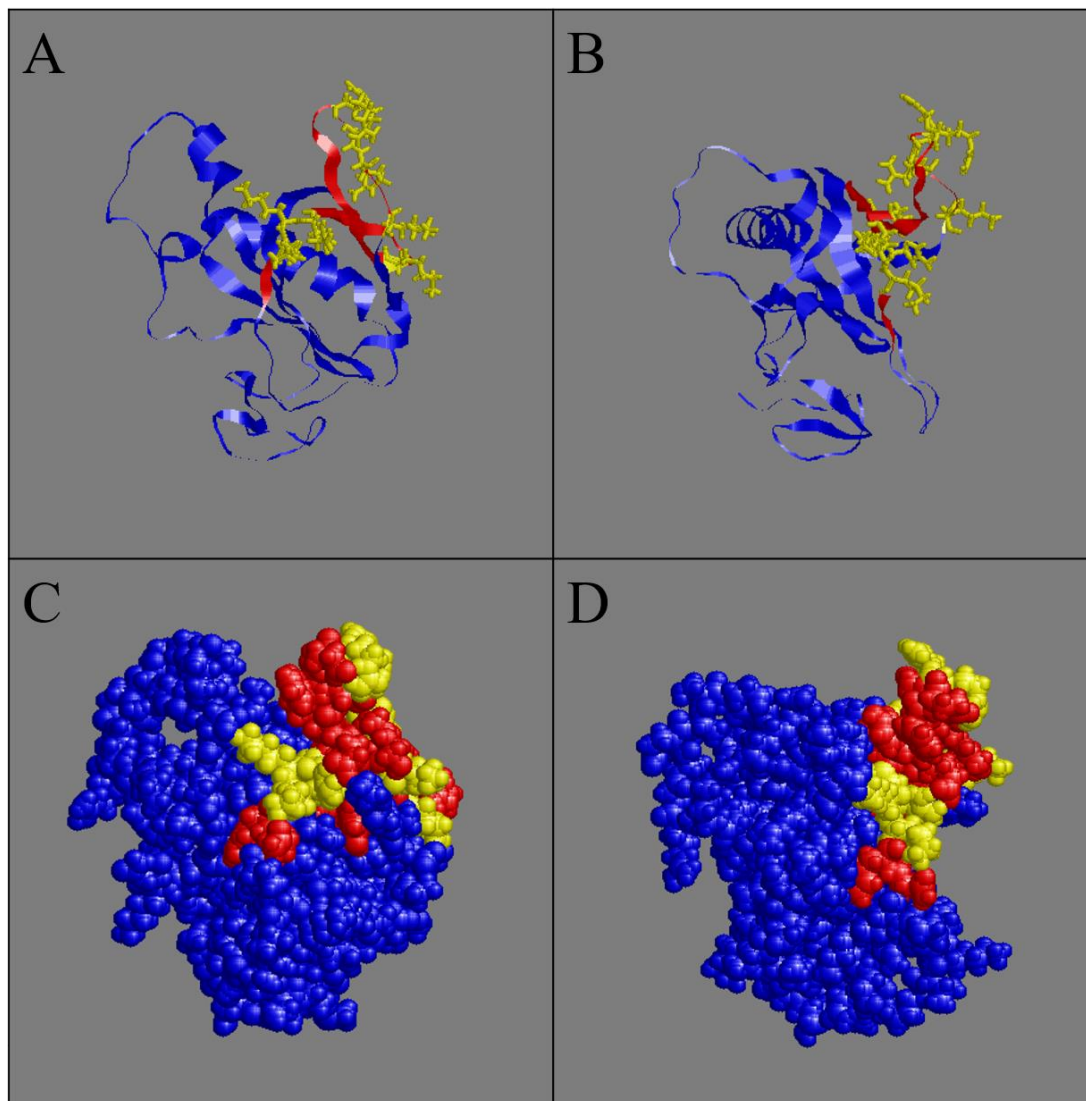
Figure 26 The location of the putative NLS in BTK. Panels A & C and B & D show the same rotation with one being a ribbon model (A & B) and the other being a space fill model (C & D). The NLS (red) is shown to be located on the exterior of the PH domain with the basic residues (yellow). Panel E shows the location of the NLS within the amino acid sequence. The PH domain is shown in green font. The putative NLS is highlighted in green. The basic residues of the NLS are marked by asterisks above.

References

1.   Rowland LP, Shneider NA. Amyotrophic lateral sclerosis. N Engl J Med. 2001;344(22):1688–1700.

2.   Strong MJ. The evidence for altered RNA metabolism in amyotrophic lateral sclerosis (ALS). J Neurol Sci. 2010;288(1–2):1–12.

3.   Strong MJ. Amyotrophic lateral sclerosis: contemporary concepts in etiopathogenesis and pharmacotherapy. Expert Opin Investig Drugs. 2004;13(12):1593–1614.

4.   Miller RG, Mitchell JD, H MD, Moore DH. Riluzole for amyotrophic lateral sclerosis (ALS)/ motor neuron disease (MND). Cochrane Database Syst Rev. 2012;3(3):191–206.

5.   Cudkowicz ME, McKenna-Yasek D, Sapp PE, Chin W, Geller B, Hayden DL, et al. Epidemiology of mutations in superoxide dismutase in amyotrophic lateral sclerosis. Ann Neurol. 1997;41:210–221.

6.   Renton AE, Majounie E, Waite A, Simón-Sánchez J, Rollinson S, Gibbs JR, et al. A hexanucleotide repeat expansion in C9ORF72 is the cause of chromosome 9p21-linked ALS-FTD. Neuron. 2011;72(2):257–268.

7.   Boeynaems S, Bogaert E, Michiels E, Gijselinck I, Sieben A, Jovičić A, et al. Drosophila screen connects nuclear transport genes to DPR pathology in c9ALS/FTD. Sci Rep. 2016;6:1–8.

8.   Jovičić A, Mertens J, Boeynaems S, Bogaert E, Chai N, Yamada SB, et al. Modifiers of C9orf72 dipeptide repeat toxicity connect nucleocytoplasmic transport defects to FTD/ALS. Nat Neurosci. 2015;18(9):1226–1229.

9.   Kwon I, Xiang S, Kato M, Wu L, Theodoropoulos P, Wang T, et al. Poly-dipeptides encoded by the C9ORF72 repeats bind nucleoli, impede RNA biogenesis, and kill cells. Science. 2014;345(6201):1139–1145.

10.   Robinson R, editor. Biology - Macmillian Science Library (4 Volume Set). Hardcover. New York: Macmillian Reference USA; 2001.

11.   Lange A, Mills RE, Lange CJ, Stewart M, Devine SE, Corbett AH. Classical nuclear

localization signals: definition, function, and interaction with importin alpha. J Biol Chem. 2007;282(8):5101–5105.

12. Kalderon D, Richardson WD, Markham AF, Smith AE. Sequence requirements for nuclear location of simian virus 40 large-T antigen. Nature. 1984;311:33–38.

13. Kalderon D, Roberts BL, Richardson WD, Smith AE. A short amino acid sequence able to specify nuclear location. Cell. 1984;39:499–509.

14. Hübner S, Xiao CY, Jans DA. The protein kinase CK2 site (Ser 111/112) enhances recognition of the simian virus 40 large T-antigen nuclear localization sequence by importin. J Biol Chem. 1997;272(27):17191–17195.

15. Fahrenkrog B, Aebi U. The nuclear pore complex: nucleocytoplasmic transport and beyond. Nat Rev Mol Cell Biol. 2003;4(10):757–766.

16. Matsuura Y, Stewart M. Structural basis for the assembly of a nuclear export complex. Nature. 2004;432(7019):872–877.

17. Rossman KL, Der CJ, Sondek J. GEF means go: turning on Rho GTPases with guanine nucleotide-exchange factors. Nat Rev Mol Cell Biol. 2005;6:167–180.

18. Yan J, Wen W, Chan LN, Zhang M. Split pleckstrin homology domain-mediated cytoplasmic-nuclear localization of PI3-kinase enhancer GTPase. J Mol Biol. 2008;378:425–435.

19. Droppelmann CA, Keller BA, Campos-Melo D, Volkening K, Strong MJ. Rho guanine nucleotide exchange factor is an NFL mRNA destabilizing factor that forms cytoplasmic inclusions in amyotrophic lateral sclerosis. Neurobiol Aging. 2013;34(1):248–262.

20. Droppelmann CA, Wang J, Campos-Melo D, Keller B, Volkening K, Hegele RA, et al. Detection of a novel frameshift mutation and regions with homozygosis within ARHGEF28 gene in familial amyotrophic lateral sclerosis. Amyotroph Lateral Scler Frontotemporal Degener. 2013;14(5–6):444–451.

21. Keller BA, Volkening K, Droppelmann CA, Ang LC, Rademakers R, Strong MJ. Co-aggregation of RNA binding proteins in ALS spinal motor neurons: evidence of a

common pathogenic mechanism. Acta Neuropathol. 2012;124(5):733–747.

22. Volkening K, Leystra-Lantz C, Strong MJ. Human low molecular weight neurofilament (NFL) mRNA interacts with a predicted p190RhoGEF homologue (RGNEF) in humans. Amyotroph lateral Scler. 2010;11:97–103.

23. Al-Chalabi A, Hardiman O. The epidemiology of ALS: a conspiracy of genes, environment and time. Nat Rev Neurol. 2013;9(11):617–628.

24. Scotton WJ, Scott KM, Moore DH, Almedom L, Wijesekera LC, Janssen A, et al. Prognostic categories for amyotrophic lateral sclerosis. Amyotroph Lateral Scler. 2012;13(6):502–508.

25. Garruto RM. A commentary on neuronal degeneration and cell death in Guam ALS and PD: an evolutionary process of understanding. Curr Alzheimer Res. 2006;3(4):397–401.

26. Plato CC, Garruto RM, Galasko D, Craig UK, Plato M, Gamst A, et al. Amyotrophic lateral sclerosis and parkinsonism-dementia complex of Guam: changing incidence rates during the past 60 years. Am J Epidemiol. 2002;157(2):149–157.

27. Cox PA, Sacks OW. Cycad neurotoxins, consumption of flying foxes, and ALS-PDC disease in Guam. Neurology. 2002;58:956–959.

28. Steele JC, McGeer PL. The ALS/PDC syndrome of Guam and the cycad hypothesis. Neurology. 2008;70:1984–1990.

29. Simpson CL, Al-Chalabi A. Amyotrophic lateral sclerosis as a complex genetic disease. Biochim Biophys Acta. 2006;1762:973–985.

30. Hanby MF, Scott KM, Scotton W, Wijesekera L, Mole T, Ellis CE, et al. The risk to relatives of patients with sporadic amyotrophic lateral sclerosis. Brain. 2011;134:3451–3454.

31. Strong MJ, Kesavapany S, Pant HC. The pathobiology of amyotrophic lateral sclerosis: a proteinopathy? J Neuropathol Exp Neurol. 2005;64(8):649–664.

32. Leigh PN, Whitwell H, Garofalo O, Buller J, Swash M, Martin JE, et al. Ubiquitin-immunoreactive intraneuronal inclusions in amyotrophic lateral sclerosis morphology,

distribution, and specificity. Brain. 1991;114:775–788.

33.   Neumann M, Sampathu DM, Kwong LK, Truax AC, Micsenyi MC, Chou TT, et al. Ubiquitinated TDP-43 in frontotemporal lobar degeneration and amyotrophic lateral sclerosis. Science . 2006;314(5796):130–133.

34.   Deng HX, Zhai H, Bigio EH, Yan J, Fecto F, Ajroud K, et al. FUS-immunoreactive inclusions are a common feature in sporadic and non-SOD1 familial amyotrophic lateral sclerosis. Ann Neurol. 2010;67:739–748.

35.   Ince PG, Lowe J, Shaw PJ. Amyotrophic lateral sclerosis: current issues in classification, pathogenesis and molecular pathology. Neuropathol Appl Neurobiol. 1998;24:104–117.

36.   Hays AP, Naini A, He CZ, Mitsumoto H, Rowland LP. Sporadic amyotrophic lateral sclerosis and breast cancer: hyaline conglomerate inclusions lead to identification of SOD1 mutation. J Neurol Sci. 2006;242:67–69.

37.   Lee MK, Xu Z, Wong PC, Cleveland DW. Neurofilaments are obligate heteropolymers in vivo. J Cell Biol. 1993;122(6):1337–1350.

38.   Szaro B, Strong M. Post-transcriptional control of neurofilaments: New roles in development, regeneration and neurodegenerative disease. Trends Neurosci. 2010;33:27–37.

39.   Strong MJ, Volkening K, Hammond R, Yang W, Strong W, Leystra-Lantz C, et al. TDP43 is a human low molecular weight neurofilament (hNFL) mRNA-binding protein. Mol Cell Neurosci. 2007;35(2):320–327.

40.   Seilhean D, Takahashi J, El Hachimi KH, Fujigasaki H, Levre A-S, Biancalana V, et al. Amyotrophic lateral sclerosis with neuronal intranuclear protein inclusions. Acta Neuropathol. 2004;108(1):81–87.

41.   Mackenzie IRA, Feldman HH. Immunohistochemistry suggests classic motor neuron disease, motor neuron disease with dementia, and frontotemporal dementia of the motor neuron disease type. J Neuropathol Exp Neurol. 2005;64(8):730–739.

42.   Zhang H, Tan C-F, Mori F, Tanji K, Kakita A, Takanhashi H, et al. TDP-43 -

immunoreactive neuronal and glial inclusions in the neostriatum in amyotrophic lateral sclerosis with and without dementia. Acta Neuropathol. 2008;115(1):115–122.

43.   Mackenzie IR. A, Strong M, Zinman L, Baker M. Pathological heterogeneity in amyotrophic lateral sclerosis with FUS mutations: two distinct patterns correlating with disease severity and mutation. 2012;122(1):87–98.

44.   Renton AE, Chiò A, Traynor BJ. State of play in amyotrophic lateral sclerosis genetics. Nat Neurosci. 2014;17(1):17–23.

45.   DeJesus-Hernandez M, Mackenzie IR, Boeve BF, Boxer AL, Baker M, Rutherford NJ, et al. Expanded GGGGCC hexanucleotide repeat in noncoding region of C9ORF72 causes chromosome 9p-linked FTD and ALS. Neuron. 2011;72(2):245–256.

46.   Al-Chalabi A, Jones A, Troakes C, King A, Al-Sarraj S, van den Berg LH. The genetics and neuropathology of amyotrophic lateral sclerosis. Acta Neuropathol. 2012 Sep;124(3):339–352.

47.   Zu T, Gibbens B, Doty NS, Gomes-pereira M, Huguet A, Stone MD. Non-ATG – initiated translation directed by microsatellite expansions. PNAS. 2010;108(1):260–265.

48.   Neumann M, Sampathu DM, Kwong LK, Truax AC, Micsenyi MC, Chou TT, et al. Ubiquitinated TDP-43 in frontotemporal lobar degeneration and amyotrophic lateral sclerosis. Science. 2006;314(5796):130–133.

49.   Arai T, Hasegawa M, Akiyama H, Ikeda K, Nonaka T, Mori H, et al. TDP-43 is a component of ubiquitin-positive tau-negative inclusions in frontotemporal lobar degeneration and amyotrophic lateral sclerosis. Biochem Biophys Res Commun. 2006;351(3):602–611.

50.   Sreedharan J, Blair IP, Tripathi VB, Hu X, Vance C, Ackerley S, et al. TDP-43 mutations in familial and sporadic amyotrophic lateral sclerosis. Science. 2008;319(5870):1668–1672.

51.   Buratti E, Dork T, Zuccato E, Pagani F, Romano M, Baralle FE. Nuclear factor TDP-43 and SR proteins promote in vitro and in vivo CFTR exon 9 skipping. EMBO J. 2001;20(7):1774–1784.

52. Jovičić A, Paul JW, Gitler AD. Nuclear transport dysfunction: a common theme in amyotrophic lateral sclerosis and frontotemporal dementia. J Neurochem. 2016;43:1–11.

53. Nishimura AL, Upunski V, Troakes C, Kathe C, Fratta P, Howell M, et al. Nuclear import impairment causes cytoplasmic trans-activation response DNA-binding protein accumulation and is associated with frontotemporal lobar degeneration. Brain. 2010;133(6):1763–1771.

54. Winton MJ, Igaz LM, Wong MM, Kwong LK, Trojanowski JQ, Lee VMY. Disturbance of nuclear and cytoplasmic TAR DNA-binding protein (TDP-43) induces disease-like redistribution, sequestration, and aggregate formation. J Biol Chem. 2008;283(19):13302–13309.

55. Ayala YM, Zago P, D'Ambrogio A, Xu Y-F, Petrucelli L, Buratti E, et al. Structural determinants of the cellular localization and shuttling of TDP-43. J Cell Sci. 2008;121(22):3778–3785.

56. Lee EB, Lee VM-Y, Trojanowski JQ. Gains or losses: molecular mechanisms of TDP43-mediated neurodegeneration. Nat Rev Neurosci. 2012;13(1):38–50.

57. Lagier-Tourenne C, Polymenidou M, Cleveland DW. TDP-43 and FUS/TLS: emerging roles in RNA processing and neurodegeneration. Hum Mol Genet. 2010;19(R1):46–64.

58. Moisse K, Volkening K, Leystra-Lantz C, Welch I, Hill T, Strong MJ. Divergent patterns of cytosolic TDP-43 and neuronal progranulin expression following axotomy: implications for TDP-43 in the physiological response to neuronal injury. Brain Res. 2009;1249:202–211.

59. Bekenstein U, Soreq H. Heterogeneous nuclear ribonucleoprotein A1 in health and neurodegenerative disease: from structural insights to post-transcriptional regulatory roles. Mol Cell Neurosci. 2013;56:436–446.

60. Kim HJ, Kim NC, Wang Y, Scarborough EA, Diaz Z, Maclea KS, et al. Prion-like domain mutations in hnRNPs cause multisystem proteinopathy and ALS. NIH public access. 2013;495(7442):467–473.

61. Guil S, Long JC, Cáceres JF. hnRNP A1 relocalization to the stress granules reflects a role

in the stress response. Mol Cell Biol. 2006;26(15):5744–5758.

62. Siomi H, Dreyfuss G. A nuclear localization domain in the hnRMP A1 protein. J Cell Bio. 1995;129(3):551–560.

63. Weighardt F, Biamonti G, Riva S. Nucleo-cytoplasmic distribution of human hnRNP proteins: a search for the targeting domains in hnRNP A1. J Cell Sci. 1995;108:545–555.

64. Pollard VW, Michael M, Nakielny S, Siomi MC, Wang F, Dreyfuss G. A novel receptor-medicated nuclear protein import pathway. Cell. 1996;86:985–993.

65. Matthew Michael W, Choi M, Dreyfuss G. A nuclear export signal in hnRNP A1: A signal-mediated, temperature-dependent nuclear protein export pathway. Cell. 1995;83(3):415–422.

66. Fridell RA, Truant R, Thorne L, Benson RE, Cullen BR. Nuclear import of hnRNP A1 is mediated by a novel cellular cofactor related to karyopherin-beta. J Cell Sci. 1997;110:1325–1331.

67. Rebane A, Aab A, Steitz JA. Transportins 1 and 2 are redundant nuclear import factors for hnRNP A1 and HuR. RNA. 2004;10(4):590–599.

68. Dormann D, Rodde R, Edbauer D, Bentmann E, Fischer I, Hruscha A, et al. ALS-associated fused in sarcoma (FUS) mutations disrupt transportin-mediated nuclear import. EMBO J. 2010;29(16):2841–2857.

69. Tan AY, Manley JL. The TET family of proteins: functions and roles in disease. J Mol Cell Biol. 2009;1(2):82–92.

70. Neumann M, Bentmann E, Dormann D, Jawaid A, Dejesus-Hernandez M, Ansorge O, et al. FET proteins TAF15 and EWS are selective markers that distinguish FTLD with FUS pathology from amyotrophic lateral sclerosis with FUS mutations. Brain. 2011;134(9):2595–2609.

71. Couthouis J, Hart MP, Erion R, King OD, Diaz Z, Nakaya T, et al. Evaluating the role of the FUS/TLS-related gene EWSR1 in amyotrophic lateral sclerosis. Hum Mol Genet. 2012;21(13):2899–2911.

72. Zakaryan RP, Gehring H. Identification and characterization of the nuclear localization/retention signal in the EWS proto-oncoprotein. J Mol Biol. 2006;363(1):27–38.

73. Leemann-Zakaryan RP, Pahlich S, Grossenbacher D, Gehring H. Tyrosine phosphorylation in the C-terminal nuclear localization and retention signal (C-NLS) of the EWS protein. Sarcoma. 2011;2011:1–6.

74. Couthouis J, Hart MP, Shorter J, Dejesus-hernandez M, Erion R, Oristano R, et al. A yeast functional screen predicts new candidate ALS disease genes. Proc Natl Acad Sci U S A. 2011;108(52):20881–20890.

75. Marko M, Vlassis A, Guialis A, Leichter M. Domains involved in TAF15 subcellular localisation: dependence on cell type and ongoing transcription. Gene. 2012;506(2):331–338.

76. Jobert L, Argentini M, Tora L. PRMT1 mediated methylation of TAF15 is required for its positive gene regulatory function. Exp Cell Res. 2009;315(7):1273–1286.

77. Maeshima K, Iino H, Hihara S, Funakoshi T, Watanabe A, Nishimura M, et al. Nuclear pore formation but not nuclear growth is governed by cyclin-dependent kinases (Cdks) during interphase. Nat Struct Mol Biol. 2010;17(9):1065–1071.

78. Reichelt R, Holzenburg A, Buhle EL, Jarnik M, Engel A, Aebi U. Correlation between structure and mass-distribution of the nuclear pore complex and of distinct pore complex components. J Cell Biol. 1990;110(4):883–894.

79. Akey CW, Radermacher M. Architecture of the Xenopus nuclear pore complex revealed by three-dimensional cryo-electron microscopy. J Cell Biol. 1993;122(1):1831–1839.

80. Stoffler D, Feja B, Fahrenkrog B, Walz J, Typke D, Aebi U. Cryo-electron tomography provides novel insights into nuclear pore architecture: Implications for nucleocytoplasmic transport. J Mol Biol. 2003;328(1):119–130.

81. Rollenhagen C, Muhlhausser P, Kutay U, Pante N. Importin β-depending nuclear import pathways: role of the adapter proteins in the docking and releasing steps. Mol Biol Cell. 2003;14:2559–2569.

82. Shah S, Tugendreich S, Forbes D. Major binding sites for the nuclear import receptor are the internal nucleoporin Nup153 and the adjacent nuclear filament protein Tpr. J Cell Biol. 1998;141(1):31–49.

83. Rexach M, Blobel G. Protein import into nuclei: association and dissociation reactions involving transport substrate, transport factors, and nucleoporins. Cell. 1995;83(5):683–692.

84. Marfori M, Mynott A, Ellis JJ, Mehdi AM, Saunders NFW, Curmi PM, et al. Molecular basis for specificity of nuclear import and prediction of nuclear localization. Biochim Biophys Acta. 2011;1813(9):1562–1577.

85. Peters R. Nucleo-cytoplasmic flux and intracellular mobility in single hepatocytes measured by fluorescence microphotolysis. EMBO J. 1984;3(8):1831–1836.

86. Fontes MR, Teh T, Kobe B. Structural basis of recognition of monopartite and bipartite nuclear localization sequences by mammalian importin-alpha. J Mol Biol. 2000 14;297:1183–1194.

87. Görlich D, Mattaj LW. Nucleocytoplasmic transport. Science. 1996;271(5255):1513–1518.

88. Mattaj IW, Englmeier L. Nucleocytoplasmic transport: the soluble phase. Annu Rev Biochem. 1998;67(1):265–306.

89. Wang R, Brattain MG. The maximal size of protein to diffuse through the nuclear pore is larger than 60 kDa. FEBS Lett. 2007;581(17):3164–3170.

90. Radu A, Blobel G, Moore MS. Identification of a protein complex that is required for nuclear protein import and mediates docking of import substrate to distinct nucleoporins. Proc Natl Acad Sci U S A. 1995;92(5):1769–1773.

91. Mosammaparast N, Pemberton LF. Karyopherins: from nuclear-transport mediators to nuclear-function regulators. Trends Cell Biol. 2004;14(10):547–556.

92. Kobe B, Kemp BE. Active site-directed protein regulation. Nature. 1999;402(6760):373–376.

93. Moroianu J, Blobel G, Radu A. The binding site of karyopherin alpha for karyopherin beta overlaps with a nuclear localization sequence. Proc Natl Acad Sci U S A. 1996;93(13):6572–6576.

94. Dingwall C, Laskey RA. Nuclear targeting sequences - a consensus? Trends Biochem Sci. 1991;16:478–481.

95. Lange A, McLane LM, Mills RE, Devine SE, Corbett AH. Expanding the definition of the classical bipartite nuclear localization signal. Traffic. 2010;11(3):311–323.

96. Conti E, Uy M, Leighton L, Blobel G, Kuriyan J. Crystallographic analysis of the recognition of a nuclear localization signal by the nuclear import factor karyopherin α. Cell. 1998;94:193–204.

97. Kosugi S, Hasebe M, Matsumura N, Takashima H, Miyamoto-Sato E, Tomita M, et al. Six classes of nuclear localization signals specific to different binding grooves of importin alpha. J Biol Chem. 2009;284(1):478–485.

98. Lee SJ, Matsuura Y, Liu SM, Stewart M. Structural basis for nuclear import complex dissociation by RanGTP. Nature. 2005;435(7042):693–696.

99. Moore W, Zhang C, Clarke P. Targeting of RCC1 to chromosomes is required for proper mitotic spindle assembly in human cells. 2002;12(2):1442–1447.

100. Nemergut ME, Mizzen CA, Stukenberg T, Allis CD, Macara IG. Chromatin docking and exchange activity enhancement of RCC1 by histones H2A and H2B. Science. 2001;292(5521):1540–1543.

101. Bhardwaj A, Cingolani G. Conformational selection in the recognition of the snurportin importin β binding domain by importin β. Biochemistry. 2010;49(24):5042–5047.

102. Mitrousis G, Olia AS, Walker-Kopp N, Cingolani G. Molecular basis for the recognition of snurportin 1 by importin. J Biol Chem. 2008;283(12):7877–7884.

103. Strasser A, Dickmanns A, Lührmann R, Ficner R. Structural basis for m3G-cap-mediated nuclear import of spliceosomal UsnRNPs by snurportin1. EMBO J. 2005;24(13):2235–2243.

104. Wohlwend D, Strasser A, Dickmanns A, Ficner R. Structural basis for RanGTP independent entry of spliceosomal U snRNPs into the nucleus. J Mol Biol. 2007;374(4):1129–1138.

105. Jäkel S, Görlich D. Importin β, transportin, RanBP5 and RanBP7 mediate nuclear import of ribosomal proteins in mammalian cells. EMBO J. 1998;17(15):4491–4502.

106. Lam MHC, Briggs LJ, Hu W, Martin TJ, Gillespie MT, Jans DA. Importin beta recognizes parathyroid hormone-related protein (PTHrP) with high affinity and mediates its nuclear import in the absence of importin alpha. J Biol Chem. 1999;274(11):7391–7398.

107. Forwood JK, Lam MH, Jans DA. Nuclear import of Creb and AP-1 transcription factors requires importin-beta 1 and Ran but is independent of importin-alpha. Biochemistry. 2001;40(17):5208–5217.

108. Moore JD, Yang J, Truant R, Kornbluth S. Nuclear import of Cdk/cyclin complexes: Identification of distinct mechanisms for import of Cdk2/cyclin E and Cdc2/cyclin B1. J Cell Biol. 1999;144(2):213–224.

109. Truant R, Cullen BR. The arginine-rich domains present in human immunodeficiency virus type 1 Tat and Rev function as direct importin beta-dependent nuclear localization signals. Mol Cell Biol. 1999;19(2):1210–1217.

110. Palmeri D, Malim MH. Importin beta can mediate the nuclear import of an arginine-rich nuclear localization signal in the absence of importin alpha. Mol Cell Biol. 1999;19(2):1218–1225.

111. Cingolani G, Bednenko J, Gillespie MT, Gerace L. Molecular basis for the recognition of a nonclassical nuclear localization signal by importin beta. Mol Cell. 2002;10:1345–1353.

112. Lee BJ, Cansizoglu AE, Suel KE, Louis TH, Zhang Z, Chook YM. Rules for nuclear localization sequence recognition by karyopherinβ2. Cell. 2006;126(3):543–558.

113. Lemmon MA, Ferguson KM. Signal-dependent membrane targeting by pleckstrin homology (PH) domains. Biochem J. 2000;350:1–18.

114. Blomberg N, Baraldi E, Nilges M, Saraste M. The PH superfold: a structural scaffold for multiple functions. Trends Biochem Sci. 1999;24(11):441–445.

115. Tyers M, Rachubinski R ichard A, Stewart MI, Varrichio A ngela M, Shorr RGL, Haslam RJ, et al. Molecular cloning and expression of the major protein kinase C substrate of platelets. Nature. 1988;333(2):470–473.

116. Roy A, Kucukural A, Zhang Y. I-TASSER: a unified platform for automated protein structure and function prediction. Nat Protoc. 2010;5(4):725–738.

117. Yang J, Yan R, Roy A, Xu D, Poisson J, Zhang Y. The I-TASSER Suite: protein structure and function prediction. Nat Methods. 2015;12(1):7–8.

118. Zhang Y. I-TASSER server for protein 3D structure prediction. BMC Bioinformatics. 2008;9(40):1–8.

119. Wen W, Yan J, Zhang M. Structural characterization of the split pleckstrin homology domain in phospholipase C-gamma1 and its interaction with TRPC3. J Biol Chem. 2006;281(17):12060–12068.

120. Yan J, Wen W, Xu W, Long J, Adams ME, Froehner SC, et al. Structure of the split PH domain and distinct lipid-binding properties of the PH-PDZ supramodule of alpha-syntrophin. Embo J. 2005;24:3985–3995.

121. Ma Y, Tang L, Chen L, Zhang B, Deng P, Wang J, et al. ARHGEF28 gene exon 6/intron 6 junction mutations in Chinese amyotrophic lateral sclerosis cohort. Amyotroph Lateral Scler Frontotemporal Degener. 2014;15(3–4):309–311.

122. Zhang M, Xi Z, Ghani M, Jia P, Pal M, Werynska K, et al. Genetic and epigenetic study of ALS-discordant identical twins with double mutations in SOD1 and ARHGEF28. J Neurol Neurosurg Psychiatry. 2016;87(5):1–2.

123. Cheung KWH. The role of the RNA-binding protein rho guanine nucleotide exchange factor in the cellular stress response. Univ West Ontario - Electron Thesis Diss Repos. 2014;Paper 2440:1–128.

124. Kosugi S, Hasebe M, Entani T, Takayama S, Tomita M, Yanagawa H. Design of peptide

inhibitors for the importin alpha/beta nuclear import pathway by activity-based profiling. Chem Biol. 2008;15:940–949.

125. Kosugi S, Hasebe M, Tomita M, Yanagawa H. Systematic identification of cell cycle-dependent yeast nucleocytoplasmic shuttling proteins by prediction of composite motifs. Proc Natl Acad Sci USA. 2009;106(25):10171–10176.

126. Shaw G, Morse S, Ararat M, Graham FL. Preferential transformation of human neuronal cells by human adenoviruses and the origin of HEK 293 cells. Faseb J. 2002;10(2):1–15.

127. Encinas M, Iglesias M, Liu Y, Wang H, Muhaisen A, Cena V, et al. Sequential treatment of SH-SY5Y cells with retinoic acid and brain-derived neurotrophic factor gives rise. J Neurochem. 2000;75(3):991–1003.

128. Ho SN, Hunt HD, Horton RM, Pullen JK, Pease LR. Site-directed mutagenesis by overlap extension using the polymerase chain reaction. Gene. 1989;77:51–59.

129. Liu X, Fagotto F. A method to separate nuclear, cytosolic, and membrane-associated signaling molecules in cultured cells. Sci Signal. 2011;4(203):1–12.

130. Roth DM, Moseley GW, Pouton CW, Jans DA. Mechanism of microtubule-facilitated "fast track" nuclear import. J Biol Chem. 2011;286(16):14335–14351.

131. Phung-Koskas T, Pilon A, Poüs C, Betzina C, Sturm M, Bourguet-Kondracki ML, et al. STAT5B-mediated growth hormone signaling is organized by highly dynamic microtubules in hepatic cells. J Biol Chem. 2005;280(2):1123–1131.

132. Droppelmann C a, Campos-Melo D, Ishtiaq M, Volkening K, Strong MJ. RNA metabolism in ALS: when normal processes become pathological. Amyotroph Lateral Scler Frontotemporal Degener. 2014;15:321–336.

133. Meier J, Couillard-Després S, Jacomy H, Gravel C, Julien JP. Extra neurofilament NF-L subunits rescue motor neuron disease caused by overexpression of the human NF-H gene in mice. J Neuropathol Exp Neurol. 1999;58(10):1099–1110.

134. Tang Y, Katuri V, Dillner A, Mishra B, Deng C, Mishra L. Disruption of transforming growth factor-beta signaling in ELF beta-spectrin deficient mice. Science.

2003;299(January):1996–1999.

135. Kim CG, Park D, Rhee SG. The Role of carboxyl-terminal basic amino acids in G q alpha -dependent activation, particulate association, and nuclear localization of phospholipase C-beta1. J Biol Chem. 1996;271(35):21187–1192.

136. Nore BF, Vargas L, Mohamed a J, Brandén LJ, Bäckesjö CM, Islam TC, et al. Redistribution of Bruton's tyrosine kinase by activation of phosphatidylinositol 3-kinase and Rho-family GTPases. Eur J Immunol. 2000;30:145–154.

137. Mohamed A, Yu L, Backesjo C-M, Vargas L, Faryal R, Artis A, et al. Bruton's tyrosine kinase (Btk): function, regulation, and transformation with special emphasis on the PH domain. Immunol Revies. 2009;228:58–73.

138. Mohamed J, Vargas L, Nore BF, Backesjo CM, Christensson B, Smith CI. Nucleocytoplasmic shuttling of Bruton's tyrosine kinase. J Biol Chem. 2000;275(51):40614–40619.

Appendices
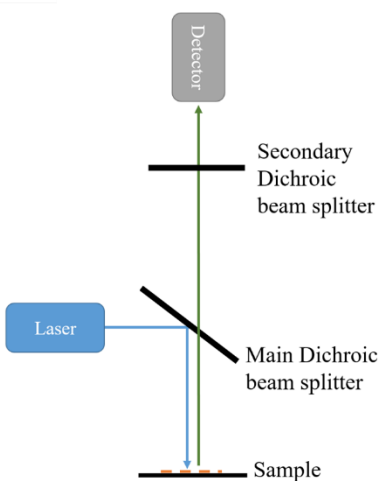
Fluorophores	Laser Wavelength	Main Dichroic beam splitter	Secondary Dichroic beam splitter
Hoechst	405nm	LP 425nm	BP 410 – 490nm
DAPI	405nm	LP 425nm	BP 410 – 490nm
eGFP	488nm	DD 488nm	BP 501 – 550nm
AlexaFlour 488	488nm	DD 488nm	BP 501 – 550nm
AlexaFlour 546	552nm	DD 552nm	BP 560 - 705nm

Appendix A: Optical Settings for Confocal Microscopy. The diagram illustrates the principles of confocal microscopy. Light generated by the laser is filtered by a main dichroic beam splitter and focused on the sample. When excited by specific wavelengths, fluorophores in the sample emit light. The light produced by this excitation is passed through a second dichroic beam splitter and is absorbed by a detector. The laser wavelengths, and main & secondary beam splitters used for each fluorophore are listed here.

BP = Band Pass Filter; DD = Double dichroic; LP = Low Pass Filter

Appendix B: Data obtained from PubMed for analysis using cNLS Mapper on other PH domain-containing proteins

Name	Access-ion Numb-er	Location of PH domain (Amino Acids)	Amino Acid Sequence of PH Domain
Spectrin beta chain, non-erythrocytic 2 [Homo sapiens]	NP_008877	2221..2324	MEGMLCRKQEMEAFGKKAANRSWQNVYCVLRRGSLGFYKDAKAASAGVPYHGEVPVSLAR AQGSVAFDYRKRKHVFKLGLQDGKEYLFQAKDEAEMSSWLRVVN
Phospholipase C-gamma [Homo sapiens]	AAA36452	29..151	LEVGTVMTLFYSKKSQRPERKTFQVKLETRQITWSRGADKIEGAIDIREIKEIRPGKTSRDFDRY QEDPAFRPDQSHCFVILYGMEFRLKTLSLQATSEDEVNMWIKGLTWLMEDTLQAPTPL
Phospholipase C-beta-2 [Homo sapiens]	AAA36453	17..144	LSQGERFIKWDDETTVASPVILRVDPKGYYLYWTYQSKEMEFLDITSIRDTRFGKFAKMPKSQ KLRDVFNMDFPDNSFLLKTLTVVSGPDMVDLTFHNFVSYKENVGKAWAEDVLALVKHPLTA NASR
Dynamin-1 [Homo Sapiens]	AAH50279	520..623	VIRKGWLTINNIGIMKGGSKEYWFVLTAENLSWYKDDEEKEKKYMLSVDNLKLRDVEKGFM SSKHIFALFNTEQRNVYKDYRQLELACETQEEVDSWKASFLRA
Phospholipase c delta 1 [Homo sapiens]	AAA73567	22..139	LLKGSQLLKVKSSSWRRERFYKLQEDCKTIWQESRKVMRTPESQLFSIEDIQEVRMGHRTEGL EKFARDVPEDRCFSIVFKDQRNTLDLIAPSPADAQHWVLGLHKIIHHSGSMDQRQ
Tyrosine-protein kinase BTK isoform 3 [Homo sapiens]	NP_001274273	40..200	LESIFLKRSQQKKKTSPLNFKKRLFLLTVHKLSYYEYDFERGRRGSKKGSIDVEKITCVETVVP EKNPPPERQIPRRGEESSEMEQISIIERFPYPFQVVYDEGPLYVFSPTEELRKRWIHQLKNVIRYN SDLVQKYHPCFWIDGQYLCCSQTAKNAMGCQ
Beta adrenergic receptor kinase [Homo Sapiens]	CAA43470	553..670	YALGKDCIMHGYMSKMGNPFLTQWQRRYFYLFPNRLEWRGEGEAPQSLLTMEEIQSVEETQI KERKCLLLKIRGGKQFILQCDSDPELVQWKKELRDAYREAQQLVQRVPKMKNKPRS
TSK / ITK tyrosine-protein kinase [Homo Sapiens]	NP_005537	7..148	LEEQLIKKSQQKRRTSPSNFKVRFFVLTKASLAYFEDRHGKKRTLKGSIELSRIKCVEIVKSDISI PCHYKYPFQVVHDNYLLYVFAPDRESRQRWVLALKEETRNNNSLVPKYHPNFWMDGKWRC CSQLEKLATGCAQYDP
(PDK1) 3-phosphoinositide-dependent protein	NP_002604	441..547	KQAGGNPWHQFVENNLILKMGPVDKRKGLFARRRQLLLTEGPHLYYVDPVNKVLKGEIPWS QELRPEAKNFKTFFVHTPNRTYYLMDPSGNAHKWCRKIQEVWRQRY

kinase 1 isoform 1 [Homo sapiens]			
RAC-alpha serine/threonine-protein kinase [Homo sapiens]	NP_00 1014432	4..111	VAIVKEGWLHKRGEYIKTWRPRYFLLKNDGTFIGYKERPQDVDQREAPLNNFSVAQCQLMKT ERPRPNTFIIRCLQWTTVIERTFHVETPEEREEWTTAIQTVADGLK
Pleckstrin homology domain-containing family A member 2 [Homo Sapiens] - N-Terminal	NP_06 7636	1..119	MPYVDRQNRICGFLDIEEHENSGKFLRRYFILDTQANCLLWYMDNPQNLAMGAGAVGALQL TYISKVSIATPKQKPKTPFCFVINALSQRYFLQANDQKDMKDWVEALNQASKITVPKG
Pleckstrin homology domain-containing family A member 2 [Homo Sapiens] - C-Terminal	NP_06 7636	199..297	LIKSGYCVKQGNVRKSWKRRFFALDDFTICYFKCEQDREPLRTIFLKDVLKTHECLVKSGDLL MRDNLFEIITSSRTFYVQADSPEDMHSWIKEIGAAV
Arno protein (ARF exchange factor) [Homo sapiens]	CAA6 8084	262..375	REGWLLKLGGRVKTWKRRWFILTDNCLYYFEYTTDKEPRGIIPLENLSIREVDDPRKPNCFELY IPNNKGQLIKACKTEADGRVVEGNHMVYRISAPTQEEKDEWIKSIQAAVS
Pleckstrin [Homo sapiens] - N terminal	NP_00 2655	3..110	PKRIREGYLVKKGSVFNTWKPMWVVLLEDGIEFYKKKSDNSPKGMIPLKGSTLTSPCQDFGKR MFVFKITTTKQQDHFFQAAFLEERDAWVRDIKKAIKCIEGGQKFA
Pleckstrin [Homo sapiens] - C-Terminal	NP_00 2655	239..346	EEFRGVIIKQGCLLKQGHRRKNWKVRKFILREDPAYLHYYDPAGAEDPLGAIHLRGCVVTSVE SNSNGRKSEEENLFEIITADEVHYFLQAATPKERTEWIRAIQMAS
Pleckstrin homology domain-containing family A member 3 [Homo sapiens]	NP_06 1964	1..100	MEGVLYKWTNYLTGWQPRWFVLDNGILSYYDSQDDVCKGSKGSIKMAVCEIKVHSADNTR MELIIPGEQHFYMKAVNAAERQRWLVALGSSKACLTDTRT
DAPP1 protein [Homo sapiens]	AAH1 2924	163..258	SLGTKEGYLTKQGGLVKTWKTRWFTLHRNELKYFKDQMSPEPIRILDLTECSAVQFDYSQER VNCFCLVFPFRTFYLCAKTGVEADEWIKILRWKL

Curriculum Vitae

Post-secondary Education and Degrees

Sept. 2014 -   **M.Sc. Pathology and Laboratory Medicine**

Aug 2016   University of Western Ontario

Thesis: "*Identification of a nuclear localization signal (NLS) within the PH domain of RGNEF*"

Advisor: Dr. Michael Strong

Sept 2008 -   **B.Sc. [H] Behavior, Cognition, & Neuroscience**

April 2013   University of Windsor

Thesis: "*Sequence learning on five item patterns in Rattus norvegicus*"

Advisor: Dr. Jerome Cohen

Related Work Experience

May 2014 –   **Research Assistant**

Sept 2014   Principal Investigator: Dr. Michael Strong

Funding: Windsor-Essex County ALS Society

As the initial work towards my Master's Thesis, I worked as a summer student performing site directed mutagenesis to create a 4.8kb construct: a 119aa deletion in the center of a 1731aa protein. The work also included subcloning and cloning into the pGEM and pcDNA3.1A vectors and transfection experiments.

Sept 2012 –   **Teaching Assistant**

April 2013   Instructor: Dr. Jerome Cohen – *Learning and Behaviour* (Psychology Department, University of Windsor)

As a teaching assistant I conducted two laboratory sessions a week where students were given hands-on experience training live animals (Rattus norvegicus) by both classical and operant conditioning. I also conducted weekly tutorials and quizzes to review lecture material.

Sept 2012 –   **Research Assistant**

April 2013   Principal Investigator: Dr. Siyaram Pandey

Funding: Michael J. Fox Foundation

In order to identify the prophylactic effects of a Co-Enzyme Q10 based drug treatment (termed Ubisol-Q10) in a mouse model (MPTP Mouse) of Parkinson's disease, I performed a series of experiments to characterize behavioural phenotypes, particularly locomotor ability.

Publications and Presentations

Publication   Manuscript in Preparation*

"*RGNEF is upregulated after axonal injury and plays a protective role in the cellular response against stress*"

Kevin Cheung, Cristian A. Droppelmann, Adam MacLellan, Michael Tavolieri, Ian Cameron, Kathryn Volkening, Michael J. Strong

Publication   Manuscript in Preparation*

What do Rats (Rattus norvegicus) learn in a Serial Reaction Time Task?"

Vara Parameswaran, Michael Tavolieri, Kaitlyn Iannicello, Siyaram Pandey, and Jerome Cohen

Poster   "*Identification of a nuclear localization signal (NLS) within the PH domain of RGNEF*"

Michael Tavolieri, Cristian A. Droppelmann, Kathryn Volkening and Michael J. Strong

London Health Research Day 2015 & 2016

Selected as a **Top 100** poster

Poster   "*Identification of a nuclear localization signal (NLS) within the PH domain of RGNEF*"

Michael Tavolieri, Cristian A. Droppelmann, Kathryn Volkening and

Michael J. Strong

Pathology and Laboratory Medicine Research Day 2015 & 2016

Oral   "*Identification of a nuclear localization signal (NLS) within the PH domain of RGNEF*

Michael Tavolieri, Cristian A. Droppelmann, Kathryn Volkening and

Michael J. Strong

Robarts Research Institute: Molecular Medicine Data Club

Poster   "*Elucidating the Role of RGNEF and Binding Partners in Neuronal Morphology*"

Michael Tavolieri, Cristian Droppelmann, Kevin Cheung, Kathryn Volkening, and

Michael J. Strong

ALS Canada Research Forum 2015 & 2016

Poster   "*Elucidating the Role of RGNEF and Binding Partners in Neuronal Morphology*"

Michael Tavolieri, Cristian Droppelmann, Kathryn Volkening, and

Michael J. Strong

International Research Workshop on Frontotemporal Dementia in ALS 2015

Oral   "*From a Frog's Eye View: Exploring the Role of Rax1 in Eye Development*"

Michael Tavolieri, Mohamed Fakhereddin, and Michael Crawford

University of Windsor Annual Biology Conference 2014

Poster   "*Sequence Learning on Five Item Patterns*"

Michael Tavolieri, and Jerome Cohen

University of Windsor Annual Psychology Conference 2013

Poster   "*What's in a rule? or What rules do rats acquire from fixed and varied sequences in the 5-choice serial reaction time task?*"

Michael Tavolieri, Siyaram Pandey, and Jerome Cohen

Comparative Cognition Society Spring Conference 2013

Oral   *"Effects of Violation Type and Location within Varied and Fixed Signal Sequences on Rats' 5-choice Serial Reaction Time Performance"*

Michael Tavolieri, Ema Sisic, and Jerome Cohen

Tri-state (plus) Conference on Animal Learning 2012

Honours and Awards

University of Western Ontario Graduate Scholarship

Top 100 Poster Presenter at London Health Research Day 2016

Invitation to join the Golden Key International Honours Society

University of Windsor Entrance Scholarship